DESIGN OF A NOVEL AXIAL-FLUX INDUCTION MACHINE FOR TRACTION APPLICATIONS

Franck C. Mushid

209532002

A thesis submitted to
the University of KwaZulu-Natal,
College of Agriculture, Engineering and Science,
in partial fulfillment of the requirements for the degree of

Master of Science

Supervisor: Professor David G. Dorrell

School of Engineering

University of KwaZulu-Natal

August 27, 2021

I, Franck C. Mushid , declare that:

(i) The research reported in this thesis, except where otherwise indicated, is my original research.

(ii) This thesis has not been submitted for any degree or examination at any other university.

(iii) This thesis does not contain other persons' data, pictures, graphs or other information, unless specifically acknowledged as being sourced from other persons.

(iv) This thesis does not contain other persons' writing, unless specifically acknowledged as being sourced from other researchers. Where other written sources have been quoted, then:

  a) their words have been re-written but the general information attributed to them has been referenced:

  b) where their exact words have been used, their writing has been placed inside quotation marks, and referenced.

(v) This thesis does not contain text, graphics or tables copied and pasted from the Internet, unless specifically acknowledged, and the source being detailed in the dissertation/thesis and in the References sections.

Candidate: Franck C. Mushid

Signature: _____

As the candidate's supervisor I agree to the submission of this thesis for examination.

Supervisor: Professor   David G. Dorrell

Signature: _____

ABSTRACT

DESIGN OF A NOVEL AXIAL-FLUX INDUCTION MACHINE FOR TRACTION
APPLICATIONS

Franck C. Mushid
School of Engineering
Master of Science

Induction motors are an important element in the industrial world; they are used in many applications, such as electric fans, elevators, pumps, conveyor belts, compressors and now even traction motors. Electric motors consume about 70 % of all industrial power consumption. Induction machines are also the source of the power generation such as in wind turbines. In recent years, the increase in price and supply-chain issues of rare earth magnets, which are currently an important material in brushless permanent machines, which are the most popular vehicular drive motor, has led to a focus on non-permanent magnet machine replacements, such as the induction machine.

The induction machine is still undergoing design development and being used in an increasing number of applications. They can be used in fixed speed (grid-connected) or variable speed (variable-frequency inverter-connected) depending on the application. Loss reduction, weight, size, as well as minimizing the cost of raw materials for manufacturing, are some of the issues in design improvement. In view of this, it is important to develop innovative methods for producing electrical machines that will reduce losses and minimizing cost of production.

The aim of this research work is to develop an appropriate analytical design procedure for designing an axial-flux induction machine and to evaluate the performance of the designed machine under various conditions. The machine must be robust and cheaper. ANSYS Maxwell software is used for 3D finite element modelling and simulation of the proposed axial-flux induction machine AFIM). For fast calculation, a simple sizing exercise is done using a pre-defined stator core. Then a radial-flux machine representation is developed in Siemens *SPEED* motor design software for fast assessment. The electromagnetic motor model is further tested to take into account the variations in rotor design. A proof-of-concept prototype was constructed for initial validation that the machine works and this design was modelled. The result of the simulation and the measurements from the laboratory design prove the possibility of the proposed AFIM for use in automotive application. Further design was carried out to improve the prototype using more substantial windings and a longer rotor. This design was tested with ANSYS Maxwell and *SPEED*. The designed machine offers a cost effective solution for future drive systems in automotive applications.

Keywords: Induction motor, axial flux machine

PUBLICATIONS ARISING

DESIGN OF A NOVEL AXIAL-FLUX INDUCTION MACHINE FOR TRACTION APPLICATIONS

Franck C. Mushid
School of Engineering
Master of Science

- F. C. Mushid and D. G. Dorrell, 'Review of Axial Flux Induction Motor for Automotive Applications', IEEE WEMDCD conference, Nottingham, U. K., 2017.

ACKNOWLEDGMENTS

Contents

List of Figures

List of Tables

List of Abbreviations

Abbreviation	Definition
2D	Two dimensions
2D	Three dimensions
AFIM	Axial flux induction machine
AFPM	Axial flow permanent magnet machine
AC	Alternating current
BLAC	Brushless alternating current
BLDC	Brushless direct current
EMF	Electromotive force
EV	Electric vehicle
HEV	Hybrid electric vehicle
FEA	Finite element analysis
DTC	Direct torque control
FOC	Field orientated control
IGBT	Insulated gate bipolar transistor
IM	Induction machine
MMF	Magneto motive force
PWM	Pulse width modulation

PMSM	Permanent magnet synchronous machine
SRM	Switched reluctance motor
SPWM	Sinusoidal pulse width modulation
VSI	Voltage source inverter

List of Symbols

Symbol	Meaning
D_o	Outer diameter of stator and rotor
D_i	Inner diameter of stator and rotor
D	Mean diameter of cores
L	Active length of stator conductor
P	Number of poles
n	Number of phases
N_{ph}	Stator turns per phase
A_{cu}	Area of copper in slot
A_{gross}	Area of slot
A_{net}	Area of slot minus the slot liner
I_{ph}	Stator current per phase
K_w	Winding factor of stator winding
f	Supply Frequency
E_{ph}	Supply voltage per phase
S_s	Number of stator slots
B_{av}	Average flux density
N_s	Synchronous speed

X_m	Magnetising reactance
X_1	Stator leakage reactance
X_2	Rotor leakage reactance
R_s	Stator winding resistance per phase
R_r	Rotor resistance per phase
s	Slip
I_{ph}	Stator phase Current
ω_s	Angular frequency
T	Torque

Chapter 1

Introduction

1.1 Background

Electric drives are used in many applications including vehicular and other transport propulsion systems. The requirements for these systems are different when compared to classical industrial applications. Vehicular propulsion systems usually operate at high torque for relatively short period during acceleration or generative braking with constant speed operation requiring much lower torque. The required speed range is wide so that a wide range of possible operating conditions are required from the drive. Recently brushless rare-earth permanent magnet machines have gained popularity in a variety of applications including drive applications due to their higher power density, efficiency and compactness. These are used in conjunction with power electronic inverters which are required for effective control. However, the high cost of rare earth permanent magnets and supply-chain issues has led manufacturers to investigate non-rare earth magnet motors in propulsion systems. There are several alternatives. Switched reluctance machines can be used in

propulsion applications, though their development for use in vehicular drives is still at the early stages. Wound-rotor synchronous machines are not commonly used due to high copper losses in the rotor, which are not easy to alleviate, and slip rings. The third alternative is the induction machine. Generally, these have a high level of robustness and reliability, and are low cost. They have been used commercially as vehicular drives by several manufacturers. Doubly-fed wound-rotor machines will have the same issues with rotor losses as the wound-rotor synchronous machine so invariably the squirrel cage machine is used where the rotor conductor fill factor using bars is much higher and no slip rings are required.

Induction motor drives are invariably conventional radial-flux machines for vehicular applications. These are high performance machines with forced fluid cooling and very high torque density. They are required to be compact with low inertia. This is demanding. To improve the performance and reduce manufacturing complexity of the induction machine for this application then this project attempts to move away from the conventional radial-flux induction machine, and use the axial flux induction machine (AFIM). For these, the rotor is not cylindrical and does not spin inside the stator, rather the rotor is disc shaped and faces the stator (or stators if double sided). By utilizing the AFIM to drive the car, the manufacture, installation and cooling of the electric motors may be easier. Therefore, in this work, the use of axial flux induction machine configuration is proposed for vehicular propulsion applications.

1.2   Research Motivation

Electric vehicles (EVs) are becoming popular. Energy storage and power delivery are two of the issues with the first generation of EVs which affect the size and weight of the vehicle and the range. The use of high quality lithium-ion and lithium polymer batteries has significantly improved these

issues. For the drive train, various machines can be used as discussed above though here the induction machine will be focused on. Conventional induction machines are designed typically for pump and fan applications if they are grid connected or variable speed industrial drives if inverter connected. Recently there has been improvement in efficiency though they can still suffer from heavy weight, poor ventilation and cooling system limitations (natural ventilation or air-over casing fan cooling) which is not particularly good for vehicular drives. This research work develops designs for a AFIM which is more compact, cheaper, and can be well cooled compared to the conventional induction motor. Aside from this, the designed machine may provide improved torque, thermal behavior and more straightforward assembly of the electric vehicle drive motor.

1.3   Aim and Objectives

The primary aims and objectives of the research work are as follows:

1. To develop an appropriate analytical design method then refine it using Ansys Maxwell and *SPEED* software for the correct preliminary design of the axial-flux induction machine for use in traction applications.

2. To investigate and analysis the performances of the designe machine.

3. To implement and construct the designed prototype of the AFIM for investigating the performance of the machine in terms of locked rotor and running light tests.

1.4 Research Methodology

Fig. 1.1 shows the steps adopted to achieve the aims and objectives of the research work.
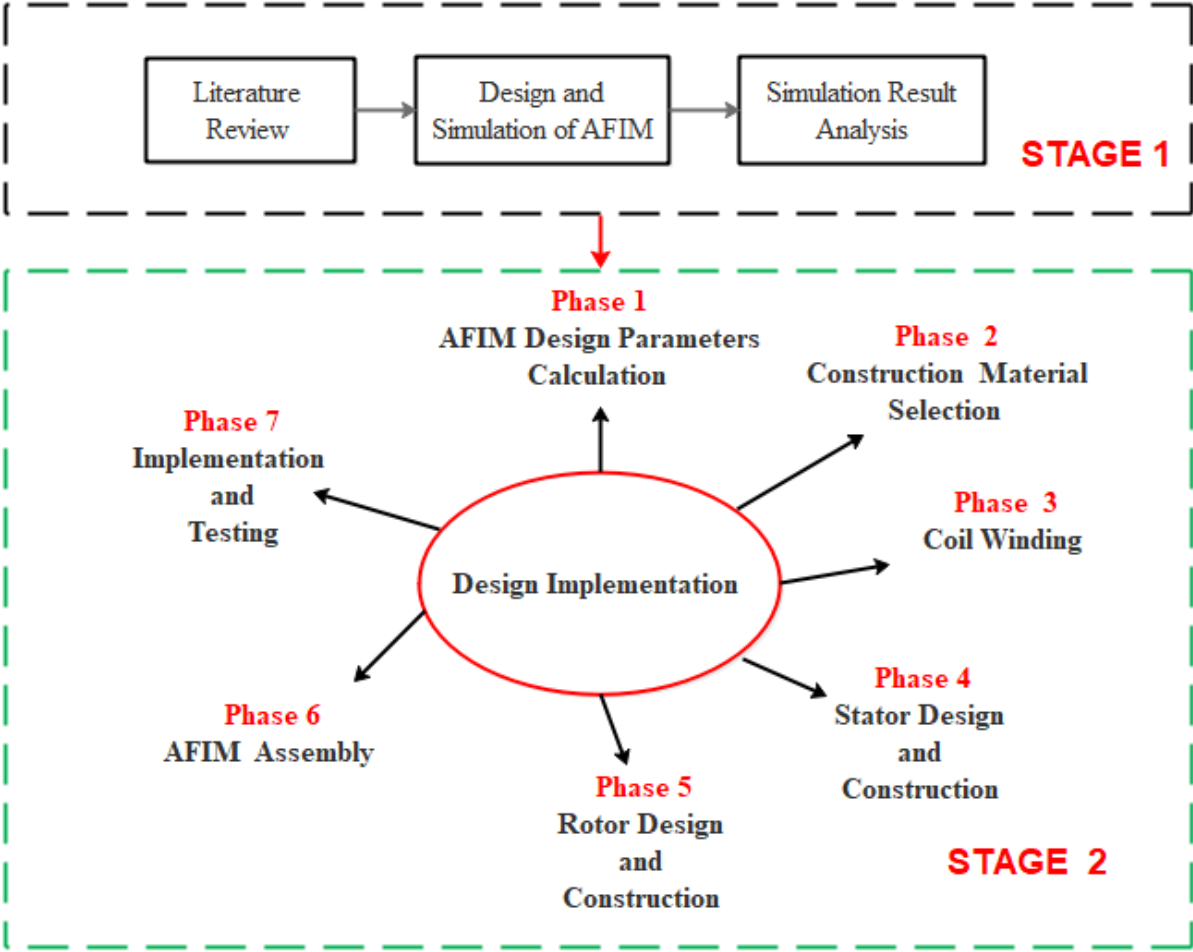
Figure 1.1 Research Methodology

1.4.1 Stage 1

- **Literature Review**

  A comprehensive literature review is conducted on the topic. Some of the areas requiring review are; history of axial flux machines, types of induction machine , principle of operation of an induction machine (IM), characteristics of IM based on the repulsion application, winding configuration of an induction machine , types and topologies of axial flux machines , comparison between axial and radial flux machines, design of AFIM and speed control and application of AFIM in an EV.

- **Design and Simulation of AFIM**

  The design and simulation of the proposed AFIM were carried out using simple sizing, then using Ansys Maxwell for finite element analysis and *SPEED* software for analytical analysis.

- **Simulation Results Analysis**

  A analysis of the simulation results was carried out.

1.4.2 Stage 2

As indicated in Fig. 1.1, the procedure for effective laboratory implementation of AFIM are:

- **Phase 1:** Proposed AFIM Parameter calculation

- **Phase 2:** Material selection

- **Phase 3:** Winding of the coil

- **Phase 4:** Stator construction

- **Phase 5:** Rotor construction

- **Phase 6:** General assembly of AFIM

- **Phase 7:** Implementation, testing and results analysis

1.5   Research Contribution

Based on the current interest in EVs, this thesis presents a novel approach to designing an axial flux induction machine for an EV. An analytical design procedure is built up for designing axial-flux Induction machines. The developed computation method uses simple sizing, then 3D finite element analysis and 2D analytical analysis to predict the performance. A fundamental comparative study on radial-flux and axial-flux induction machine topologies is presented in the work. A proof-of-concept double-stator double-sided rotor axial-flux machine is constructed. This is tested to validate the analysis methods. Further modified designs show the efficacy of the arrangement in meeting the requirements of a vehicular drive motor.

1.6   Scope and Limitations

The machine design is for an eight pole three phase axial flux induction machine using the Ansys Maxwell and Siemens *SPEED* software. The work is limited to the design and implementation of an axial flux induction machine for traction applications. The reason for using eight poles is that this is a common pole number used for commercial brushless permanent magnet vehicular drive motors such that in the Toyota Prius [6].

1.7   Structure of the Thesis

- **Chapter 1:** The general introduction to the research work is presented. This includes the aims, objectives and motivation of the work.

- **Chapter 2:** The literature review is carried out in this chapter which addresses automotive drives in general and axial flux machines in particular. There is a discussion of the general concepts of EV technologies. Historical evolution of the EVs and different configurations of the drive trains are presented. The AFIM in the context of high performance drives is put forward with axial and radial flux comparisons made. This leads to the advantages and disadvantages being described. The design aspects of an AFIM that are needed to improve its dynamic performance in order to be able to compete with the dynamic performance of the axial flux permanent magnet machine are addressed.

- **Chapter 3:** This chapter presents the simulation methods of the AFIM using Ansys Maxwell and Siemens *SPEED* software. The basic sizing is put forward here to give some dimensions.

- **Chapter 4:** This chapter presents the laboratory testing of the prototype. The proposed improved design is simulated under various load conditions.

- **Chapter 5:** The general conclusions of the work and recommendations for further investigation are presented.

Chapter 2

Literature and Technology Review

2.1 Electric Motors

There are two types of electric motors used in EVs to provide power to the wheels and these need to be variable speed. These is the direct current (DC) motor and the alternating current (AC) motor.

The DC motor is the traditional variable speed drive and comprises of three main components: field, armature and commutator. The field coils are mounted on the yoke of the motor which create the magnetic field, The wound armature on the rotor is connected to the DC supply via the commutator which mechanically switches the armature coils in sequence as the rotor rotates. The speed can be varied using the switching of the armature and field and use of resistors to control the DC supply to it. These drives predate power electronics and were used in old electric vehicles together with large lead-acid battery packs. However they are inefficient and now obsolete.

With the development of power electronic converters, firstly thyristors (using phase angle con-

trol) and later faster devices such as the IGBT (giving pulse wave modulation (PWM) control), variable frequency supplies have developed which can give variable frequency and voltage. This means AC motors can be used as variable speed drives. There are three main types of motor that are suitable for electric propulsion systems: the brushless permanent magnet motor (which can be sine or square wave current control), the squirrel cage induction motor and the reluctance motor (switched reluctance and more recently synchronous reluctance). Not all motors perform well when used in electric propulsion systems [7] [1]. All require variable frequency and variable voltage converter supply. The requirement for a vehicular drive motor are:

- High density of torque and power;

- High torque at low speed and high power at rated speed;

- Wide speed range at constant power;

- High efficiency in braking;

- High reliability and robustness;

- Low noise during operation; and

- Acceptable cost.

To manage these requirements many drive motors are not continuously rated and use fluid cooling. This is so they can deliver high torque for a limited time during acceleration and regenerative braking and not overheat during these periods.

2.2 Automotive Drive Motor Options

The motor types described above can be further dived into sub-types as shown in Fig. 2.1. This shows the choice and brief characteristics for each machine [8]. The induction motor shows itself as a suitable candidate for electric propulsion systems. Generally, the brushless permanent magnet synchronous motor is more efficient compared to induction and reluctance motors. In the following sections, a brief explanation is given for each motor type in relation to the EV drive requirement.
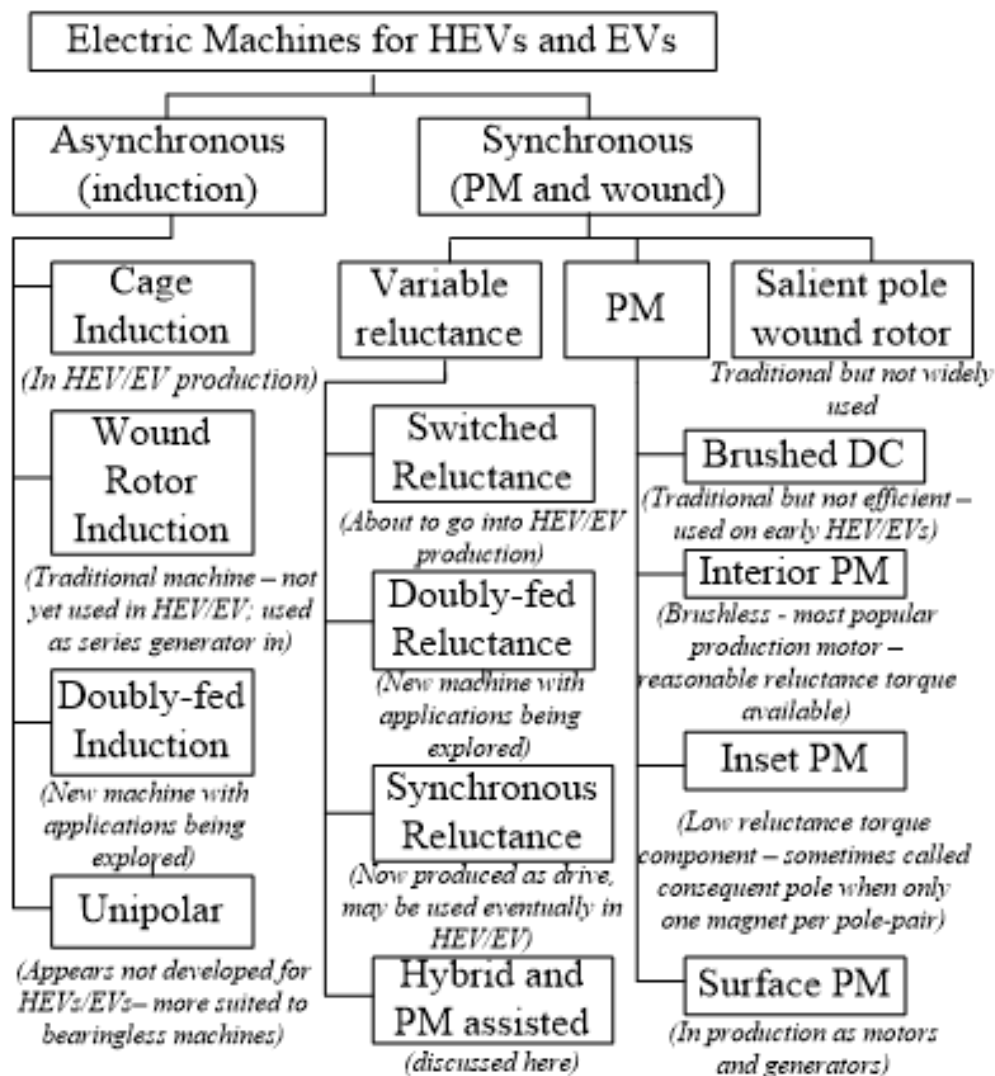
Figure 2.1 Different machines available for HEVs and EVs

[8]

2.3   Direct Current (DC) Motor

Basically, the two types of electric motors are:

- Conventional brushed DC motor
- Brushless motor

The direct current (DC) motor is the traditional variable-speed drive motor in electric propulsion systems. They are still used in some older trains and also in older industry where a variable DC supply is obtained using a Ward-Leonard system or latterly with thyristor converters. Due to the ability to produce high torque, particularly at low speeds, they present a torque - speed characteristic suitable for traction applications. They are a mature technology with simple control. To change the speed of operation it is only necessary to control the voltage applied to the motor. However, DC motors are bulkier in construction due to the commutator, and have lower efficiency. They have lower reliability and require greater maintenance because of the commutator and the brushes which need regular inspection and replacement. Structural issues with the commutator and armature windings can limit the operational speed. DC motors tend to have two, four, or six poles depending on speed, power and voltage. There are three possible connections for a DC motor depending on the field winding configuration: series, shunt or separate excitation. Separately excited motors are more flexible and allow field weakening for extended speed operation in the constant power range. However, if only one DC supply is available then shunt or series excitation is used. Some older power drives have both shunt and series windings for different modes of operation and some machines are compounded - using both shunt and series windings simultaneously. By replacing the field winding with permanent magnets, the size can be reduced and efficiency improved. However, there is a loss in control due to having a fixed field. The low permeability of the permanent magnets means the armature reaction is generally reduced and the commutation switching improved [9] [1] [10].

Brushless DC machines are a derivative of the brushed DC machines. The term "brushless" is used because there is no commutator and no brushes. Brushless DC motors essentially turn a brushed DC machine inside out so that the field is spinning and the armature is static with the switching between armature coils done electronically. They are generally 3-phase and the current is quazi-square wave (trapezoidal). They offers better performance and longer life. They are similar to brushless synchronous machines though the induced winding EMF should be trapezoidal rather than sinusoidal and the control strategies are different. They use different position feedback methods with the brushless DC machine using Hall sensors which are more straightforward while brushless AC machine use encoders. They have many applications from small single-phase self-starting motors used in computer fans through to high-efficiency high-performance drives using high energy rare earth magnets. They can be used in EVs though they can suffer from torque ripple when compared to brushless AC motors and need to be designed to minimize this.

2.4   Reluctance Motor

Although the SRM (Switched Reluctance Motor) principle has been known for more than a century, the motor has gained interest since the 1970s as the power electronic converters necessary to drive them were developed. It has potential for applications in electric propulsion systems and its magnetless arrangement with no rotor conductors makes it advantageous. The reluctance motor is a direct derivation of the variable reluctance stepping motor. It has the advantage of simple and robust construction, low cost, fault tolerance, high torque at low speeds, simple control and excellent torque or speed characteristics for applications in electric propulsion systems. The rotor structure is simple with no windings, no magnets and no slip rings. The reluctance motor has a wide speed range and is suitable for electric propulsion systems; no gearing is necessary between the motor

and the wheels in some instances. The increase in the speed range, which can reach values several times the rated speed, is obtained from the use of suitable control systems. The reluctance motor does have disadvantages: torque ripple, noise, vibration and electromagnetic interference. A special topology for the electronic converter is required. It is usually necessary to know the position of the rotor so that the motor can be properly controlled, although there are sensorless systems [9] [11].

2.5   Permanent Magnets Synchronous Motor

The permanent magnet synchronous motor (PMSM) is derived from the synchronous machine by replacing the field winding with permanent magnets. The PMSM is also called the permanent magnet brushless AC Motor (PMBLAC), sinusoidal-fed permanent magnet brushless motor or brushless AC motor (BLAC). It is sometimes erroneously called brushless direct current (BLDC) motor which is incorrect. This type of motor has the advantage of presenting high torque at low speeds as well as high power density and efficiency. The elimination of the commutator gives a reduced total weight and volume, eliminates rotor losses, provides greater efficiency, and allowing easier dissipation of heat [9] [11]. There are two main types of permanent magnet synchronous motor classification which is dictated by the position of the magnets in the rotor. The magnets can be mounted inside the rotor (interior permanent magnet - IPM) or on the rotor surface (surface permanent magnets - SPM). The former can enable q-axis saliency and inclusion of an alignment torque as well as the main excitation torque. The high performance and high efficiency of these machines, particularly IPM, makes them a popular choice for vehicular drive motors.

2.6   Induction Machine

The induction machine (IM) is relatively simple in construction, reliable, robust, low maintenance and relatively low cost. Induction machines (IMs) are often in electric propulsion applications and are probably second to the PMSM in use as a vehicular drive machine. There are wound rotor induction machines used in applications such as wind turbines that have rotor windings connected through slip rings but these are not particularly suitable for vehicular drive motors. The squirrel cage induction machine, however, has rotor conductors but no slip rings or commutator and can operate above rated speed with a wide field weakening (constant maximum power) range as required for a vehicle. Variable frequency and voltage control of induction machines can lead to the desired performance for traction systems. However, to attain this then controls such as field oriented control (FOC) and direct torque control (DTC) are required. Nonetheless, the cost of implementing FOC is greater than that for DC motor control thus these are most sophisticated [1] [9] [12].

2.6.1   Principle of Operation of an Induction Machine

A 3-phase AC power supply connected to the stator of an induction or synchronous machine generates a magnetic field that rotates at a synchronous speed. In a synchronous machine, the rotor has windings or magnets that generate a magnetic field which is constant so that the rotor has to rotate at the synchronous speed which interacts with the stator magnetic field to produce torque. However, in an induction machine , the rotor rotates at a slower speed than the stator magnetic field. In a squirrel cage induction machine the rotor conductors form a closed circuit and the difference in speed between the synchronous speed and the rotor speed will lead to the stator magnetic field inducing EMFs in the rotor conductors causing current to flow. This is an opposing current, in effect the secondary winding similar to a transformer, and will set up a rotating magnetic field rotating

at synchronous speed. The interaction of the stator and rotor fields will generate torque [13]. This torque will drive the machine.

When the rotor rotates at synchronous speed the stator field appears static with respect to the rotor and thus no rotor current or torque is generated; generally, an induction motor runs a little slower than synchronous speed. According to the standard design B torque curve, the difference or "slip", between actual and synchronous speed differs from about 0.5 % to 5.0 % for an induction machine during steady-state operation and at grid frequency [14].

The main feature of an induction machine compared to a synchronous machine is that the magnetic field is generated by induction instead of being separately excited or self-magnetised . In order to generate rotor current, the speed of the rotor must be less than the speed of the rotating magnetic field of the stator, as already stated. As the rotor rotates slower with regards to the synchronous speed, the rotating speed of the stator magnetic field increases relative to the rotor, consequently, generating more current in the windings and thus creating more torque. The "slip" is defined as the ratio between the rotor speed and the stator rotating field - the synchronous speed. Under load, the speed drops and the slip increases to create sufficient torque to turn the load. However, while the current keep increasing with slip, the torque will reach a peak before reducing (the "pull out" torque). For this reason, the induction machine is sometimes referred to as the "asynchronous machine" [15]. An induction machine can also be used as an induction generator or it can be unrolled to form a linear induction motor, which can directly generate linear motion. Generation is possible in a squirrel cage induction machine by forcing the rotor to rotate above the synchronous speed. The machine torque will try to brake the machine and thus generation occurs.

2.6.1.1 Synchronous speed of an induction machine

Generally, the synchronous speed of an induction machine is given by.

$$\eta_s = \frac{120f}{P} \tag{2.1}$$

where η_s is the rotation rate of the stator magnetic field, f is the frequency of supply, while P is the number of poles.

2.6.1.2 Slip

The ratio of the different between the synchronous speed and the operating speed of an induction machine is referred to as slip. Generally, the slip is

$$S = \frac{\eta_s - \eta_r}{\eta_s} \tag{2.2}$$

where η_s is stator synchronous speed, η_r is rotor mechanical speed. When motoring, the slip varies from zero (at synchronous speed) and unity (at standstill when starting). This is the range for motoring. Since the short-circuited rotor has low resistance, even a small slip, large currents are generated in the rotor which produces significant torque. At full rated load and grid frequency, the slip varies from more than 0.05 p.u. for small or special purpose motors to much less than 0.01 p.u. for large motors. The speed variation can leads load-sharing problem when various sized motors are mechanically connected. Nevertheless, various techniques have been employed to reduce slip. These techniques include variable frequency drives (VFDs) [16]. The slip will vary with frequency, so that the full load slip will tend to reduce with increasing frequency. This is because the speed difference at rated load tends to be constant as the frequency increases so that in (2.2) the numerator is constant while the denominator increases. This is because the frequency of the induced rotor EMFs is at slip frequency so that to produce the same rotor current at different rotor speeds (or

17

different supply frequencies) the slip frequency has to be maintained. Additionally, to keep the stator flux constant as the speed varies then the supply voltage has to vary with the frequency; i.e., $V/f \approx$ constant.

For vehicular drive motors, generative braking is required and in an induction machine this can be obtained by running the machine above the synchronous speed. At this point the slip becomes negative and generation occurs. If the vehicle is running at a set speed the the supply frequency from the inverter can be reduced to reduce the synchronous speed in line with (2.1) so that the rotor rotates above the synchronous. The frequency can then be reduced in a controlled manner to reduce the vehicle speed and recharge the batteries.

2.7 Types of Squirrel Cage Induction Machine

The squirrel cage induction machine can be grouped into two depending on the input supply. The two types are:

- Single-phase induction machine; and

- Three-phase induction machine.

The single-phase induction machine is not a self-starting motor, while the three-phase induction machine is a self-starting motor.

2.7.1 Single Phase Induction Machine

Single-phase induction machines are used in low power applications both in domestic and industrial settings. These are squirrel rotor cage machines. The main winding has a pulsating stator field

rather than a rotating stator field thus will not start with a main winding only. They are invariably grid connected. The main winding carry AC when motor is connected. Auxiliary windings are using in quadrature with the main winding to start the machine. These are much lower in rating and often have an additional resistor or capacitor connected in series with the auxiliary. The winding is often switched out when the speed approaches to full load. This is the least expensive solution for most applications. Single-phase induction machine can be grouped into different categories based on the starting methods:

- Split phase induction machine (with centrifugal switch);

- Capacitor start induction machine;

- Capacitor start capacitor run induction machine;

- Shaded pole induction machine; and

- Permanent capacitor motors.

A centrifugal switch opens and disconnects the starting winding when the motor reaches about 70 % to 80 % of the synchronous speed.

These machines are clearly unsuitable for automotive drives.

2.7.2 Three-Phase Induction Motor

Three-phase induction machines have a rotating field rather than a pulsating field and therefore are self-starting. Three-phase induction machines are grouped into squirrel cage and slip ring motors as already stated. Squirrel cage motors are rugged and simple in construction, thus, they are is widely used (in excess of 90 % of all induction motors) and are suitable for vehicular drives.

2.8 Winding Configuration of an Induction Machine

The selected machine winding configuration is very significant to the machine design as it effects motor sizing (weight), torque density, stator winding harmonics and motor speed range. The two main winding configurations are distributed and concentrated windings. Distributed windings reduce harmonic content and produce close to sinusoidal airgap flux which is necessary for an induction motor. This reduces asynchronous torques. Concentrated windings have more airgap flux harmonics and are more suitable for BPM and switched reluctance machines. Distributed winding configurations can incur higher copper loss and increase motor weight [17]. According to [18] and [19], winding configurations can grouped into:

- Single layer;

- Double layer;

- Fractional slot; and

- Concentrated winding.

The concentrated winding is not suitable for an induction machine so is not discussed here. In a single layer winding, a complete slot is occupied by a single coil side. It only allows for full pitching and is a concentric wounding. In a double layer winding, two coil sides occupy a slot. They can have lap or wave arrangements and can allow short pitching. Both of these configurations, for a 3-phase winding, have an integral number of slots per pole per phase. In a fractional slot, the slot per pole per phase is not an integer which can give additional airgap harmonics and these are often used in high pole number BPM machines.

The layout of a winding can reduce the airgap spatial harmonics, depending on the angle of the winding of each phase span and their distribution. The span of the coil of a machine phase depends

on the pitch factor. 180 electrical degrees represent a full pitch coil while if the coil is short pitched the angle in between the starting and returning point of the coil is reduced by a given angle.

2.9   Induction Machine Losses and Efficiency

For effective design and operation of electrical motors, it is important to take note of the losses which may directly affect the efficiency of the motor. Induction machines will have copper losses in the stator and rotor conductors and iron losses in the core. There are stray load losses which are small losses that cannot be accounted for but are probably due to iron loss and some additional eddy current such as proximity losses in conductors that cannot be accounted for. There are mechanical losses in the form of friction and windage losses. Generally, these losses can be divided into:

- Constant losses; and

- Variable losses.

In fixed-supply machines such as pump and fan motors, a simple efficiency-speed curve will describe the efficiency of the motor and it should be designed to operate at peak efficiency at the rated load. However, with the move to use in vehicular drives then the efficiency requirement becomes a multi-dimensional issue with the efficiency being important over a range of speeds and loads. This has led to the use of efficiency contour charts as shown in Fig. 2.2. This is a chart typical for an EV using an induction motor drive . These charts do have noticeable differences depending on the type of motor used which is illustrated in [1].
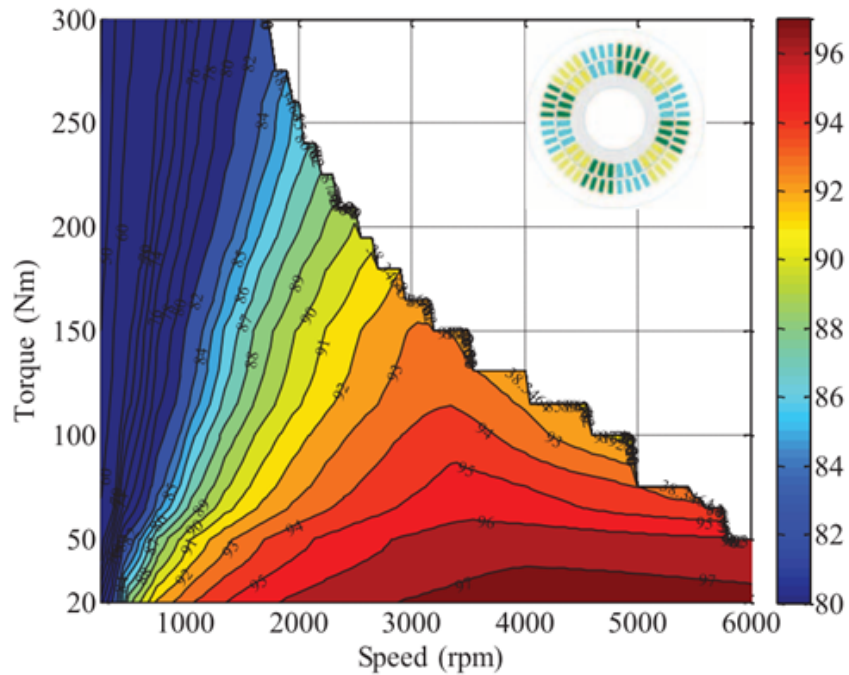
Figure 2.2 Efficiency map for automotive induction motor drive [1]

2.9.1 Constant Losses

Constant losses, also known as fixed losses, are losses that is constant during normal operation of squirrel cage IM. This assumes constant supply frequency. This loss is often measured during a no-load testing of an IM. This loss can be grouped into iron and core losses and mechanical losses due to friction and windage.

1. **Iron or Core Losses**

   Iron or core losses are further divided into hysteresis and eddy current losses. Core lamination is used to reduce eddy current losses. Laminating the core reduces the steel core cross-section that the current can circulate into much smaller sections, thus reducing eddy current. High-grade silicon steel can be used to reduce hysteresis losses. The core losses depend on the frequency of the supply. The stator frequency is equal to the supply frequency,

while the rotor frequency is equal to the slip frequency which is the slip multiplied by the supply frequency. This is much less than the stator frequency when running at steady-state or with a variable speed supply. For instance, for a supply frequency of 50 Hz, which gives a stator frequency of 50 Hz, the rotor frequency will be about 1.5 Hz when the slip is 3 %. Consequently, rotor core loss small compared to a stator core loss. In terms of vehicular drives, the supply can drive the machine to much higher speeds which means higher frequencies. For instance, if the inverter is running at 400 Hz, the 1.5 Hz speed difference range is maintained for the same torque so that the slip is 0.0375 %. This means that increased frequency is affects the stator core losses rather than the rotor core losses. Indead in this work, the rotor contains solid steel rather than laminated steel. The choice of magnetic steel for the stator is important. Low loss steel is available and also the losses are a function of frequency (hysteresis is a function of frequency and eddy current loss is a function of the square of the frequency). Different steels will have different characteristics with respect to the flux magnitude and the frequency.

2. **Friction and Windage Losses**

Losses occur at the bearings due to friction losses. These losses are zero at start and increase with speed. There will also be losses due to windage effects inside machine (in flywheels a vaccuum is often used to remove these). If the airgap is fluid cooled or forced air cooled to help remove rotor copper losses then these methods could possibly increase the windage losses. These losses tend to be constant at constant speed whatever the load.

2.9.2   Variable Losses

These losses are also called copper losses and vary with load at constant speed. Hence they are a function of torque rather than speed. These are joule losses due to current flowing in stator and rotor conductors. As the load changes, the current and hence these losses change. Therefore, these losses are called variable losses.

High losses can be cause temperature rise, which can be detrimental to the performance of the machine and can be catastrophic. This is particularly relevant in vehicular drive motors because they are not continuously rated, rather they are designed to operate at high torque for short periods of time during hard acceleration and braking. As the temperature rises so does the resistivity of copper and aluminium (often used in cage rotors via casting) which leads to even higher loss for given currents and possible thermal runaway. Many automotive drive motors have forces cooling to ensure thermal runaway does not occur.

2.10   Machine Field Weakening

The designed machine must run over the entire speed range of the vehicle when not using a gearbox with multiple gears. The speed of the machine is dependent on the frequency which varies the synchronous speed; however, the flux levels are a function of both frequency and voltage since the flux, in a coupled electromagnetic circuit, is equal to the rate of change of voltage in the coupled coils. Induction machines are torque limited since there is a limit to the flux due to saturation and limit in current due to heating. Therefore at maximum torque the voltage will increase linearly with frequency as already mentioned so that $V/f \approx$ constant. However, the inverter voltage constraint is attained at base speed where maximum output voltage is reached. Above this speed the machine

enters a constant voltage region where the flux reduces with increasing speed. The envelope of operation will be limited by maximum power since the machine can operate up to maximum voltage and speed. This is illustrated in Fig. 2.3. This is a key difference to industrial induction machine drives which tend not to operate in the field weakening region whereas vehicular drives operate very much into an extended field weakening region. At the base speed the maximum iron losses may be reached; as the speed increased beyond the base speed the flux reduces, limiting the iron losses and preventing excessive core heating.
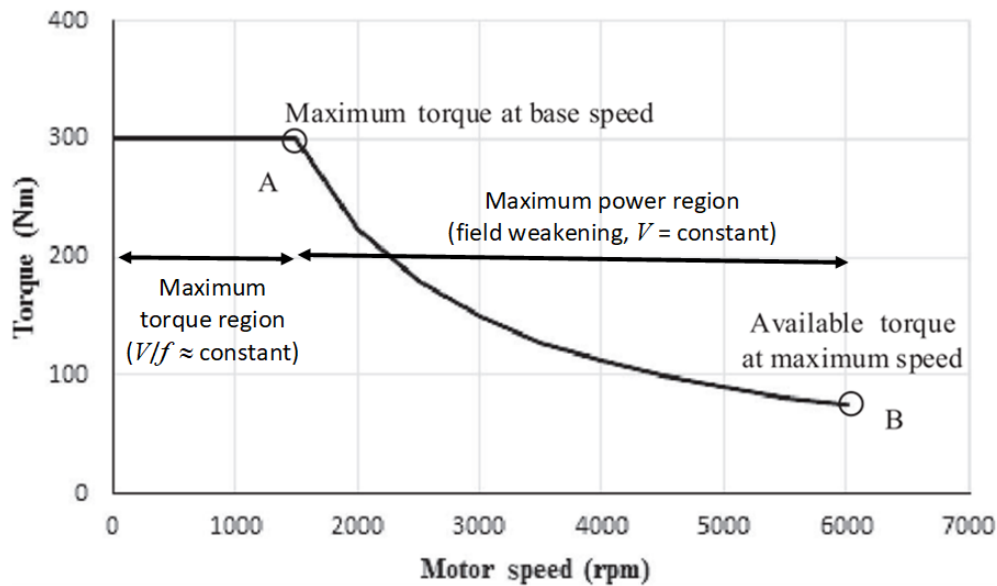
Figure 2.3 Illustration of torque-speed envelope for vehicular drive motor showing maximum torque and maximum power ranges [1]

The flux in an induction machine is straightforward to control via the voltage. For completeness, field weakening in BPM machines is discussed for comparison since they have constant flux from magnets. In a BPM machine field weakening is not as straightforward because of the fixed field flux from the magnets which makes it difficult to limit the field flux at speeds above the base speed. Field-weakening in a BPM is obtained by rotating the stator current off the q-axis and advancing by some way. The stator current flux then opposes the magnet flux [20] [21]. The arma-

ture reaction flux then has a negative d-axis direction component that opposes the field flux from the magnets. Consequently, this reduces the back EMF and allows the converter to operate at its maximum voltage at speeds exceeding the base speed. This requires careful control and use of a position encoder to detect rotor position.

2.11   Motor Characteristics for Propulsion Systems

When designing a machine for propulsion in EVs, the motor must adhere to strict design constraints. This section summarizes the drive requirements. It is crucial that the energy consumed by the machine when motoring or generating adheres to the design boundaries. This will enhance the effectiveness and durability of the batteries during the required driving range. Over the expected speed range, the machine is needed to deliver the torque for traction while maintaining a high degree of efficiency, otherwise the vehicle range will be limited due to losses. The key aspect of electric motors propulsion design are:

- High instantaneous power and high-power density for effective control of the machine; in Fig. 2.3, which is typical for mid-sized car, the motor can deliver 300 Nm for a short time - it is likely to be continuously rated at about 150 Nm.

- High starting torque at a lower speed and constant power at high speed - this allows rapid acceleration from standstill.

- Constant torque and power over a varied speed range. Most steady-state operating points will be at low torque and speed since vehicles tend to have maximum speeds well in excess of the road speed limits and to use the whole envelope requires a very aggressive driving style.

- Regeneration with high efficiency over the full speed range - the discussions put forward in this chapter are mostly couched in terms of the motoring mode. However, it is important that energy is retrieved during braking to recover kinetic energy. The efficiency chart in Fig. 2.2 is for motoring, where the torque is positive. There will be a reciprocal chart of similar ilk for generation where the torque is negative.

- Robustness and high reliability.

Low cost, high reliability, robust structure, good controllability and acceptable efficiency are some of the advantages of the induction motor that makes it stand out for use in many different applications [22]. According to [23], the mechanical and electromagnetic advantages of the axial flux induction motor shows it to have potential for use in EVs. This potential is yet to be realized.

2.12   Axial Flux Induction Machine Drives

The vast majority of industrial electrical machines are squirrel cage asynchronous machines for pumps and fans etc.. More modern variable speed drives and actuators use other types of machine in addition to the induction machine, such as the brushless PM motor and reluctance motor. These configurations are possible thanks to the technological advances in materials, numerical calculations and power electronics. EVs use variable speed drives and most use brushless PM machines.

It is of great importance to consider power density and energy for storage and conversion in an EV design because these are related indirectly to the vehicle weight and size. Brushless PM EV electric motors are designed to be either DC or AC and the motor type determines the controller used. The authors in [24], review different types of electrical motors used in hybrid electric vehicles (HEVs) and EVs.

According to the authors in [25], in 1988, proposed a slotless brushless PM AC motor with toroidal woundings, slot less and permanent magnet. In this design, the axial flux permanent magnet motor was proven highly efficient due to the high power density and high torque generated at low speed. The authors of [26] proposed axial flux induction machines that directly drove two wheels.

Induction machines can either be radial or axial flux machine depending on the direction of flux in the airgap and the electromagnetic energy conversion. The operating principle of both radial and axial flux machine is the same, these are categorised according per field orientation and their conductor geometry. Fig. 2.4 represents the radial field motor with radial airgap flux and axial-direction conductors, and the axial-flux machine has an axial airgap flux and radial-direction conductors.
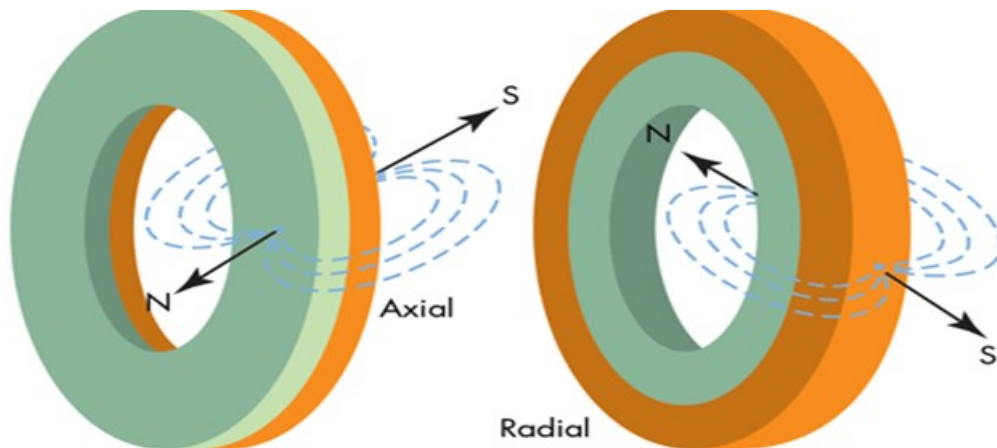
Figure 2.4 Flux orientation: a) axial, and b) radial.

Axial flux induction machines could have several applications. For instance:

- The authors in [27] compared the advantages and disadvantages of a brushless PM AC permanent and an induction machine for the same automotive application. This is because rare

earth magnet material resources are limited so that induction machine drives are considered for automotive applications.

- High-speed compressor systems utilise high-power variable speed induction machine drives for high pressure pumps. Like automotive drive machines, these machines to achieve high speed during operation and the supply frequency from the supply can go into several hundred Hertz [8][28].

The work in [29][30] stated that the axial flux induction machine is suitable for medium speed operation i.e. 3000 – 15000 rpm due to their light construction, and excellent mechanical and dynamic performance properties. The rotor design is made from solid steel that is disc shaped with an inserted cage cut from a good conductor such as copper or aluminium. There have been patents filed to address numerous features of the machine but the overall basic topology remains consistent [31][32]; therefore the validity of the patented variations seem very specific and possibly infringing on one another. The motor continues to be researched [33][34].

The axial flux induction machine has recently gained popularity in some niche applications, the main form being the brushless PM axial flux motor [35][36] [32][37].

Axial flux induction machines can be designed with different inertia ; [38] shows that the construction of an axial flux machine rotor can be varied. The axial flux machine has a greater diameter-to-length ratio than a radial flux machine with the inner diameter being larger than the shaft diameter. This allows for effective ventilation and cooling to be achieved. In order to reduce the axial-flux machine size the high specific electric loading and high specific magnetic loading are required. In an EV application, if it is meant to be in-wheel, the axial flux induction machine has to have a short axial length [8][29]. In [39] and [40], research on direct drive high torque in-wheel motors was conducted for both HEVs and EVs. These studies investigated and presented

the advantages of the axial flux induction machine for automotive drive applications. The effects of different parameters relating to the performance characteristics of axial flux induction machine were analyzed.

2.12.1   History of Axial Flux Machines

The axial flux machine is not a new technology. It has been presented in numerous topologies. The radial flux induction machine is the most popular motor type due to its high reliability and low-cost manufacturing. It is the workhorse of the industry. However, the flux path in a radial flux machine is relatively long compared to the axial flux equivalent. A large fraction of the length of a radial flux induction motor is also the end turn region of the windings. The axial flux induction machine topology has thus attracted some interest as a double-sided axial flux machine that can significantly increase torque density and where the length of the machine is a limiting design parameter. The history of electrical machines shows that the earliest machines were the axial flux machines dating back to 1831 and were built by Michael Faraday.

Some years later in 1837, Davenport patented the first radial flux machine. There are several reasons why the axial flux machine was not used for many years. For instance, there is a large attractive force between the stator and the rotor, causing difficulties in manufacturing. The laminated stator core can be high cost in manufacture and there are difficulties in assembly to maintain uniform airgap. Thus, radial flux machines have come to dominate the market. However, these issues can be overcome with improved manufacturing techniques.

In 1983, electrical machines with Neodymium-Iron-Boron (NdFeB) permanent magnets first appeared. These rare earth magnets facilitated the use of machines with axial flux in addition to machines with radial flux. During recent decades, permanent magnets have undergone much

development. This has shown the need to consider the thermal stability of the permanent magnet, as well as the sensitivity of the specific parameters of permanent magnets with increasing temperature. Axial flux rare earth PM machines are increasingly being used, for example, incorporated into the wheels of the electric propulsion systems, wind generators, pumps, and other applications [41][42]. With the availability of various materials, axial flux machines can play a major role in new and current applications.

2.12.2   Axial Flux Induction Machine Characteristics

An axial-flux induction machine (AFIM) topology in which the rotor is located between two slotted stator cores with three-phase windings, is suitable for low speed direct-drive usage as considered in this research work. They can run at higher speeds. The stators may be set up easily, and due to the double-sided interior rotor topology, the axial loading of bearings is low if the rotor is centred. In direct-drive usage, the quality of the electromagnetic torque is a crucial parameter, thus, the design has to reduce the torque pulsations as a sum of cogging torque and excitation torque ripple [43]. Cogging torque is due to alignment between the stators and rotor which gives the least reluctance path during rotation. This can occur with no rotor current. Excitation torque ripple in AFIM is due to the distortion of the sinusoidal back-emf and stator winding current. The issue of electromagnetic torque quality in the design AFIMs can be tackled by decreasing cogging torque and back-emf harmonic contents.

The disc-shaped profiles of the rotor and stator makes it possible to produce various designs. Small axial flux machines of only a few Watts or less, for hard disc drives etc., are frequently designed as simple single sided plates with magnets on the rotor plate and airgap windings on the stator with little or no iron. Larger motors will have slotted stators and may have double sided

rotors with two stators or double sided stators with two rotors.

Special attention should be given to the design of the mechanical linkage of the rotor-axis, as this is frequently the source of failures of disc-type motors, see Fig. 2.5 [44]. Lamination and magnetic composite materials are both enclosed in the design of axial flux induction machine. By the combination of these two materials restricted axial flux induction machine in a volumetric space, restricted in a height, and give a smooth torque output ripple. The rotors bars of the axial flux induction machine are skewed which help to smooth the torque pulsations of the induction machine, therefore the machine efficiency increases.
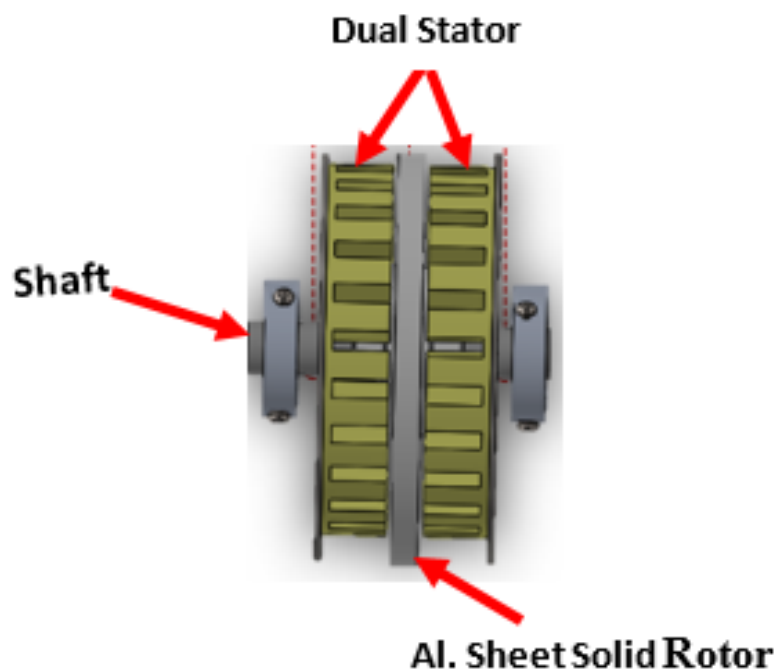
Figure 2.5 Axial flux induction machine

For applications such as electric traction and wind turbines, their reduced size (compared to the equivalent radial flux machine) and their high torque density drives the study of axial flux machines. If the machine is double sided then the increase in torque is obtained through have two

rotor surfaces and air gaps in the same machine. The active surface of the air gaps is greater than that of conventional cylindrical motor; this is also an advantage for cooling. The increase in the number of poles results in an increase in the diameter and therefore a decrease in the axial length. As a result, the volume of the active parts is less compared to the radial flux machines.

2.12.3   Types and Topologies of Axial Flux Machines

Axial flux induction machines have three main arrangements: single sided machines, double-sided machines and multistage machines.

The radial length from the stator inner radius to the outer radius is the active part which produces the torque and the axial length is dependent on the yoke design of the stator and the rotor; i.e., the flux density in the stator and the rotor yokes. Nevertheless, as the number of poles increases, the active radial length of the motor remains unchanged, and the axial length depends on the flux density in the stator yokes [45]. The different arrangements for single sided and double-sided motors are shown in Fig. 2.6.

The single sided machine has one arrangement but the double-sided arrangement can have several different arrangements. The double-gap, internal stator, machine was studied in references [46][47]. For this structure, the interest was focused on the winding. In [44], Gieras, Wang and Kamper, in their book, analysed double rotor motors with an internal stator; the stator was ironless with airgap windings. Two different types of windings were proposed and compared to standard distributed windings. The authors compared the windings in terms of torque and copper mass. Three stator prototypes were constructed and tested with the same permanent magnet rotor discs. The motors were 1 kW at 200 rpm with 12 pole-pairs. The finite element analsys (FEA) results and experiments show that the tape coil windings are better in terms of torque performance because of
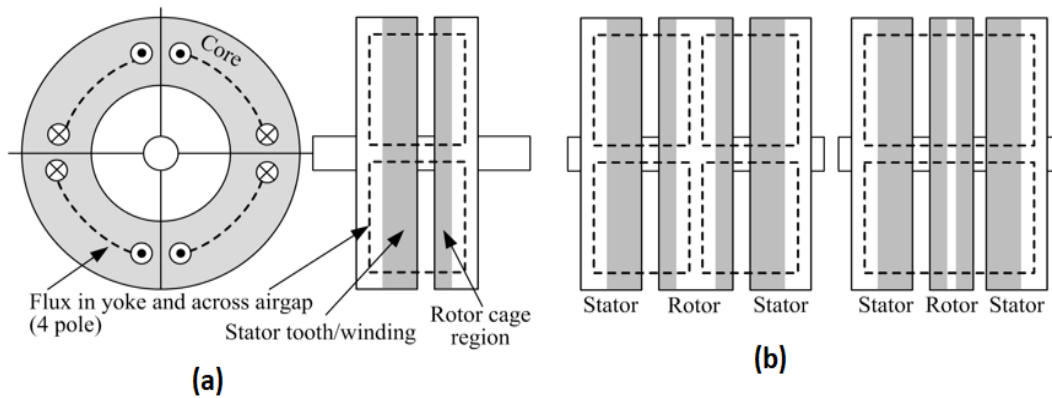
Figure 2.6 Axial-flux induction machines: (a) Single sided motor; and (b) Double-side motor with two stators

the winding distribution and a 15 % reduction in copper mass.

De Doneto *et al.* [48] compared a radial flux and axial flux and the different ways to calculate torque. This is an interesting comparison between the topologies of a brushless PM machine. Two winding types were compared in [49] for a 10 kW double-rotor axial-flux machine with an internal stator running at 800 rpm. The rotor had 10 pole-pairs. The topology in Fig. 2.6 (b) is specific to internal rotor between to stators. What can be seen is that there are two arrangements where the flux goes through the rotor or is reversed in the rotor core back; i.e., the opposite stator poles are either of opposite polarity or the same polarity. The advantage of have the flux going through the rotor is that the rotor core back, or yoke, can be substantially reduced in thickness or removed completely. This is advantageous in terms of reducing rotor inertia and also, if it is an induction machine, rotor iron losses.

In brushless permanent magnet machines fractional slot poles are often used in high pole number machines. There is no reason why these cannot be used in an axial flux machine. Different radial-flux arrangements are compared in [50]. The forces within the machine are assessed and

this sort of work would need to be considered when transferring this type of arrangement to the axial-flux topology.

In [51], the double sided stator is considered. This can be wound in different ways. This paper considers (a) a Toroidal winding; (b) a dual-side concentrated winding; and (c) a dual-side, single-layer lap winding.

The authors of [52] assessed different flux paths in a PM dual-rotor internal-stator machine and introduced a design using magnetic circuits to analyse the different flux paths in the motor. They were particularly interested in leakage flux. They tested a 6 KVA 2 pole-pair prototype for use as a portable generator. Compared to the conventional 8 kVA wound rotor generator, this motor is more compact but it is more expensive (30 % more in 2003) due to the presence of permanent magnets.

Evens Electric in Sydney, Australia, has been developing an axial Flux dual-stator 90 kW induction machine with a maximum torque of 300 Nm. In terms of performance, this new motor should compare to the induction machine used in the Tesla Roadster that also has an induction machine. Due to its short axial length, it is reduced to a third of its usual size. The design could be used for other applications, such as electric buses.

The single-sided rotor axial flux induction motor is a configuration has a single stator and a single rotor and the stator core can be slotted or slot less. The flux has to flow in the circumferential direction on both stator and rotor so that the flux enters and leaves the same sides of both the stator and rotor. This will necessitate the use of steel yokes behind the windings and cage. There is substantial axial force between the rotor and stator when excited.

The double-sided axial-flux induction machine has either the double stator with a single rotor or single stator with double rotor. These can be described:

- **Double stator with a single rotor**

In this type of arrangement, the rotor is between the two stators. One issue in this kind of configuration is that the core of the rotor can be removed if the machine is a permanent magnet type to obtain a coreless rotor structure. In an induction machine with a cage rotor, the rotor can be made from a solid steel disc with radial slots for the rotor bars. This is because the slip frequency should be low giving low eddy currents in the steel.

Since the rotor is between the two stators there should be an equal distance between the two stators, this will result in no axial force rotor because the axial forces on each side of the place will be in the equilibrium. However, this is an unstable point. This arrangement is shown in Fig. 2.6 (b). When the flux allowed traveling through the rotor, as shown on the right, the axial length is less since the rotor is thinner. If the flux path reverses in the rotor, as shown on the left, then the flux paths on each side are independent and if there is a change in airgap on one side with respect to the other, then there may be unequal axial forces on the rotor faces leading to an axial force.

- **Single stator with double rotor**

This has an interior stator between the two rotors. This configuration is based on the direction of the flux in the stator core. This is illustrated in Fig. 2.7. Two topologies can be derived from this configuration, the North-North (NN) topology and the North-South (NS) topology. In the NN topology, the direction of the magnetic flux is returned the stator yoke so that a stator core is needed. The stator is laminated with tape wound iron core. The winding can be wound in a toroidal fashion if this arrangement is used. For the NS topology, the magnetic flux passes through the stator and then closed through the rotor yokes. The magnetic flux path through the stator yoke is short, so that the yoke can be eliminated, leading to a lighter stator core consisting only the teeth and windings. It is possible to remove the core completely with the windings being airgap windings. The NS topology is not possible with toroidal

windings since there is no effective flux linkage between the stator windings and rotors [51]. One possibility when using two rotors is to mechanically decouple the rotors so that it could be used for the differential between the two drive wheels. If a brushless PM machine is used then this requires the flux on each side to be independent so that the arrangement in Fig. 2.7 (a) is needed. However, this is quite advanced, and more torque needs to be transmitted to the faster rotor. In an induction machine, while the rotors are not synchronous so that the arrangement in Fig. 2.7 (b) may be possible with decoupled rotors. However, it will give more torque to the slower rotor, so at this point this seems impractical. Hence, it is assumed that one inverter will be used to produce the drive to the motor and the rotors fixed together.
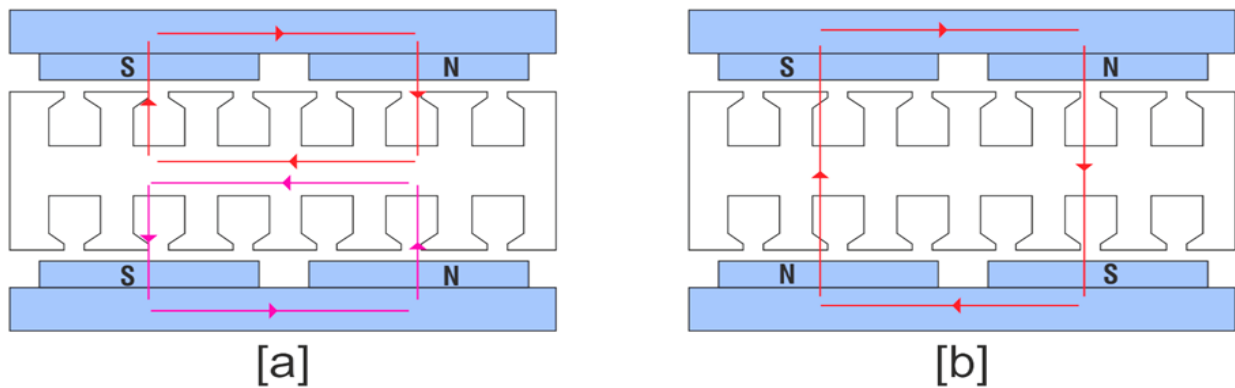
Figure 2.7 Flux directions of (a) Flux NN type axial flux machine (b) NS type axial flux.

2.13   Comparison between Axial and Radial FluxMachines

With the application of new materials, more novelty in construction, and improved cooling techniques, there has been increased power density (mass or volume) in motors. There are characteristic limits for conventional radial magnet motors due to the following:

- The heat in the stator winding has to move to the teeth and then to the stator yoke and casing.

Losses in the rotor and very high current density in the stator windings may require the use of forced cooling. If the rotor has PMs then the cooling will be down the stator slots. If it is an induction motor then rotor cooling is still an issue. These limitations are fundamental to the radial flux structure.

- A new axial flux induction machine topology can give better cooling with airgap cooling where the rotor conductors are close to the coolant. This can give higher power density than the radial flux induction machine. Other advantages are [23]:

    1. Long axial length is not required for production of high torque.

    2. Axial machines have an air gap that can be adjusted.

    3. Cooling is improved.

    4. Efficient utilization of rotor core.

Axial type machines are are typically pump machines, servo drives, traction drives, and other applications for specific purpose where their properties offer distinct advantages over radial motors. In vehicular applications it is important for use a machine with low inertia because if a gearbox is used this inertia is amplified through the drive train and the vehicle will feel like an internal combustion engine car that is running in gear that is too low with an over-revving engine. An axial flux machine can have low inertia.

There are disadvantages to an axial flux machine; the normal magnetic force on the rotor is an axial force. A radial flux machine has magnetic forces that are radial and they are diametrically cancelling forces in a balanced machine with a centered rotor. Equivalent cancelling axial forces can only be found in double-sided machines, not single sided machines, which may require high rated thrust bearings. These axial forces are always present in permanent magnet machines because the magnets cannot be switched off [44].

In [53], a new topology of axial and radial flux induction machine was proposed in which the rotor has an axial and a radial-cage winding and the motor has a single stator with a double rotor topology. This topology will reduce the airgap length to give high efficiency and low power factor as stated above. High torque is obtained with a large airgap length; however, this leads to a large magnetising current, which affects the efficiency and power factor, especially at low power. This is an important design criterion, which needs critical investigation.

2.14   Axial Flux Induction Machine Drive Systems

The power supply and controller for AFIM drives are similar to those used in conventional propulsion systems with radial flux machines. AFIMs can be used for electric vehicles with a traditional geared mechanical transmission, with reduction gearbox with possible more than one gear, or without a gearbox driving the wheels are directly with motors integrated inside wheels or close to the wheel. Obviously this requires the drive wheels to have individual motors. This does reduce the need for a gearbox and differential.

To reduce the volume of the motor, a reduction gearbox must be used. Motors are torque limited and a gearbox works as a "mechanical gearbox" - the power must be maintained through the gearbox if losses are negligible to that the torque $\times$ speed must be constant, hence as the speed is reduced the torque increases.

In a multi-motor drive system, several power amplifier inverters are required in a multi-motor drive system, so that they are very rare. This is because the motors are acting as an electronic differential so the motors will be at different speeds requiring operation at different frequencies with different controls. The torque has to be carefully controlled to ensure that excessive over-

steer and under-steer does not occur.

In a single-motor system with double rotors, the rotors will probably be mechanically linked so that the two rotors are synchronous so that one 3-phase inverter is required.

2.14.1   Speed Control of AFIM

The induction machine can be fixed speed when connected to the grid or an adjustable speed drive (VSD), which includes high performance servo drives. The latter requires a variable frequency inverter supply. There are a variety of controls but essentially these are torque control or speed control with most being the latter.

When a variable speed drive operates in speed control, the load is driven at the reference speed and the torque is determined by load. When operating in torque control mode technique, the load is driven by the reference torque, meanwhile the speed changes to the level where the load torque equals to the delivered motor torque.

Direct torque control (DTC) is one of the advanced motor control technique that permits direct control the motor variables, such as stator flux and torque. Consequently, it can control the torque and speed of the motor. This often does not need speed feedback until close to zero speed. However, speed feedback is often used for precision.

In controlling frequency and voltage of the motor, one of the advantage of DTC technique is the absence of a separate modulator compared to a pulse width modulator (PWM) drive which considerably increases the response time of the drives to the variations in required torque [54]. Open loop speed control precision for DTC is similar to closed loop flux vector control but has

closer control of the torque. Speed control using DTC is well established with a response time less than 5 ms.

While a simple scalar control method is possible as the motor control technique, where the frequency and voltage are the main control variables, this is not effective in controlling the motor effectively and efficiently.

The induction motor is controlled by the inverter in the form of PWM pulse train commanding both the voltage and frequency. The flux in the motor remains the same over the maximum torque range as shown in Fig.2.3 when the ratio of voltage and frequency is kept approximately constant [55]. Above this point the motor goes into the field weakening range where the voltage will be almost constant with increasing frequency and the flux reduces linearly with frequency.

Magnetization identification of the motor is done during the start-up period of the motor. In order to create an accurate motor model for the drive, the start command is given and the motor is magnetized at zero speed for period. When the operating speed is changed when the accelerator is pressed, the motor is identified then the speed change will take place. The acceleration and deceleration time and the ramp shape determines the rate of the motor acceleration and deceleration. The speed controller is automatically adjusted in the course of the motor identification in order to maximize the efficiency of the motor. The advantages and disadvantages of different motor speed control techniques is shown in Table 2.1.

Table 2.1 Summary of the advantages and disadvantages of motor speed control methods

Method	Advantages	Disadvantages
Frequency Control	Very cheap	No control of torque and flux
	No feedback required	Delays in modulation
Field Oriented Vector Control	Good torque response	Costly, delays in modulator
	Exact speed control	feedback is compulsory
Direct Torque Control	Quick torque response	Increase current distortion
	Quite simple	and torque ripple
	No position OR	Unstable switching, it change
	Speed encoder required	as the motor speed changes

2.15   The Concept of Electric Vehicle Technology

EVs are not new. The first electric vehicles appear around 1830 when Joseph Henry invented the first DC motor. Thomas Davenport was regarded as the builder of the first electric vehicle in 1834. In 1847 Moses Farmer built a two-passenger EV, and in 1851 Charles Page developed an EV that reached a speed of 32 km/h. Gaston Plante, in 1859, took a major step in EV technology by building the "rechargeable" battery. In 1899 Camille Jenatzy developed the car "Jamais Contente" (Fig. 2.8) which reached 106 km/h. It was equipped with two 12 V electric motors of 12 V. This was a record speed. In 1900, an EV developed by BGS (a French company) travelled 290 km in a single charge. At the beginning of the 20th century, the EV began to suffer competition from

combustion engine vehicles. At a technological level, the EV was always ahead of the internal combustion engine vehicle but presented the problem of loading and the price of the batteries. With the improvement of the roads, in cities and between cities, internal combustion engine vehicles began to dominate the vehicle market due to charging and range issues of EVs [2].

Figure 2.8 Electric car "Never Satisfied" [2]

The invention of electric ignition for internal combustion engines by Charles Kettering in 1912 (eliminating the need to crank the engine), and the discovery of oil in Texas, which led to the reduction of the price of gasoline, were major drivers for internal combustion engine vehicles. In 1908, Henry Ford began mass production of the Ford Model T, which cost between $500 and $1,000, contributing to the popularization of internal combustion engine vehicles. This led to the disappearance of the EV by the 1930s apart from niche vehicles. In the 1970s, the EV was once again the subject of study due to the oil crisis. In 1996 General Motors launched EV1 (Fig. 2.9), the first production EV. However, in 2001 most of these EVs has been taken off the road, and in many cases had been scrapped GM.

In 2003 Tesla Motors was created, which presented the Tesla Roadster model in 2006. This car, shown in Fig. 2.10, is capable of reaching 100 km/h in 3.9 s thanks to a 250 hp induction

Figure 2.9 EV1 from General Motor [3]

motor. It had a top speed of 232 km/h (electronically limited), and has a range of 400 km. In 2007

Figure 2.10 Tesla Roadster [4]

there was another oil crisis. Since then there has been a great deal of interest in the development

of EVs in order to reduce the dependence on oil and to reduce the emission of greenhouse gases.

Several models of EVs are currently under development or in production [56]. Portugal is one of

the first countries to join the extended use of EVs with the government entering an agreement with

Renault-Nissan. The commercialization of the Nissan Leaf EV started in 2010.

2.15.1 Advantages and Disadvantages of Electric Vehicles

The main advantages and disadvantages of EVs are highlighted here:

1. **Advantages**

   - Efficient at most speeds;

   - It emits less noise than an internal combustion vehicle;

   - Reduced energy consumption compared to the internal combustion vehicle since electric motors are more efficient than internal combustion engines;

   - High torque at low speeds;

   - In most configurations the clutch and multiple gears are not required;

   - They do not emit pollutants;

   - Do not produce waste oil;

   - Less engine maintenance; and

   - Allows regenerative braking.

2. **Disadvantages**

   - Limited range and slow recharge;

   - Batteries are expensive, contributing to the high EV prices; and

   - There may be problems caused by the absence of noise and pedestrians not hearing their presence. This is being addressed using artificial noise being generated to simulate the typical noise of an internal combustion vehicle.

2.15.2   Electric Vehicle Configurations

There are various configurations of EVs, depending on the type of motor, energy storage system technology and the location of both in the vehicle. Focusing only on the location of the motor in the vehicle, some possible alternatives for EVs are given below. [57].

- The simplest configuration that can be used is shown in Fig. 2.11 (a), where the internal combustion engine is simply replaced by the electric motor (M), containing the clutch (E), the gearbox (GB) and the differential (D).

- Another possible configuration is to remove the internal combustion engine and the clutch, taking advantage of only the gearbox and the differential as shown in Fig. 2.11 (b).

- In the configuration in Fig. 2.11 (c), only the differential is coupled to the electric motor in order to eliminate some mechanical losses, which is the configuration used by Tesla Roadster (Fig. 2.10).

- In Fig. 2.11 (d), the electric motors are coupled to gearboxes (CR), which are connected to the axles of each rear wheel.

- In Fig. 2.11 (e), the electric motors are directly coupled to the axles of each rear wheel.

- The configuration used in Fig. 2.11 (f) is used by Mitsubishi in the Colt EV, being an optimum configuration for the construction of new EVs. The motors are incorporated into the wheels, and described as in-wheel motors as shown in Fig. 2.12.

The arrangement in Fig. 2.12 is used for rear-wheel drive vehicles. The advantages of rear-wheel drive in EVs are the same as in internal combustion engine vehicles: uniform tire wear and better weight distribution. However, rear-wheel-drive vehicles have disadvantages: straight-
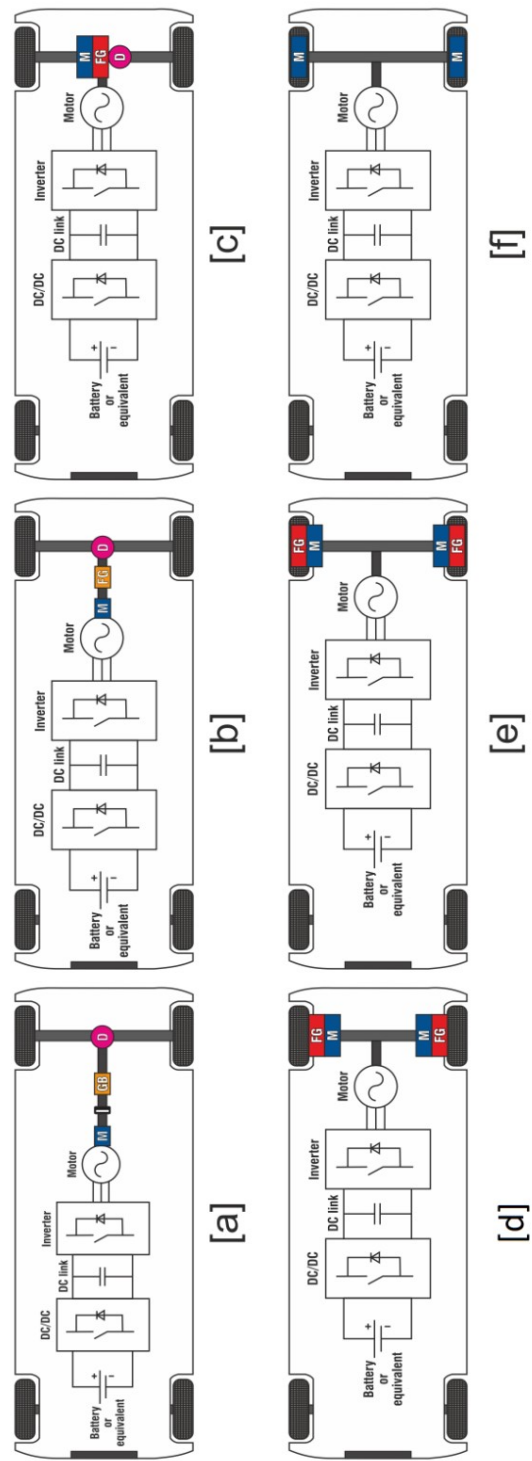
Figure 2.11 Types of configurations for electric vehicles with rear wheel drive [5]

line acceleration presents an unstable equilibrium, more mechanical losses, less space inside the vehicle, handling issues in slippery conditions.

Front-wheel drive EVs, have identical to configurations compared to rear-wheel-drive vehicles; the rear-wheel drive system is now applied to the front wheels. Front-wheel drive vehicles have the following advantages: lower mechanical losses and straight-line acceleration with a more stable balance. They will also be more effective in regenerative braking since most breaking is on the front wheels. However, they give greater wear on the front tires.
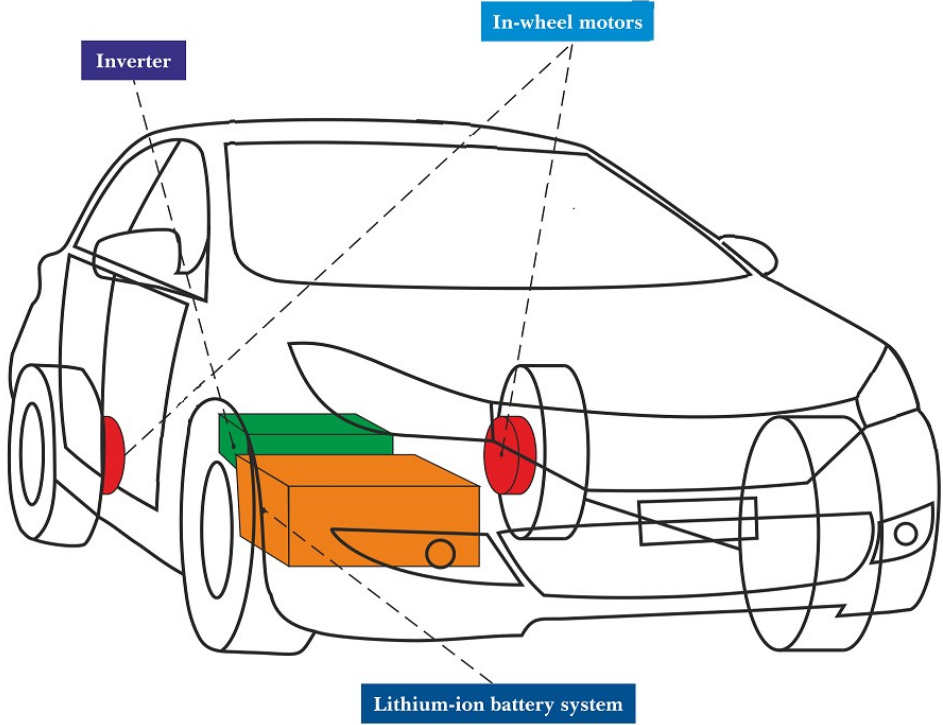
Figure 2.12 Types of in-wheel motor

2.15.3   Hybrid Vehicles

Like electric vehicles, hybrid vehicles are not new. The first hybrid vehicle model dates back to 1899. It was built by the German Ferdinand Porsche, and was named Mixte. This vehicle used an internal combustion engine, with constant speed, coupled to a dynamo that carried a bank of batteries. The electric motors were inserted in the hubs of the front wheels. This was the first vehicle to have front-wheel drive, the use of motors connected to the wheels with transmission shafts allowed gearing. The efficiency was estimated at 83 %.

In 1900, the Belgian company Pieper introduced a hybrid car. This car had a 3.5 hp internal combustion engine being coupled to an electric motor/generator through to the road wheels. When the car cruised, the motor/generator acted as a generator, recharging the batteries. When the car needed more torque, the electric motor/generator acted as a motor and helped the internal combustion engine.

As with EVs, hybrid vehicles had a relapse from the 1920s. In 1966, during a congress in the United States, the use of electric and hybrid vehicles was recommended for the first time in order to reduce air pollution.

Between 1968 and 1971, three scientists from the company TRW, Baruch Berman, George H. Gelb and Neal A. Richardson, developed, demonstrated, and patented a traction system to be used in hybrid vehicles. This was called electromechanical transmission. Many of the mechanical concepts developed by these scientists are still used in modern hybrid vehicles.

In 1969, General Motors introduced the GM512, a Hybrid Vehicle with very low weight, which allowed a top speed of 64 km/h. It had three modes of operation: up to 16 km/h it operated only with the electric motor; between 16 km/h and 21 km/h it combined the two sources of propulsion:

the electric motor and the two-cylinder internal combustion engine; and above 21 km/h it operated only with the internal combustion engine.

The oil crisis of 1973, as with EVs, led to an increase in interest in hybrid vehicles. The US Department of Energy conducted several tests on electric and hybrid vehicles from various automotive manufacturers including the Volkswagen taxi.

In 1993, the US government of President Bill Clinton announced a partnership with the North American manufacturers for the development of a new generation of hybrid and electric vehicles. In Japan, Toyota launched the first generation Prius in 1997 and they sold almost 18,000 in the first year. In the same year Audi became the first European manufacturer to have a mass-produced hybrid vehicle, based on the Audi A4. The Audi Duo III was a sales failure, having sold only 60 units. This led European car manufacturers to focus on the research and development of the refinement of diesel internal combustion engines.

There are currently several models of hybrid vehicles in development and production. As an example, Toyota is currently in the third generation of the Prius and Honda in the second generation of the Insight. Hybrid vehicles were initially classified into two types: series and parallel. Currently, with the introduction of some new types of hybrid vehicles, this classification has become of three types: series, parallel and series-parallel.

2.15.4 Advantages and Disadvantages of Hybrid Vehicles

The advantages and disadvantages of hybrid vehicles are discussed in this section

1. **Advantages**

- Economy of 30 % to 50 % in fuel consumption compared to a conventional internal combustion vehicle;

- Reduction in the emission of polluting gases to the atmosphere;

- Flexibility to use petroleum;

- High torque at low speeds;

- In some configurations the clutch and the gearbox are not required;

- Reduction of audible noise;

- Allow regenerative braking;

- Greater range than an EV or even a conventional combustion vehicle; and

- It is not necessary to charge the batteries through an outlet.

2. **Disadvantages**

- Expensive batteries; and

- Some of the available hybrid vehicles still have a very high purchase price.

2.16   Design of the Motor Control in an Electric Vehicle

In EVs, the throttle represents a torque command. Therefore, for any motor closed-loop control there is a need for torque with good dynamic response to give good response to the throttle while limiting the current. The system efficiency can be improved by running at the optimum magnetic flux level. If a precision cruise control is required; an external speed-control loop may be necessary. According to [58], some of the major issues that need to be considered in designing the motor controller for EV propulsion systems are:

- Maximization of the motor output torque;

- Optimization of flux level for performance purposes;

- To avoid possible excitation of resonance in the mechanical transmission smooth control of torque over the full speed range is required;

- Strength contrasted with parameters variation; and

- Smooth limitation of current and voltage when regenerative braking; and stability over the entire speed range.

This aspect must be carefully considered because in most traction applications flux weakening is required (i.e., there is a fixed reduction gear or direct connection so that a wide operating range is required). The DTC block diagram comprises of two loops is shown in Fig. 2.13. There is the speed control loop and the torque control loop. The speed control loop is used to generate the reference for the torque and flux. The output of the speed control loop is limited by the torque limits and the DC bus voltage. The speed control loop consists of a Proportional Integral (PI) and acceleration compensator which are used to control the reference torque. The torque control loop is used to estimates the flux and torque. It is used to compare the reference values of torque and flux to the measured values. This loop also comprises of switching table which generates pulses for the inverter.
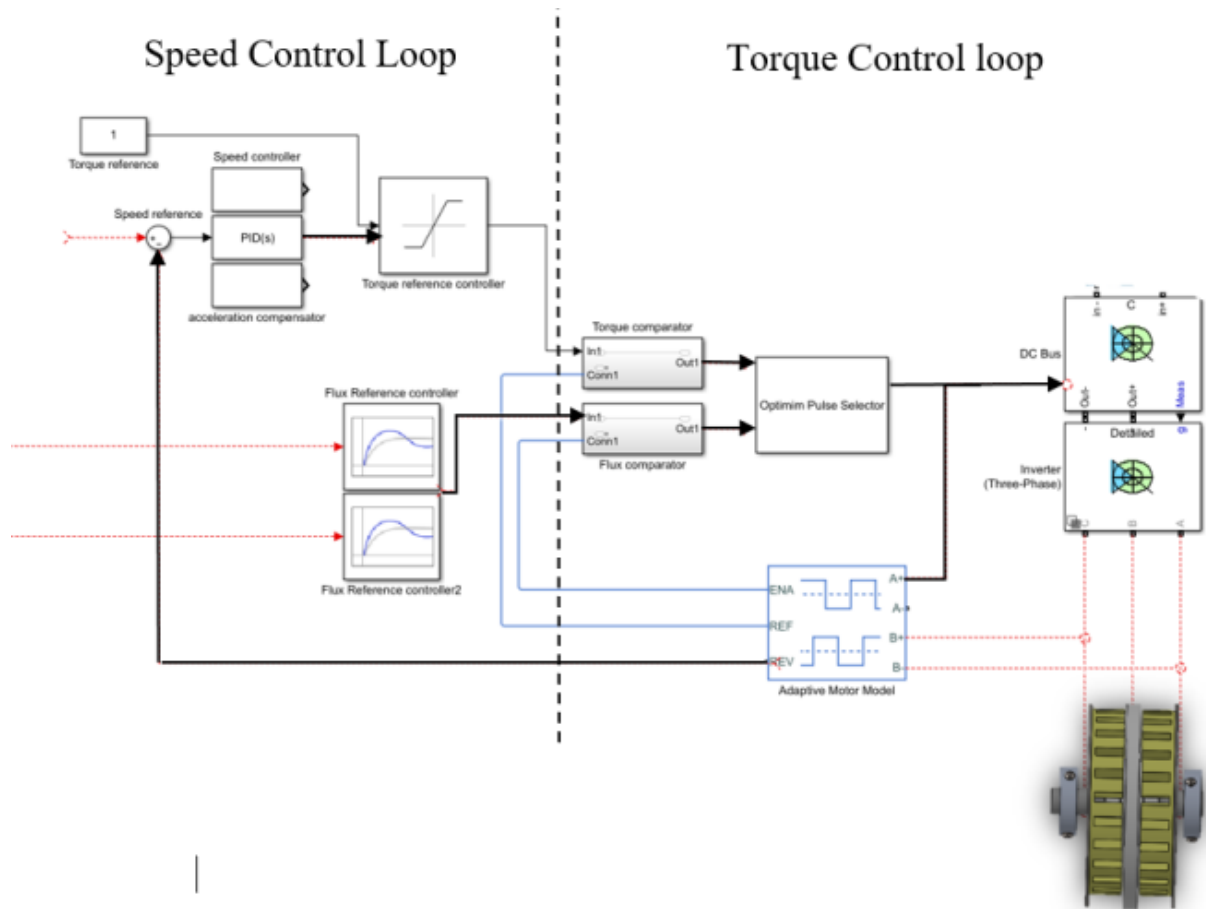
Figure 2.13 Overall control scheme of DTC

2.17   Aspects Consideration on the Design of AFIM Drives

In the design of an axial flux induction machine, the high ratio of diameter to length as well as having a larger inner diameter than the shaft diameter can provide good ventilation and cooling. In order to further reduce the axial flux machine size, it is crucial to use high electrical and magnetic loading. The short axial length of the axial flux induction machine gives it an advantage in automotive applications when compared to other electrical machines.

There are several aspects to consider in the fast design of the axial flux induction machine and they may be classified by their conductor geometry and field orientation. Note that the outer and inner diameters of the stator are most significant parameters in the design of an axial flux induction machine because these parameters have a fundamental effect on the motor characteristics, such as efficiency, output torque, copper losses, and iron losses. There are other design parameters to consider such as, size of the conductor, material types and number of turns. Below are some of the critical aspects to consider for effective design and reliable performance of an AFIM drive:

- Stator and rotor configuration;

- Stator winding arrangement;

- Rotor structure;

- Magnetic core design;

- Motor supply;

- Stator slot arrangement;

- Motor materials;

- Phase number; and

- airgap length.

2.18   Conclusion

In this part of the work a review of axial-flux induction machines is offered within the context of automotive drive systems. Different types of axial flux machine (synchronous and induction machines) and their geometries are discussed.

The AFIM machine has been chosen as the motor for EV motor drives as an alternative drive to the brushless PM machine. The AFIM design is a possible favourable solution either in a single motor arrangement or multiple motor arrangement that can behave as an electromagnetic differential supplied by duel inverters in a two wheel drive arrangement.

A brief contrast between the axial flux machine and radial flux machine was presented. This allows the comparison of these machines in terms of operating principles, characteristics, and motor considerations. This chapter also presented the concepts of electric vehicle technology.

Chapter 3

Design and Simulation of AFIM

3.1 Simulation Approach

The aims and objectives of the work is to develop a suitable analytical design procedure for designing an axial-flux induction machine and to evaluate the performance of the designed machine under various conditions. Therefore, in this chapter, the design and simulation procedure of the machine is described and the simulation results are discussed.

The machine is selected for high-torque performance for use in EVs. Analytical analysis is carried out using a 2D representation of machine to obtain approximations for the rated operational parameters. For more accuracy the modelling of the AFIM is carried out with 3D time-stepping FEA. The models of AFIM are constructed and simulated in the RMxprt-Maxwell a template-based design tool of Anys software.

It has to be stated here that while the 3D FEA gives more more accurate results it is more time

consuming to carry out. This is because the induction motor is voltage fed since the rotor currents have to be calculated in the solution. Therefore it has to be a time stepped (or transient) solution. This is very time consuming, even if only one pole is modelled due to the symmetry. This is unlike the brushless PM machine which is current fed so can be solved with static solutions which run much faster. Hence the use of the analytical 2D solutions.

3.2   Brief Description of Ansys-Maxwell Software

Ansys-Maxwell is a computer-aided engineering software. It is a high-performance, low frequency electromagnetic field simulation interactive software package that uses FEA to solve electromagnetic problems by solving Maxwell's equations in a finite region of space with appropriate boundary and user-specified initial conditions for 2D/3D electromagnetic and electromechanical devices, as well as motors, actuators, transformers, sensors and coils. Maxwell uses the finite element technique to solve static, frequency-domain, and time varying electromagnetic and electric fields. In order to mesh the domain and linear interpolation functions to approximate the solution, Maxwell software uses triangular/tetrahedral element [59] .

3.3   Finite Element Analysis

For effective design and analysis of an AFIM, accurate parameters such as voltage, current, magnetic flux density and speed parameters are needed, either are inputs or outputs. Finite difference methods and finite element analysis methods are two techniques that can be used for determining magneto-dynamic analysis of a machine. However, due to the lack of accuracy, especially

with non-linear magnetic cores, the finite difference method is not suitable for use for magneto-dynamic analysis. The FEA method is more suitable due to its flexibility and accuracy in solving electromagnetic problems.

The FEA method is employed before prototyping and manufacturing of an electrical machine. Using the attributes of the materials and the physical dimensions of the motor, FEA can calculate flux distributions and generated torque in the no load or the load conditions [60]. To use FEA, the following principles are required;

- The system must be composed of an enclosed area or volume - system components can be omitted only if there is symmetry via a periodicity or imaging;

- The physical properties of all materials used in the system must be defined; and

- Functions must be defined at each point in the system. A flowchart for the FEA analysis is shown in Fig. 3.1.

In order to explore and to evaluate the design procedure shown in Fig. 3.1, the certain topological decisions must be made. It was decided that the proposed AFIM structure will consist of dual stators and a single rotor, with constraints in terms of voltage, pole number, speed, and materials. The first step is the geometry choice of the prototype machine .The next step is the mesh generation for the proposed machine which in modern FEA packages is automatic within the choice of element size. For Maxwell, the input of a design is simplified by the use of RMxprt which allows some analytical simulation and input of motor geometry, windings and materials through a front-end spreadsheet template entry process.

Details of the design procedure is described in the next section.

Figure 3.1 FEA Procedure Flow Chart

3.4 AFIM Theory, Analytical Design, RMxprt and *SPEED*

3.4.1 AFIM Design - Magnetic Principles

3.4.1.1 Stator design

At this point design choices need to be made. In this instance the AFIM was chosen to have 3 phases and 8 poles. This is because the current technology uses this pole number in many vehicular applications. For instance, the Toyota Prius hybrid EV uses an 8 pole brushless PM machine which runs at 6000 rpm in the Generation II vehicle and 14000 rpm in the Generation III vehicle. Obviously this is not necessarily the correct pole number for an induction motor but it will allow higher frequency operation which gives better efficiency in an induction machine. This was looked at in [61] who used a 6 pole machine though the difference with an 8 pole machine is not great [23]. Therefore the minimal number of stator slots is $3 \times 8 = 24$ slots for an integral number of slots per pole. For a compact design which is rugged, a low slot number is advantageous. Also, it decreases production machine cost. This work includes the building of a proof-of-concept machine and the stators utilize a 24 slot stator design from a permanent magnet machine that was made available for study. These are laminated strip-wound stacks where the external and internal diameters together with length and slot number are user defined inputs when designing a new stator and change with the type of motor modelled. However, for prototyping purposes in this design then the analysis is applied to the proof-of-concept design with the available stator cores, then further analysis is carried out to obtain better operation via rotor design improvement and tighter winding that would occur with a mass manufactured rather than one-off prototyped design.

The stacking factor is to computed as part the total stator steel area. This is usually set to 0.9

to 0.95 depending on the tightness and compression of the laminations. The software can use a defined type of steel. The steel parameters are known along with coefficients of core loss K_e, K_c, K_h. RMxprt provides six different types of slot that may be chosen. The best fit for the prototype stators was used The average diameter D_{av} and length of active conductor, similar to stack length of rotating motor *Ldisc* can be expressed:

$$D_{av} = \frac{D_o + D_i}{2} \tag{3.1}$$

$$L_{disc} = \frac{D_o - D_i}{2} \tag{3.2}$$

where D_o and D_i are the stator outer and inner diameters respectively. These will be used for the radial-flux equivalent of the machine in the *SPEED* simulations.

3.4.1.2 Stator winding

The winding configuration is important because this has a serious impact on the speed range, torque density, weight and airgap. For inductions it is important to have a winding close to sinusoidal distribution to minimize the winding harmonics that can generate asynchronous harmonics. Nevertheless, in the case where the motor is constructed with the distributed type of windings there is an increase in motor weight and motor copper losses. There are four basic groups of winding arrangements [62], [63]:

1. The double layer configuration is where there are two coils sides per slot. This winding is usually arranged in a lap winding arrangement and allowed short pitching. This is used in larger induction machines.

2. The single layer is where there is a single coil side per slot. This required a concentric winding that is effectively fully pitched. This is used in smaller induction machine.

3. The fractional slot arrangement is when the slot per pole per phase is not an integer. This is not suitable for induction machines - it tends to be used in high pole number brushless permanent magnet machine.

4. The configuration in which the coils of a phase coil wrapped round one slot with no phase overlap, it is called the concentrated winding. However, this is not suitable for an induction motor - it tends to be used for switched reluctance machines.

In this work it was decided to use a double layer lap winding with short pitching. With 8 poles and one slot short pitching, the winding is shown in Fig. 3.2 from the *SPEED* simulation and in Fig. 3.3 for Ansys using the RMxpert package. The lay out of the winding can be reduced the airgap harmonics. This winding can be entered using a spreadsheet entry system.
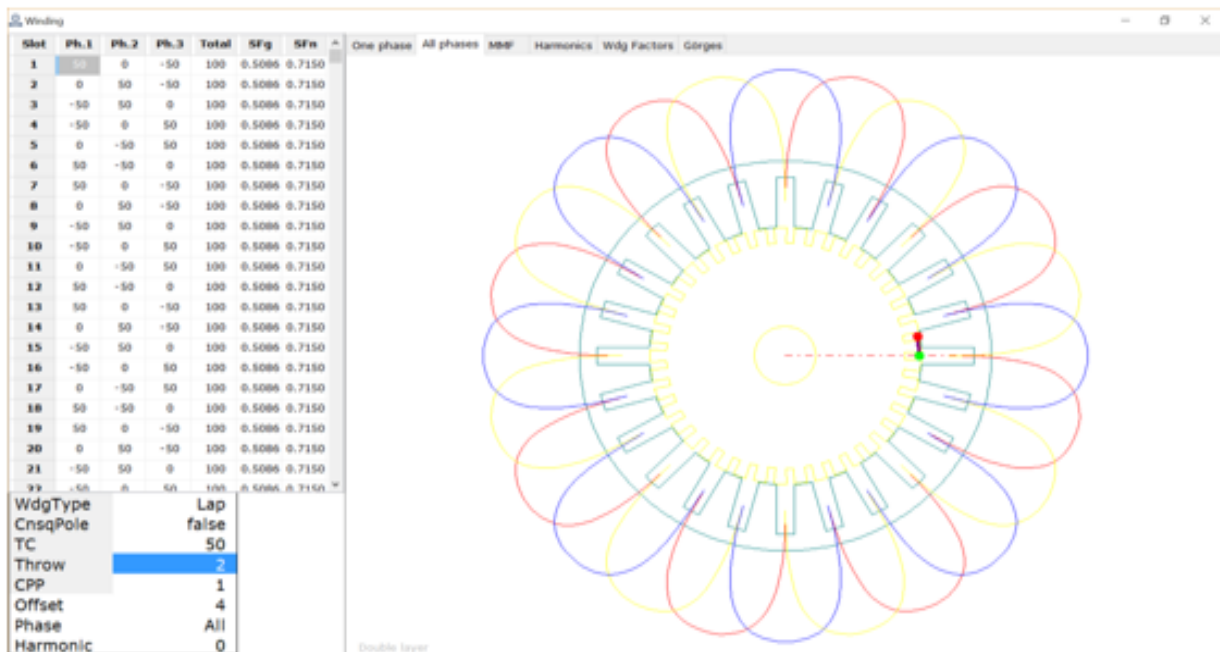
Figure 3.2 Winding configuration from Winding Template in *SPEED* software

The winding factor K_w is determined from the distribution factor K_d and the pitch factor K_p
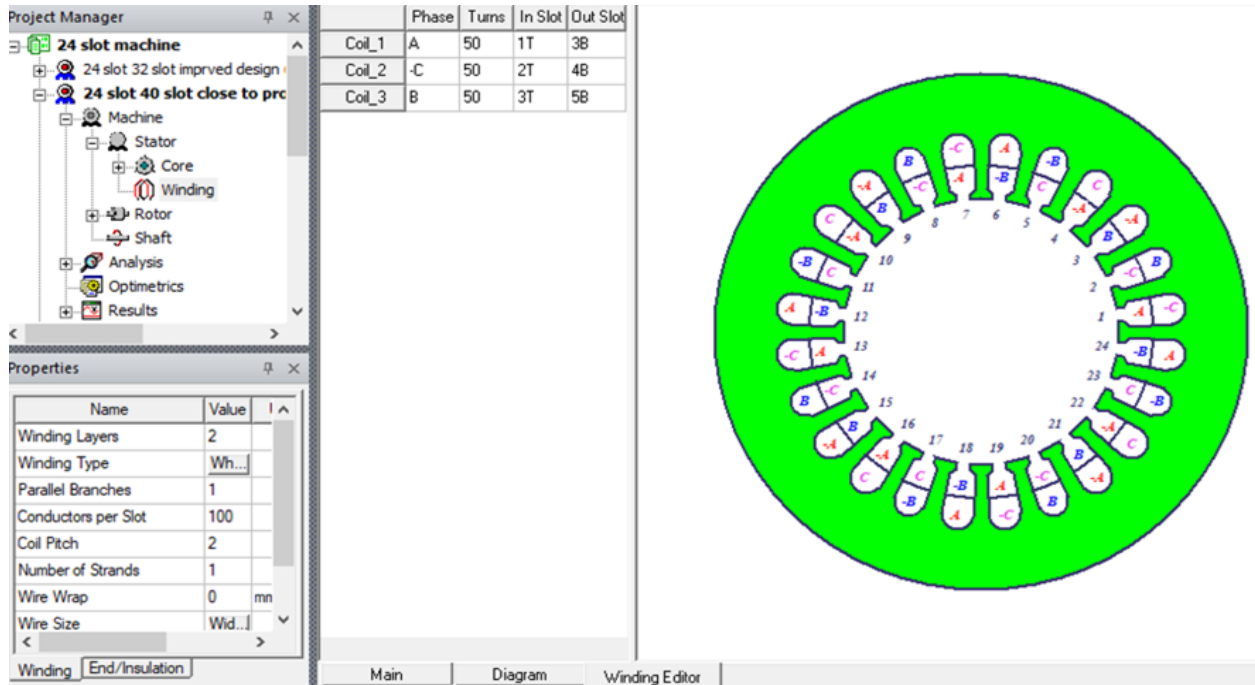
Figure 3.3 Winding Configuration from Ansys RMxpert software

and is given as [64]:

$$K_w = K_p K_d \tag{3.3}$$

For the fundamental flux wave, the pitch factor K_p can be calculated from [64]:

$$K_p = \frac{B \text{ produced by short-pitch coil}}{B \text{ produced by full-pitch coil}} \tag{3.4}$$

$$K_p = \sin \frac{\alpha}{2} \tag{3.5}$$

where α is the pitch or span of the coils. For this winding the pitch is $2/3$ to reduce the end winding size and stator winding resistance. This is often done in synchronous machines to eliminate third harmonics. Therefore here $K_p = 0.886$. This may seem like a large reduction but the compactness in end-winding, particularly in the inner surface of the stator, appears an option worth taking.

For the distribution factor K_d [64]:

$$K_d = \frac{\sin\left[\frac{m\gamma}{2}\right]}{m\left[\frac{\gamma}{2}\right]} \qquad (3.6)$$

where m is the number of coils per phase belt and γ is the angular distribution between the coils. In this case with 24 slots and 8 poles there there is one coil per pole per phase so that $m = 1$. in this case $K_d = 1$.

Hence $K_w = 0.886$ for the winding arrangement chosen.

3.4.1.3 Winding EMF

From Lenz's Law the flux and winding voltage can be related to each other. From

$$e_{ph} = -\frac{\mathrm{d}\lambda}{\mathrm{d}t} = -\frac{\mathrm{d}N_{ph}\phi}{\mathrm{d}t} \qquad (3.7)$$

The EMF should be an RMS value while the flux is usually dealt with in terms of a peak:

$$\sqrt{2}e_{ph(RMS)} = -N_{ph}\frac{\mathrm{d}\phi}{\mathrm{d}t} \qquad (3.8)$$

It can also be assumed that the variables are sinusoidal so that

$$e_{ph(RMS)} = E_{ph}\sin(2\pi f) \qquad (3.9)$$

$$\phi = \Phi_{ph}\cos(2\pi ft) \qquad (3.10)$$

$$-\frac{\mathrm{d}\phi}{\mathrm{d}t} = 2\pi f\Phi_{ph}\sin(2\pi ft) \qquad (3.11)$$

Considering one phase then from the above equations

$$N_{ph} = \frac{E_{ph}}{4.44 f\Phi_{ph}K_w} \qquad (3.12)$$

64

where, E_{ph} is the RMS voltage induced in stator phase and f is the supply frequency of the motor. The total flux Φ_{gap} from the flux per phase Φ_{ph}. There are three phases offset by 120 electrical degrees then when a phase current is at peak, then the other two are at negative half peak magnitude. In addition there is a spatial offset and again when there is full alignment with a phase there is negative half alignment with the other two phases so that:

$$\Phi_{gap} = \left(1 + (-0.5 \times -0.5) + (-0.5 \times -0.5)\right) \Phi_{ph} = \frac{3}{2}\Phi_{ph} \tag{3.13}$$

$$\Phi_{gap} = \frac{3E_{ph}}{8.88 f N_{ph}} \approx \frac{E_{ph}}{3 f N_{ph} K_w} \tag{3.14}$$

This represents the flux per pole and it is useful to relate this to the peak flux density in order to rate the voltage. In a radial flux machine the flux density down the axial length of the machine would be constant. Assuming that the flux varies sinusoidally then

$$\Phi_{gap} = L \int_{-\tau/2}^{\tau/2} b(x)\, dx \tag{3.15}$$

where, τ is the pole pitch. But

$$b_x = \hat{B}\cos\left(\theta_{elec}\right) = \hat{B}\cos\left(\frac{\pi}{\tau}x\right) \tag{3.16}$$

and

$$\tau = \frac{\pi D}{P} \tag{3.17}$$

where D is the stator diameter and P is the pole number. Therefore from these equations

$$\Phi_{gap} = L \int_{-\tau/2}^{\tau/2} \hat{B}\cos\left(\frac{\pi}{\tau}x\right) dx = \frac{2\tau L}{\pi}\hat{B} \tag{3.18}$$

Putting this into (3.14) gives

$$\hat{B} = \frac{\pi}{2\tau L} \times \frac{E_{ph}}{3 f N_{ph} K_w} \tag{3.19}$$

and adding (3.17) gives

$$\hat{B} = \frac{P}{\pi D} \times \frac{\pi}{2L} \times \frac{E_{ph}}{3 f N_{ph} K_w} = \frac{P}{LD} \times \frac{E_{ph}}{6 f N_{ph} K_w} \tag{3.20}$$

65

This equation is for a radial flux machine if the flux density is fixed, due to steel saturation levels, then it can be observed that the voltage will increase with the axial length and diameter. It also increases with frequency and phase voltage which is to be expected. It does, however, decrease with pole number.

This has to be applied to an axial flux machine. The question here is how the airgap flux varies in the radial direction. using Ampere's circuital law

$$\oint_L B.\mathrm{d}l = \mu_0 NI \tag{3.21}$$

On any radial line in the airgap the *NI* will be constant when neglecting the slotting so that the assumption is made that the airgap flux density is constant in the radial direction. Therefore, from (3.20), for the axial flux machine airgap can be expressed as

$$\hat{B} = \frac{P}{L_{disc}D_{av}} \times \frac{E_{ph}}{3fN_{ph}K_w} \tag{3.22}$$

Putting (3.1) and (3.2) in then

$$\hat{B} = \frac{4P}{\left(D_o^2 - D_i^2\right)} \times \frac{E_{ph}}{3fN_{ph}K_w} \tag{3.23}$$

An alternative way for addressing this is that in (3.20) the term πLD represents the surface area of the airgap when treated as a cylinder so that if surface areas are equated

$$\pi LD = \frac{\pi \left(D_o^2 - D_i^2\right)}{4} \tag{3.24}$$

This gives the same solution.

3.4.1.4 Double sided machine

The treatment for the flux density for the axial machine given in (3.23) is for a single sided machine. When the FEA is carried out one pole of one side will be modelled and the Method of Images for a magnetic system used since if the stators are aligned, there is a mirror image around the radial centre plane of the rotor.

In the analytical analysis then it can be seen in (3.23) that including the second stator on the opposite side of the rotor, as a series connection, will double the phase winding turns thus doubling the phase EMF. If the second stator is connected in parallel then the phase winding turns will remain constant.

For a double stator machine there are therefore four available connections -they can be connected in star or delta and can be connected in series or parallel. In this study is as assumed that the stator windings are connected in star to prevent any harmonic circulating current and connected series to prevent unbalanced currents between the two sides.

To calculate an approximate back-EMF (line-to-line) from (3.23) for the prototype machine from a grid-connected 50 Hz supply then assume the peak airgap flux density is 0.5 T. In the prototype machine each coil had 100 turns so that $N_{ph} = 800$. The short pitched winding gives $k_w = 0.866$, and the phase voltage is multiplied by $2\sqrt{3}$ to get the line voltage with both sides connected in series. Hence

$$E_{line} = 2\sqrt{3}E_{ph} = 2\sqrt{3} \times \hat{B} \times \frac{LD}{P} \times 6fN_{ph}K_w = 2\sqrt{3} \times \hat{B} \times \frac{\left(D_o^2 - D_i^2\right)}{4P} \times 6fN_{ph}K_w \quad (3.25)$$

$$E_{line} = 2\sqrt{3} \times 0.5 \times \frac{\left(0.22^2 - 0.133^2\right)}{4 \times 8} \times 6 \times 50 \times 800 \times 0.866 = 345.5 \text{ V} \quad (3.26)$$

This shows that the machine can be tested up to the maximum voltage from a 420 V 3-phase autotransformer supply.

3.4.1.5 Magnetizing MMF and reactance

From (3.21) the required MMF can be calculated for a given

$$\oint_L \hat{B}.dl = 2g\hat{B} = \frac{2}{P} \times \mu_0 \frac{3}{2} K_w N_{ph} \sqrt{2} I_{ph(RMS)} \quad (3.27)$$

where g is the airgap length and $\mu_0 = 4\pi \times 10^{-7}$ H/m. This is the flux crosses the airgap twice. The turns per pole pair is required, hence the division by the number is pole pairs. This relates

the peak flux density to the RMS magnetizing current and assumes a balanced three phase set and the the steel is ideal so that all the MMF is dropped across the airgap. This is suitable for a series connected machine. For the prototype machine with $g = 1$ mm then

$$I_{ph(RMS)} = \frac{4 \times 2 \times (2 \times 0.001 \times 0.5)}{4\pi \times 10^{-7} \times 3\sqrt{2} \times 0.866 \times 800} = 2.17 \text{ A} \tag{3.28}$$

If we take the results from (3.25) then the magnetizing reactance can be calculated where

$$X_m = \frac{E_{line}}{\sqrt{3}I_{ph(RMS)}} = \frac{345.5}{\sqrt{3} \times 2.17} = 91.9 \ \Omega \tag{3.29}$$

This is for the series star connected machine and the magnetizing reactance in a per-phase equivalent circuit. If the the two stator sides were connected in parallel the voltage would halve and the current double reducing X_m by four. This is a relatively low reactance due to the large airgap. This is used due to the nature of the prototype machine and also because a larger airgap can produce higher torque. In a variable speed operation the frequency is not fixed so that the magnetizing inductance should be used where

$$L_m = \frac{X_m}{2\pi \times 50} = \frac{91.9}{100\pi} = 0.293 \text{ H} \tag{3.30}$$

3.4.1.6 Electric loading

The available slot area and the maximum slot fill factor will dictate how much copper conductor can be put in the slot. The slots are 34 mm deep and 12 mm wide so that the slot area is 12 mm $\times$ 34 mm = 408 mm^2. However, this is the gross area A_{gross} and the slot liner needs to be included usually using a slot liner thickness on the slot sides and bottom so that

$$A_{net} = (12 - 0.5) \times (34 \times 2 \times 0.5) = 379.5 \text{ mm}^2 \tag{3.31}$$

Generally, for a well packed slot, the slot fill factor C_S is not more than about 70 % where

$$C_S = \frac{A_{cu}}{A_{net}} \tag{3.32}$$

A_{cu} is the area of conductor in the slot. For 100 coil sides per slot then the maximum cross section of each conductor can be calculated as $379.5 \times 0.7 \div 200 = 1.33$ mm^2. This is a round conductor of 1.30 mm diameter. For a naturally cooled machine with a reasonable cooling system about 5 A/mm^2 is possible which gives a current of 6.64 A. For fluid cooled machine this could rise to 10 A/mm^2 giving 13.28 A. For an automotive drive machine the transient current can rise to possibly 25 A/mm^2, or 33.2 A; however, this for an brushless permanent magnet machine [65].

In automotive applications, to obtain the wide speed range without needing an excessive voltage level it usual to use only a few turns per slot with large conductors, or several bundled parallel conductors. This is illustrated in Fig. 3.4 for a radial flux 4-pole 20,000 rpm machine. This allows the machine at frequency in excess of 650 Hz (as in this case). However, in the machine designed here, for investigation, the frequency at the base speed is 50 Hz so a higher number of turns is used.

Figure 3.4 Stator winding in radial flux automotive drive motor (www.refreedrive.eu)

With the maximum level of continuous electric loading then the power can be estimated to be $\sqrt{3} \times 345 \times 13.28 \div 1000 \times 0.5 = 3.97$ kW with a conservative power factor of 0.5, a frequency of 50 Hz and running close to 750 rpm with 13.28 A. This is a torque of about 50.6 Nm. However, this assumes correct design of the induction machine in terms of electromagnetic and thermal design.

If the transient 25 A/mm^2 current density is used then the power could rise to 9.93 kW. Though this is an extreme value. Usually vehicular drive motors are gears so power can be obtained by running at a much faster speed.

For the prototype machine then much thinner wire was used to allow easy manufacture within the university workshop; 1 mm diameter wire was used giving a total copper cross section of $\pi \times 1^2 \times 200 \div 4 = 157.1 \text{mm}^2$ so that the slot fill factor is

$$C_S = \frac{78}{379.5} = 41.4\% \tag{3.33}$$

The prototype winding is not impregnated with varnish to help with cooling so assume the machine the maximum current 5 A/mm^2. The conductor area s 0.785 mm^2 giving a current of 3.9 A. In the experimental rig. This can go a little higher during short-time testing. However, it is limited by poor thermal design.

3.4.1.7 Rotor design

The rotor here is novel. It is formed from aluminium with steel inserts to form the magnetic circuit rather than steel with cast or fabricated aluminium or copper conductors. This will mean better heat dissipation in the conductors.

An approximate calculation for the rotor design is to assume there is the same amount of conductor in the rotor as in the stator. In this case the rotor is formed from aluminium which has approximately double the resistivity of copper so there is a factor or two in the calculated amount of aluminium aluminium. The amount of copper in the stator with full slots of 1.3 mm wire is $A_{cu-stat} = 2 \times 24 \times 1.33 \times 200 = 12751.2$ mm^2. This accounts for both sides of the stator. As a rough rule of thumb, the amount of aluminium to steel can be split evenly at the radial centre of

the rotor so that the amount of aluminium in the rotor is

$$A_{al} = \frac{1}{2}\pi\frac{(D_o + D_i)}{2} \times L_{rot} \qquad (3.34)$$

where L_{rot} is the axial length of the machine. Rearranging this and assuming $A_{al} = 2 \times A_{cu-stat}$ then

$$L_{rot} = \frac{4A_{al}}{\pi(D_o + D_i)} = \frac{4 \times 2 \times 12751.2}{\pi(220 + 133)} = 91.9 \text{ mm} \qquad (3.35)$$

This is a very approximate calculation but should lead to the machine being stator critical. Another way to do this is consider that the stator, at the average core radius, has a slot pitch (centre slot to centre slot distance) of 23 mm so that the net stator slot width to slot pitch ratio is about 0.5. With a net slot depth of 33 mm, double siding, and resistivity ratio of 2, the rotor length will be $33 \times 0.7 \times 2 \times 2 = 92.4$ mm which is a similar answer.

The rotor can be cooled using radial ducts.

For the prototype machine with 1 mm wire the copper $A_{cu} = 2 \times 24 \times 0.79 \times 200 = 7584.0$ mm^2 so that

$$L_{rot} = \frac{4 \times 2 \times}{\pi(220 + 133)} = 54.4 \text{ mm} \qquad (3.36)$$

This should ensure that the rotor has low resistance - and lower than the stator resistance.

The outside diameter of the rotor should be greater than the outside diameter of the stator core in order to accommodate the outer rotor end-ring. This depends on the number of rotor conductors. For the prototype machine it was 273 mm which was about the same diameter as the stator with windings.

The rotor disc was fabricated from aluminium disc which was 15 mm thick to utilize materials available. The rotor core was formed from mild steel studs. An initial design choice was to put many studs in to ensure a good magnetic circuit and minimize the slotting effects of the stator.

However, this probably meant that the were 50 % more studs than needed so that effective bar to core width was 0.35. It is therefore estimated that the rotor will have a high rotor resistance - probably higher than the stator resistance. This will produce a machine with high starting torque but low efficiency because at rated load the slip will be high. However, this is a proof-of-concept machine.

3.4.2   Prototype Machine Parameters

Table 3.1 shows the parameters for the prototype machine. In the simulations different slot fills and rotor arrangements will be studied.

Table 3.1 Simulation Parameters

Parameters	Dimension	Unit
Stator outer diameter	220	mm
Stator inner diameter	133	mm
Rotor outor Diameter	273	mm
Rotor disc width	15	mm
Height of the stator	45	mm
Width of stator slots	12	mm
Height of stator slots	34	mm
Stator core back	11	mm
Frequency	50	Hz
Line Voltage	400	V
Number of stator slots	24	
Number of effective rotor bars	36	
Pole number	8	
Phase number	3	
Winding	Lap	Double layer
Turns per coil	100	
Coil pitch	2/3	

3.4.3 Mechanical System and Torque of a Variable Speed Induction Machine

The mechanical equations of motions must be added to the system of the electric equation, with the aim of making an electromechanical study of the operation of the motor. The mechanical equation

of motion depends on the characteristics of the load, which differs greatly from one application to another. For simplicity, in this case, assume that the torque, which opposes that produced by the machine, consists only of an inertial load and an external load torque, which are known.

$$J_T \frac{d\omega_r}{dt} = T_e - T_L \tag{3.37}$$

where ω_r is the speed in rad/s, J_T is the total moment of inertia of the system, T_L is the load torque and T_e is the electromagnetic torque produced by the motor.

The electromagnetic torque produced by a fixed frequency connected machine is well known and a torque-time example is shown in Fig. 3.10. The equivalent circuit analysis is put forward in terms of the running light and locked rotor testing in Section 4.3.1. Here, the torque-speed characteristics for varying frequency to meet the requirements in (3.37). If the machine frequency is varied then a set of cuves can be obtained as illustrated in Fig. 3.5 (a). At lower frequencies V/f is constant and the peak torques are equal. Once the base speed is reached, where the voltage and current are maximum, the peak torque is reached and this is the maximum power region, also know as the field weakening region. The maximum possible torque reduces with increasing speed.

Vehicular drive machines are required to contribute to the braking (just as in an internal combustion engine where it is possible slow using engine braking) but an added role for this is to regenerate the vehicle kinetic energy back into stored battery energy via regenerative braking. This is known to save about 25 % of the energy. In an induction motor it is possible to do this by reducing the supply frequency so that it is running super-synchronously where the induction machine will generate. The torque-speed curves can be modified to include the generation as shown in Fig. 3.5 (b).

Lines of constant frequency

Constant voltage

Load torque

Maximum voltage point

Constant voltage/ frequency ratio

Reduced torque at low frequency

Speed

Variable Synchronous speed

Decreasing frequency

Torque

Continuous rating | Intermittent rating and overloading

(a) Motoring curves

Motoring

Speed

Constant voltage/ frequency ratio

Generating

Reduced torque at low frequency
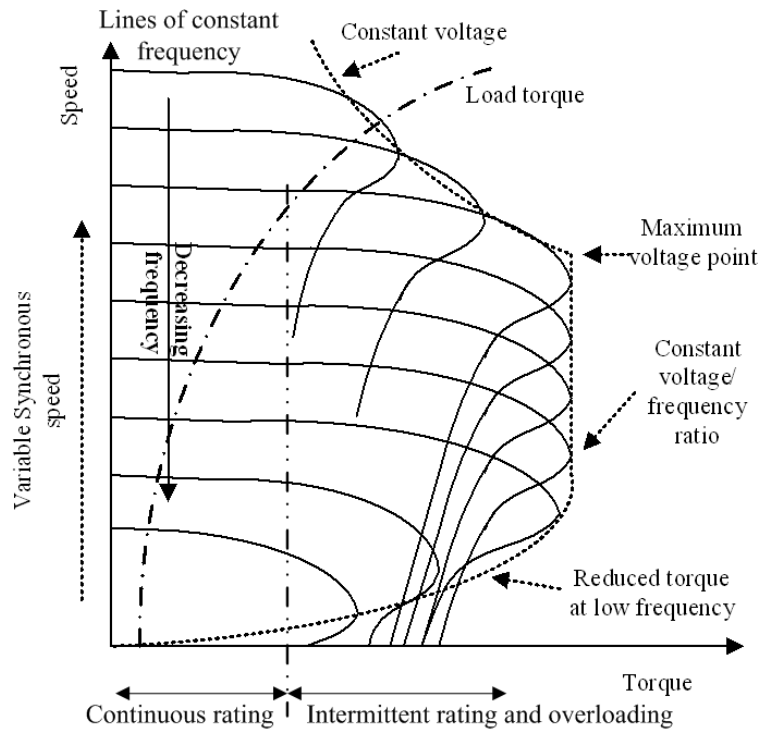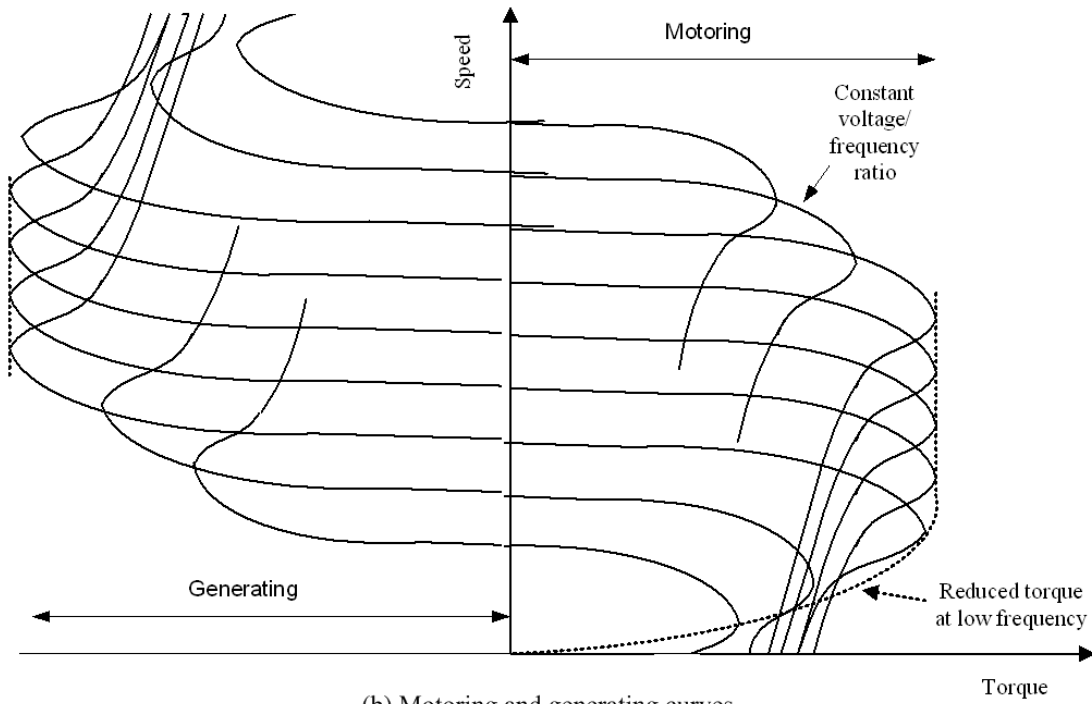
Torque

(b) Motoring and generating curves

Figure 3.5 Torque-speed curves for varying frequency

75

3.4.4 Simulation Examples

3.4.4.1 Radial flux machine simulation example using RMxpert

RMxport is used as the front end for Ansys Maxwell to allow a spreadsheet entry system. In this section a 4-pole radial-flux example is run to illustrate RMxpert. M600-60 material is used for the laminated steel of the rotor and stator of the design AFIM. The stator windings are copper and the shaft is ST1010 steel. The user interface of RMxprt is shown in Fig. 3.6. This is a front-end analytical calculation tool so that the time require for the analysis is in order of seconds.

Table 3.2 shows the results at the steady state point which is about half the peak torque. Some output RMxprt graphs are shown in Figs. 3.7 to 3.10. This machine represents a good machine. It can be seen that the stator slots and rotor slots are semi-closed, the slot areas are well proportioned and the stator yoke in about the correct thickness for a 4 pole machine.
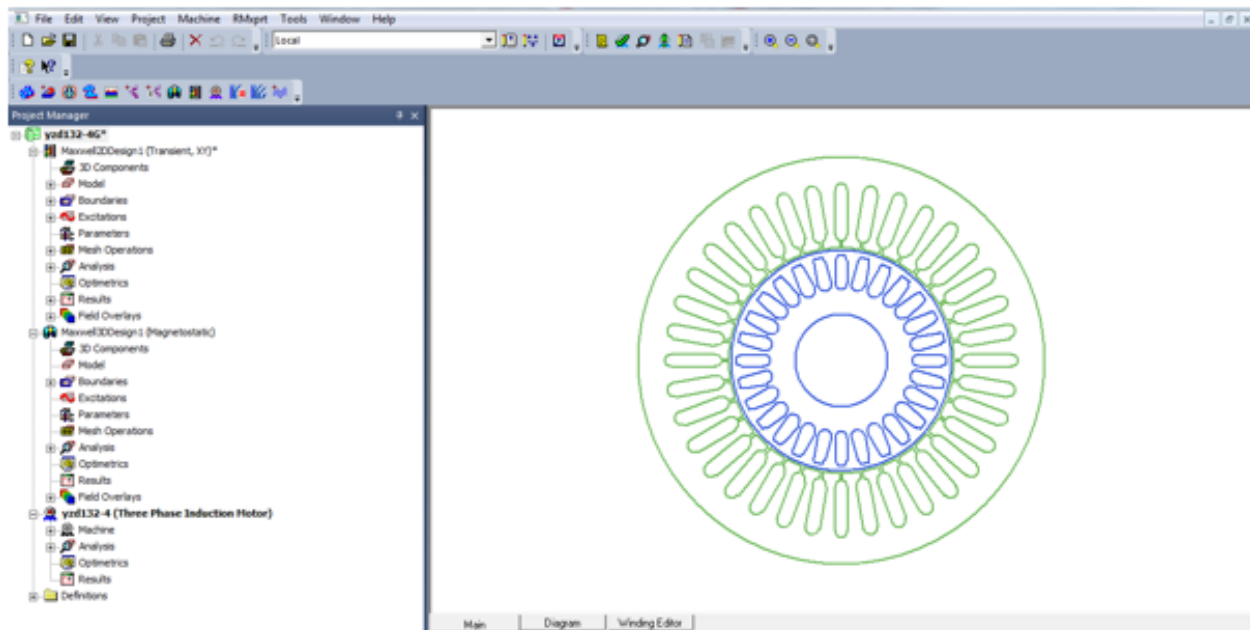
Figure 3.6 RMxprt User Interface

Table 3.2 RMxprt Result

| Parameters	RMxprt Result	Unit
Number of Revolution	1360	rpm
Stator Phase Current	4.5	A
Stator Resistance	2.3	Ω
Torque	10	Nm
Total Losses	0.356	kW
$\cos \theta$ - power factor	0.66	
Efficiency	80	%
Output Power	14.24	kW
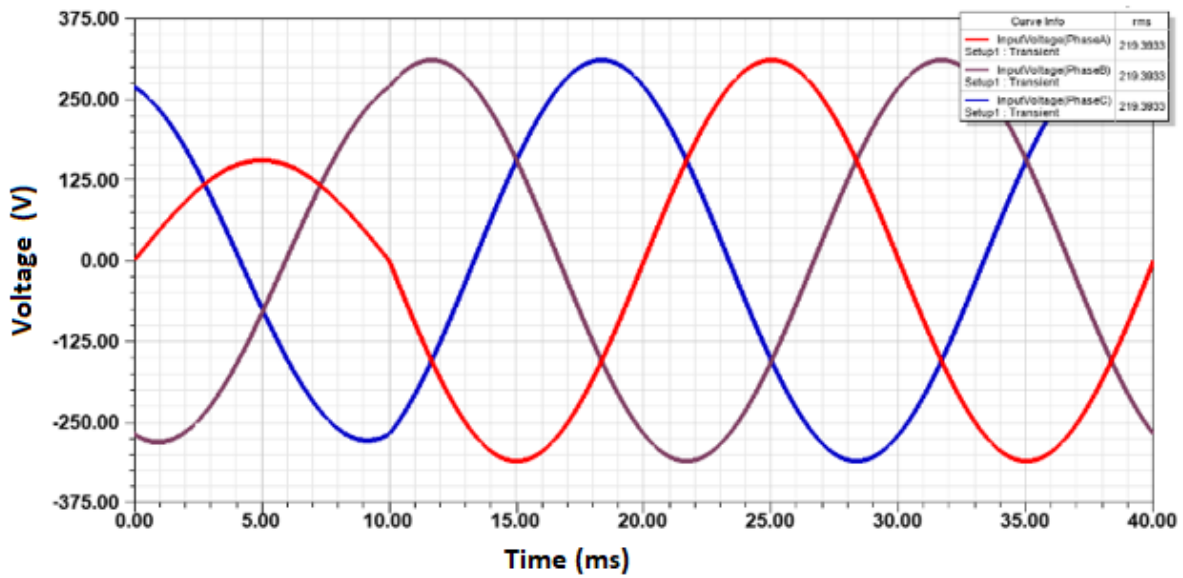
**Figure 3.7** Induced Voltage
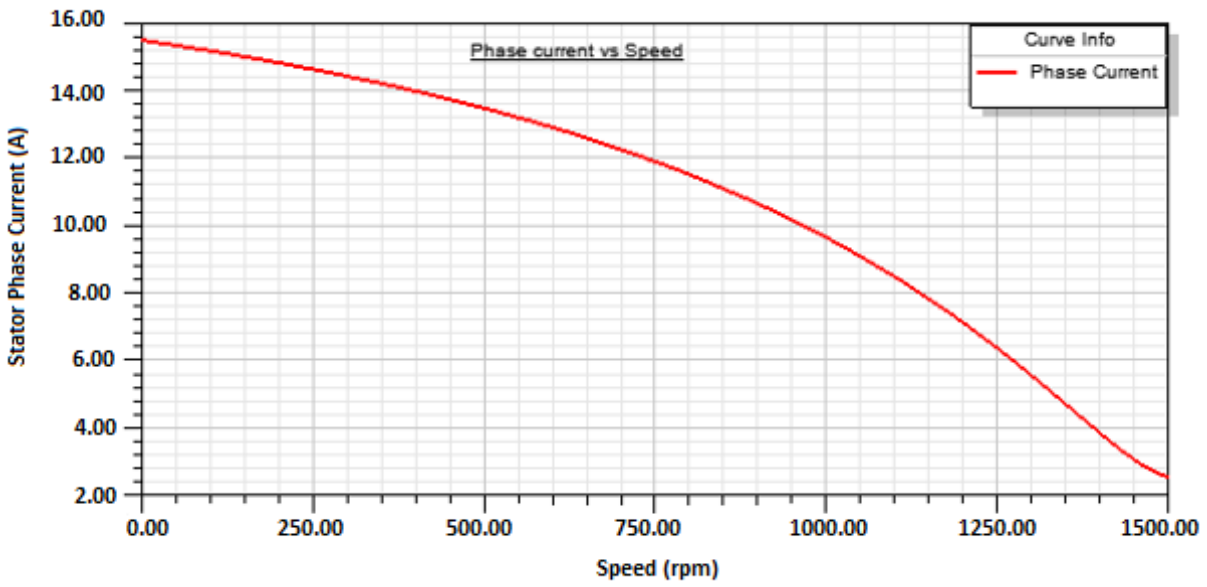
**Figure 3.8** Stator Phase Current Vs Speed
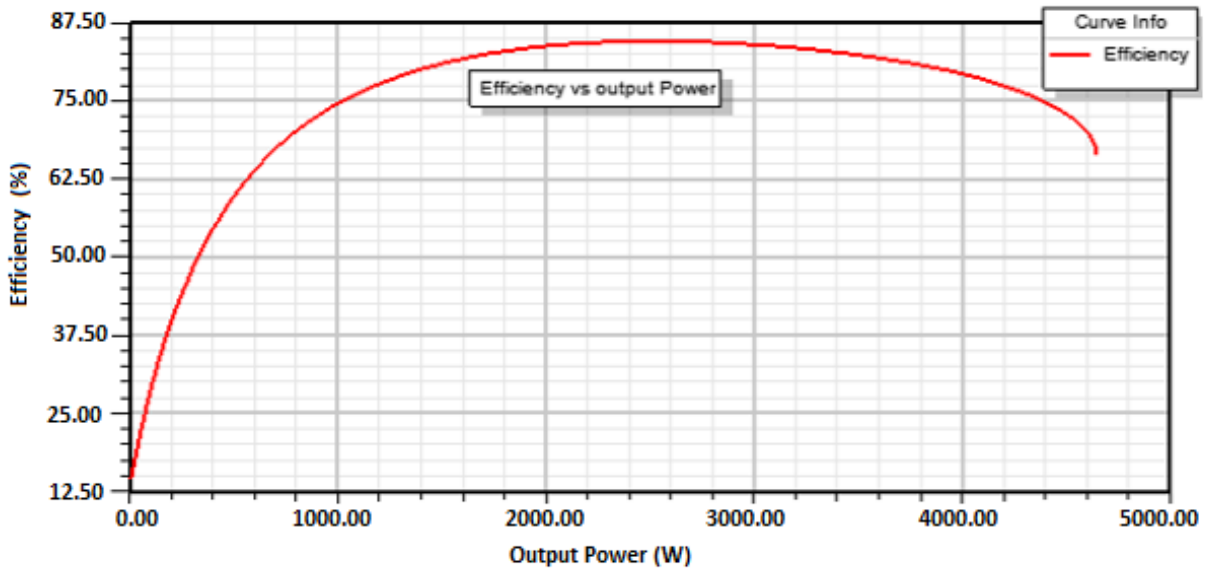
Figure 3.9 Efficiency Vs Output Power

The simulation is a transient simulation with the characteristic torque oscillation at the start.

The results are for the voltages, efficiency, stator phase current and torque. The torque starts low and peaks at just over 22 Nm before reaching the steady state which is typical for an induction machine. This is illustrated in Fig. 3.10.
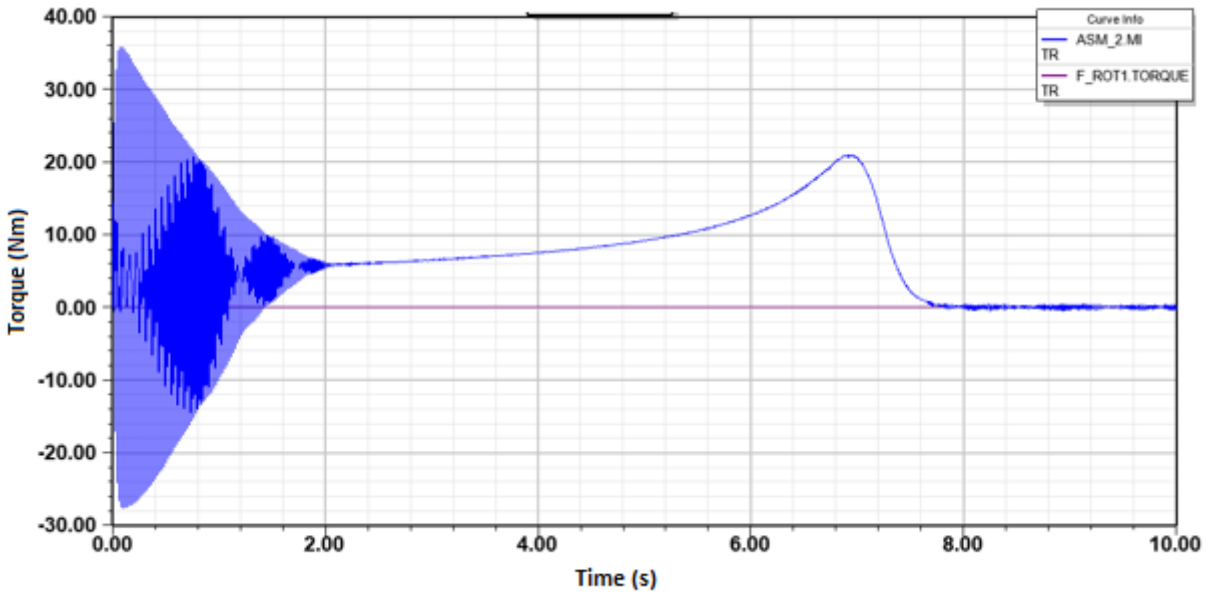
Figure 3.10 Torque Vs Time

3.4.4.2 Example with Ansys Maxwell 3D

The prototype axial flux machine is transferred from RMxprt to Ansys Maxwell with a direct link. Maxwell uses FEA to solve static, frequency-domain, and time varying electromagnetic and electric fields. The parameters of the motor, as defined in Table 3.1 are used (though the yoke is thinner). The automatic adaptive meshing technique of Maxwell 3D is used for meshing. A stator mesh model is shown in Fig. 3.11. 3D FEA requires much processing time and interpretation It is
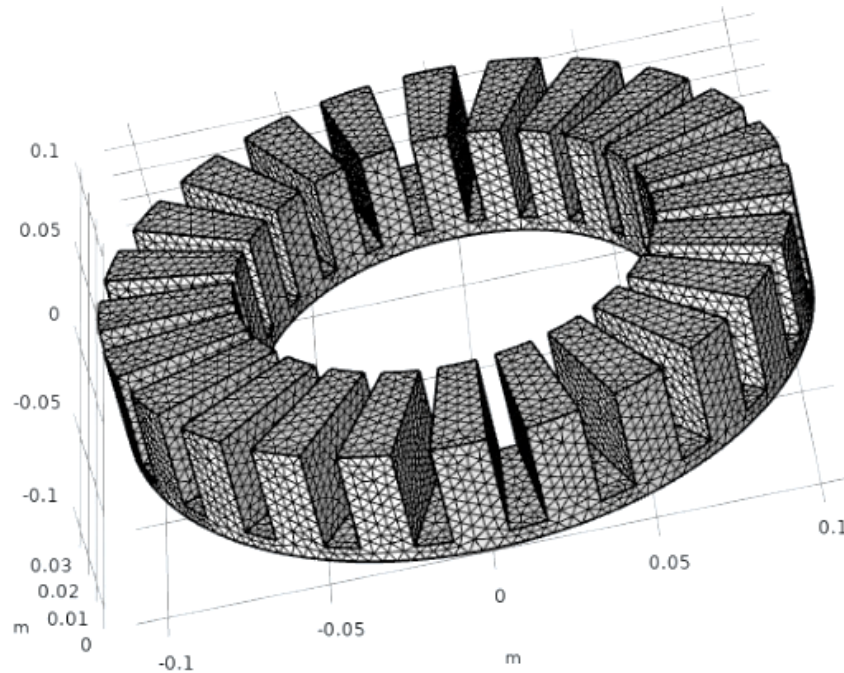
Figure 3.11 Maxwell-3D Mesh model of the stator

possible to use a 2D representation as discussed in the next section.

3.4.5 Magnetic Flux Density Distribution Analysis Using *SPEED* 2D and Maxwell 3D FEA

FEA can be used to analyze the magnetic flux density distribution and thermal distribution. For the flux density, it can check the saturation effects of the motor structure in a nonlinear model under no-load and loaded operating conditions. Flux distribution in different parts of the magnetic circuit can be investigated. The evaluation of magnetic flux density distribution in different parts of an AFIM is very important because if the flux density of the core gets to saturation levels, it will affect the operation of the motor and decrease performance. Therefore, the aim is to obtain the flux density values at the important locations of the motor (airgap, rotor and stator teeth and yoke). The

layout of the flux lines makes it possible to visualize the passage of the flux in the entire motor. Fig. 3.12 illustrates the magnetic flux density distribution in a 2D machine From *SPEED* PC-FEA which is a 2D FEA bolt-on to analytical induction motor package PC-IMD. In the stator teeth, the maximum magnetic flux density is 0.95 T at the tooth centre while the average value is 0.67 T. The flux density reaches 1.5 T at the tooth tip which is which is the usual saturation location - the peak level depends on the limitation of the material used. Here, the mesh has to be dense because the flux is changing quickly in both magnitude and direction and a poorly meshed model can give erroneous results.

Fig. 3.13 is the magnetic field distribution in vector form at the average radius for a stator tooth. Note that this is a 3D model and it can be seen that the elements are trapizoidal in 3D rather than triangular which are usually used in 2D FEA.
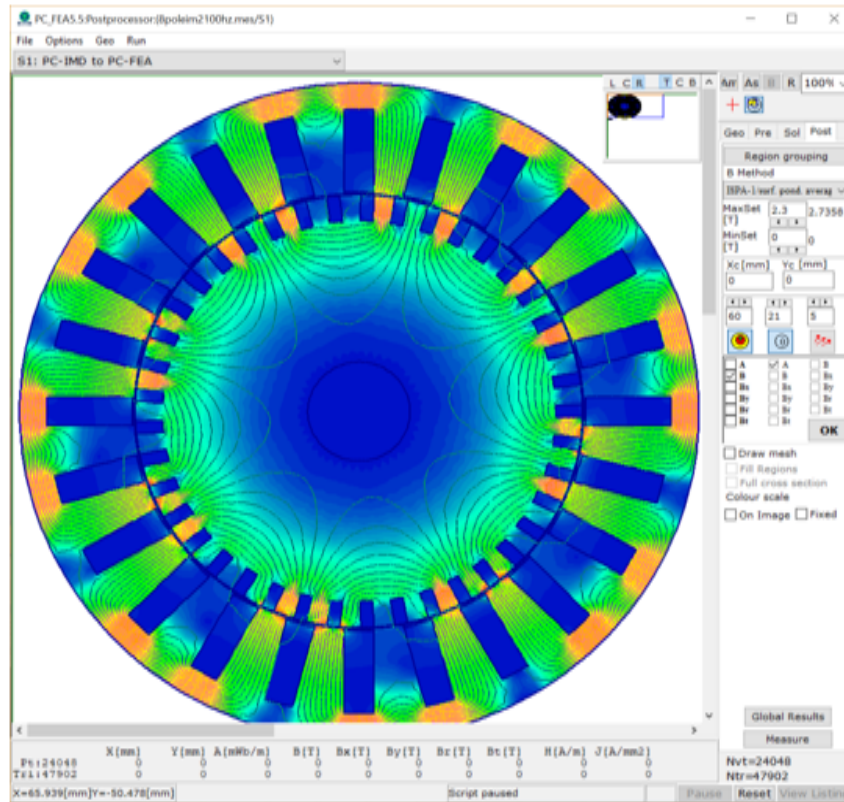
**Figure 3.12** Magnetic flux density distribution in 2D Model
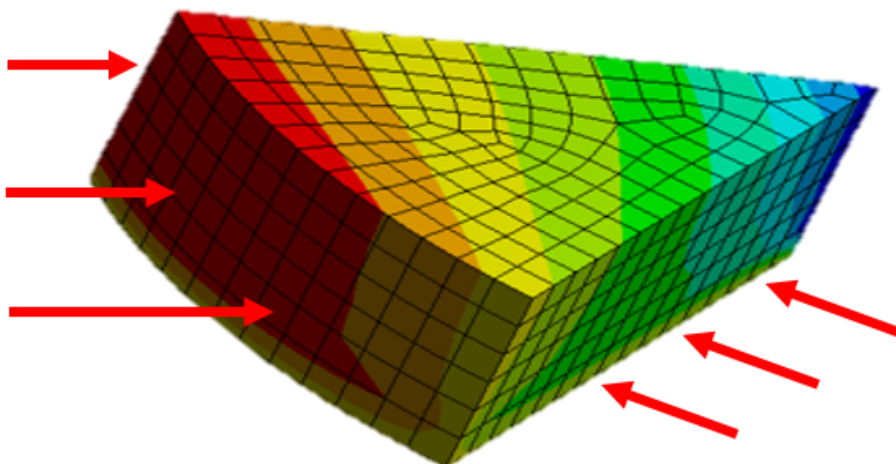
Figure 3.13 Magnetic field distribution in vector form in 3D Model

3.4.6 Flux Harmonics and Peripheral Effects

Analytical methods often account for only the main flux harmonic in the airgap or a few of the winding harmonics (5th, 7th, 11th, 13th, etc.). However, there will be additional slotting effects. These will induce voltages into different components of the machine which can generate hysteresis losses, eddy currents and asynchronous torques. These will be over a range of frequencies. Superposition is used to obtain the asynchronous torques due to each space harmonic to determine the total field. The treatment of non-linearity is incompatible with the principle of superposition, so this must be considered with caution. Time-stepped FEA can give a better solution to these .

The calculation of induction machines is generally done in 2D. To do this additional winding end-effects and skew effects calculations have to be added. For the 2D solution, a section is taken in the centre of the machine. For example, a 2D model should, ideally, incorporate the 3D effects of:

- The stator coil end windings;

- The rotor cage end-rings;

- The skew of the rotor bars; and

- Possible inter-bar currents.

The latter is difficult to calculate and often neglected.

3.4.7 Effects of Heat on an AFIM

Temperature is one of the most important issues that affects the performance of an induction machine. Premature insulation breakdown due to increased aging from overheating can reduce the machine lifetime. In an induction motor the torque produced decreases at a set slip point because

the rotor resistance increases. This means the machine will run possibly at reduced efficiency sue to the higher slip. If thermal runaway occurs then there can be a catastrophic failure with stator winding burn out or failure of the rotor cage with bar cracking or melting - aluminium melts at relatively low temperature compared to steel (hence they are easily cast into a steel core).

The geometry and size of an AFIM will affect the thermal rating of the machine. Thermal factors have to be taken in account on the design of the prototype machine in order to predict machine temperatures. Much of the thermal design is dependant on the manufacture of the machine. Particularly the varnish impregnation of the windings after dipping and the material boundary conditions [66]. The type of cooling will affect the thermal performance. These are usually natural, fan-over and forced fluid cooling. The transient performance requirement of vehicular drives usually required forces fluid ducts down the conductor slots or a wet jacket around the stator or even fluid cooling in the airgap. However, for an in-wheel drive motor, or a motor on a motorcycle, this can be difficult because of the additional fluid pipework and heat exchanger requirement.

Thermal exchanges are based on the laws of thermodynamics and are by conduction, convection or radiation. Thermal conduction is the transfer of heat quantity by direct interaction, under the influence of a temperature gradient, within a medium or between direct physical contacts without material flow. For solids that do not emit radiation, conduction remains the only means of heat transfer.

Induction machines are very common and therefore have been the subject of much research aimed at improving its thermal modelling and optimising its design. Thermal modelling is not straightforward for an induction motor. Indeed, the coupling that exists between electromagnetic and thermal modelling requires simultaneous modelling of the two phenomena [66].

A complete thermal model must represent all the electromagnetic and thermal states of the mo-

tor when the load torque is known; this complex problem that needs be solved in a reasonable time which often leads to simplifications. If the temperature is known at any point, the electromagnetic problem can be solved, and deduce the powers dissipated locally. Conversely, knowledge of these powers solves the thermal problem. The coupling of these two problems is important because of the dependence of the conductivity of the materials relative to their temperature. However, in many instances the electromagnetic design is decoupled from the thermal design with the temperatures being set. After the electromagnetic design the thermal design is done to meet the losses dissipation requirements. Design software such as Motor-CAD (https://www.motor-design.com) can link the two processes.

Another difficulty is taking into account of the rotor movement. In this case, it is necessary to devise methods to transfer heat from the rotor. Brushless permanent magnet machines do have the advantage of having much less rotor loss - essentially eddy current loss in magnet and metal materials.

The operation of the machine is greatly affected by its external environment so that fluctuations in ambient temperature conditions can create harmful heating for insulation and for rotating parts (bearings). This has to be included in any thermal calculation.

The local study of temperature distribution often uses the finite element method as shown in Figs. 3.14 to 3.17. Heat can be treated in a similar manner to current in an electric circuit with a temperature difference between the heat source (at the top of the teeth of a stator core in Fig. 3.14) to the ambient (at the back of the yoke in Fig. 3.14). There will be a heat flow, or flux component as shown in Fig. 3.15. Similar heat flows are shown for a rotor disc in Figs. 3.16 and 3.17 where the heat sources are the eddy currents in the rotor steel inserts rather than the aluminium conductors.
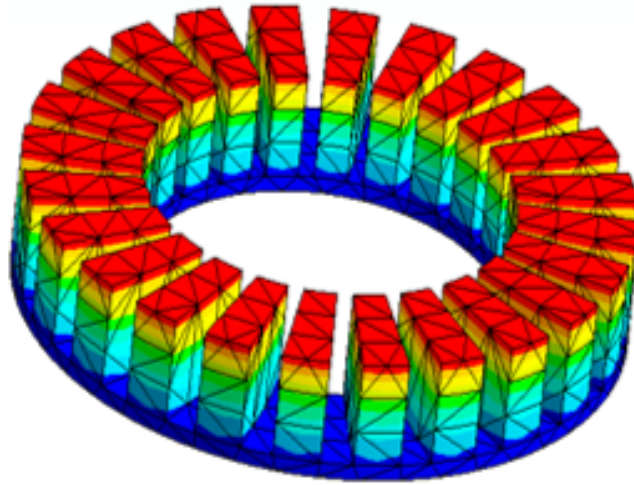
Figure 3.14 Maximum heat on the stator teeth in 3D Model
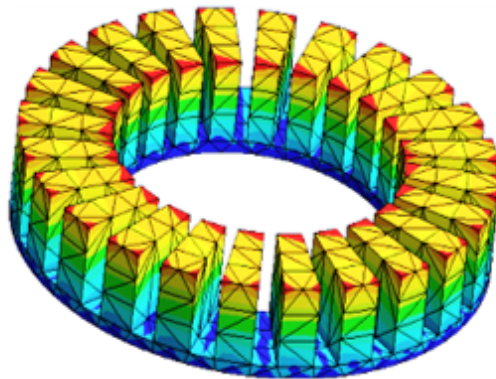
Figure 3.15 Total Heat Flux on Stator teeth
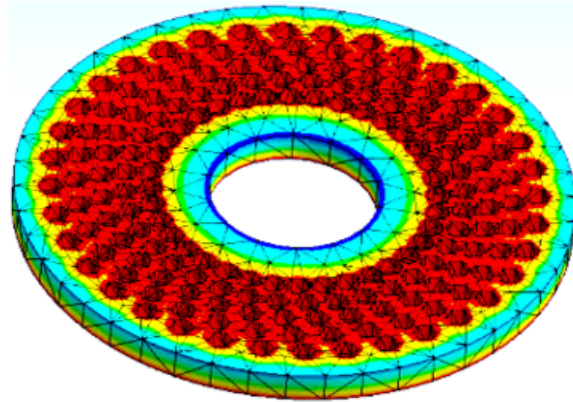
Figure 3.16 Maximum temperature on the Al solid- Rotor surface.
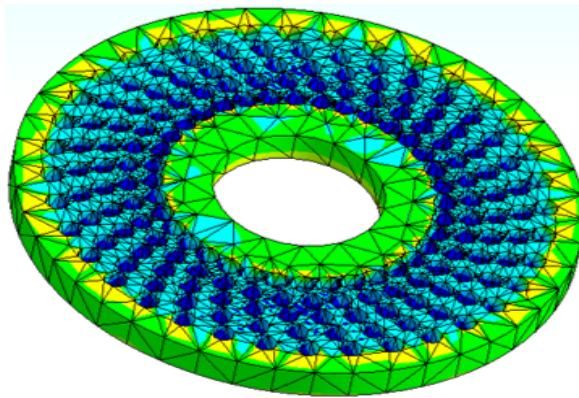
Figure 3.17 Total heat flux on the Aluminium rotor surface

The 2D studies on a radial or axial plane do not always provide reliable temperature fields; however, it is common to use analytical thermal networks to represent a motor where there are thermal resistances (mostly at material boundaries) and thermal capacitances (bulk materials). This is what Motor-CAD does. A 3D study can take into account of real phenomena however the boundary conditions are very much a function of manufacturing and this needs careful consideration as already stated. Such a model is cumbersome to be implemented, particularly in the study of transient conditions such as during hard accelerations of an vehicular motor or hard regenerative braking.

Transient thermal analysis can be time consuming so that often only short transient conditions are considered (much less than one minute), particularly if 3D models are considered.

3.4.8 *SPEED* **2D Representation**

This is used to do fast 2D simulations to obtain results across a set of solutions and build an operating chart. Two models are considered. One to assess the accuracy against the prototype, then a model that has a correctly sized rotor and can be used for developing the operating Chart

To represent the double-sided axial flux machine in a radial flux package such as *SPEED* then some approximations have to be made:

- The first is that the airgap diameter is set the the mean radius of the axial-flux stators;

- The second is to assume the axial length of the machine is double the difference of the outer and inner radii of the stator. This is because the rotor is double sided;

- The airgap is set to the same airgap as on one side, not the sum of the two;

- The end-winding length has to be adjusted because the AFIM has four sets of endwindings whereas the radial flux machine has two; and The rotor cage thickness is set to half of the thickness of the axial-flux rotor. The same coils winding as on one side is used for the radial flux representation.

This should ensure the radial flux representation is close to that of the AFIM.

SPEED is a spreadsheet package that has various editors. The Outline Editor allows various geometrical data to be entered. The prototype machine representation is shown in Fig. 3.18 while one sheet of the Main Template is shown in Fig. 3.19. The Winding Template is shown in Fig. 3.2. From this simulation many outputs can be analysed such as a torque-speed curve at constant frequency as shown in Fig. 3.20.

Outline Editor

(x,y)=(-75.706,118.622)

RadSh	20.0000
Rad0	20.0000
Rad1	88.2500
Gap	1.2500
Poles	8
Slots	24
LamShape	Circle
Rad3	133.0000
S_Slot	PllSquare
SD_S	34.0000
SWid	11.4000
SO_S	11.4000
TGD_S	1.0000
TGANG_S	20.0000
Lstk	87.0000
Stf	0.9700
TGorSO	TGang
R_Bars	37
NumHoles	0
RHole	Round
PCDia	54.1926
HoleDia	10.8385
MConfig	Int
DblCage	false
Bar1	Type2
RoShift	0.0000
Edit View	Full motor

Figure 3.18 *SPEED* Outline Editor for prototype machine

Template Editor

Configuration and dimensions

Connex	3-Ph Wye	Poles	8	Slots	24	MConfig	Int
Rad3	133.0000	Rad1	88.2500	S_Slot	PllSquare	Lstk	87.0000

Control

Vs	345.5000	CalcMode	f/rpm	TorqCalc	Load Pt	DoPart	false
Freq	50.0000	Slip	1.0000	*rpm	0.0000	rpmS	750.0000
PowrSh..	0.0000	TorqSh..	0.0000	rpmNL	1500.0000		

Windings

WdgType	Lap	TC	100	PPaths	1	R_Bars	37

Rotor

PC1	50.0000	PCEndR	50.0000	Skew	0.0000	Bar1	Type2

Losses

Wf0	10.0000	RPM0	700.0000	NWFT	1.0000

Temperatures

TempCalc	Fixed	Ambient	20.0000	
T_wdg	75.0000	T_rtr	100.0000	

\Main /Winding /Rotor /Losses /Thermal /Test data /Simulation /Settings /

**Figure 3.19** *SPEED* Main Editor for prototype machine

89
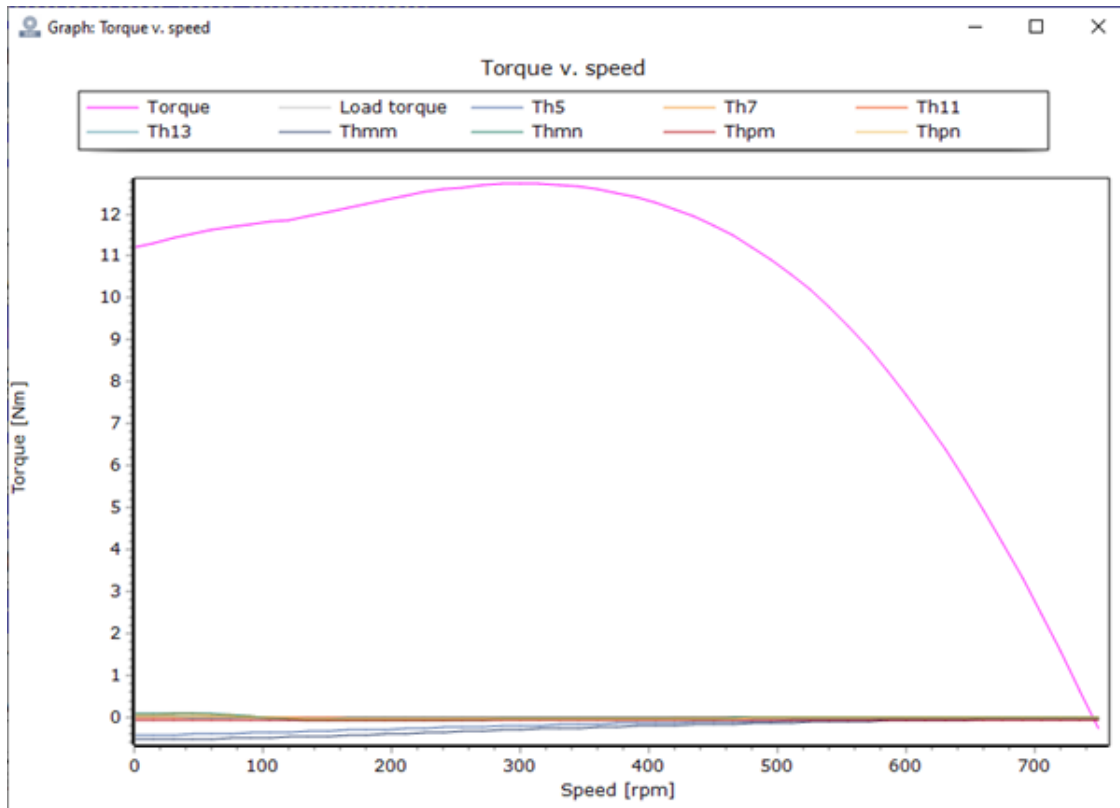
Figure 3.20 *SPEED* Torque-speed curve for prototype machine

The prototype machine is not a very good machine as shown in Fig. 3.20 where the peak of the torque is at a low speed. This shows the rotor resistance is too high as discussed earlier. For the improved machine with a long rotor and full stator slots then the Outline Editor is shown in Fig. 3.21. The reason for the deap bars is that this represents axial direction in the AFIM. The torque-speed curve is given in Fig. 3.22 for this.

Outline Editor   — □ ✕

RadSh	20.0000
Rad0	20.0000
Rad1	88.2500
Gap	1.0000
Poles	8
Slots	24
LamShape	Circle
Rad3	133.0000
S_Slot	PllSquare
SD_S	34.0000
SWid	11.4000
SO_S	11.4000
TGD_S	1.0000
TGANG_S	20.0000
Lstk	87.0000
Stf	0.9700
TGorSO	TGang
R_Bars	40
NumHoles	0
RHole	Round
PCDia	54.1926
HoleDia	10.8385
MConfig	Int
DblCage	false
Bar1	Type3
RoShift	0.0000
Edit View	Full motor

(x,y)=(-136.781,135.660)

Figure 3.21 *SPEED* Outline Editor for fully rated machine
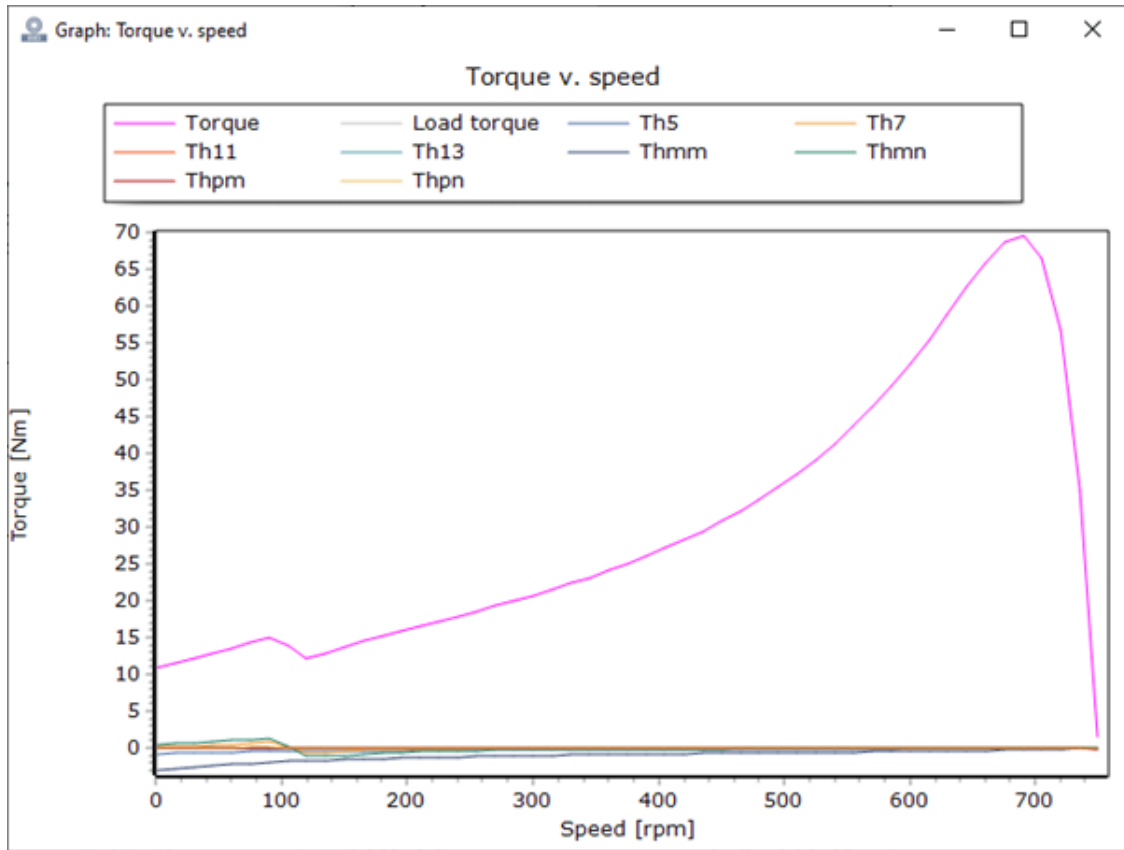
Figure 3.22 *SPEED* torque-speed for fully rated machine

3.5 Conclusion

This section has detailed various aspects of calculating and modelling an AFIM using simple sizing calculations, FEA and analytical methods. The next section will give the testing and simulations of the AFIM using the prototype to verify the simulations then going on to illustrate how the design can be improved.

Chapter 4

Testing and Simulation of the AFIM

4.1   Background

Axial Flux induction machines are planar and the airgap is adjustable in a prototype if designed to be so. If AFIM is not designed properly their power density and power factor can be very low compared to other machines, which is the case for the proof-of-concept machine constructed here.

Compared to conventional induction machine, the compacted axial flux induction machine design may allow run-up with lower current density and as a result the power losses are reduced. Therefore, the torque and power density of the machine may increase at low speed applications [67].

When designing high-speed AFIM with double-stator-one-rotor structure, distinct considera-tion must be given to the presumption of the airgap flux wave harmonics. These harmonics can generate eddy-current at the aluminium rotor disc surface. Some of the sources of the harmon-

ics are: stator and rotor slotting, stator windings harmonic current linkage, core saturation and non-sinusoidal supply voltage. More losses can be generated when the motor is running at high speed and connected to a power electronic converter. These are the result to the supplementary time-harmonics from the converter [68].

4.2 AFIM Prototype Design Procedure

The design configuration of axial flux induction machine is consisting of double-stator one-rotor topology. The airgap length of the axial flux induction machine can be adjusted in order to balance the load in the stators - the rotor should be axially centred between the stators. The synchronous speed is 750 rpm at 50 Hz though for a vehicular drive the supply will vary.
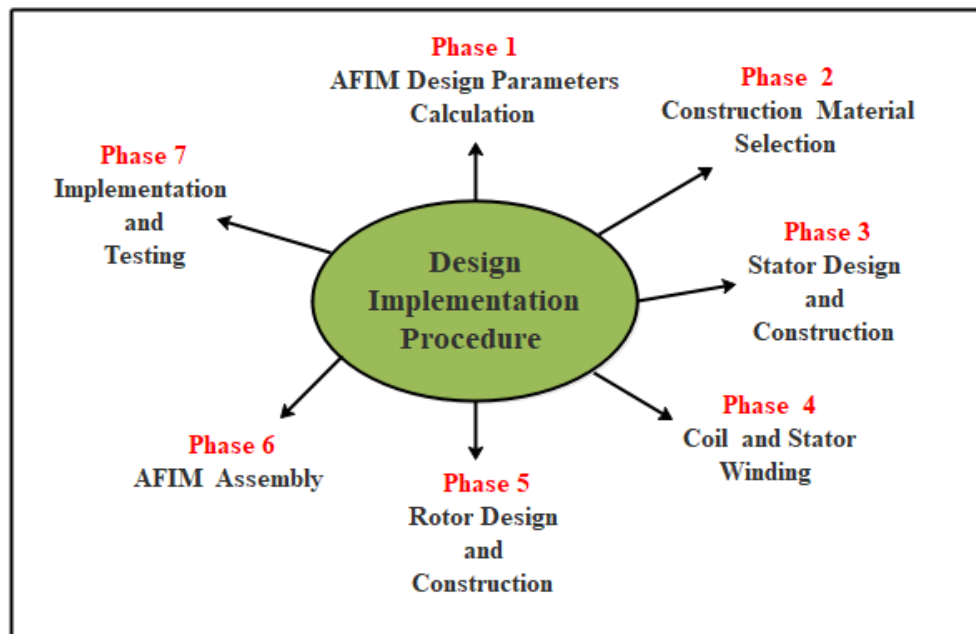

Figure 4.1 AFIM design Procedure

Fig.4.1 shows the prototype motor design procedure. The phases are:

- **Phase 1: AFIM design parameter calculation**

  In this research, the approximate dimensions and sizes of some parts of the proposed motor are determined by the use of fixed sized stators that were sourced as proof-of-concept stators though not designed for the applications Details of the basic design calculations for the AFIM design were discussed in Section 3.4

- **Phase 2: Construction material selection**

  The materials used for the design, construction are: the aluminum disc, copper wire, slot liner paper and strip-wound laminated stator cores of steel type ST37.

- **Phase 3: Stator design and construction**

  The most complex component to manufacture is the strip-wound laminated stators that require the steel strip to to be wound with the slots punched in the correct position which will become further apart as the strip core is wound. Therefore two identical cores were sourced to simplify construction. These came from single-sided brushless permanent magnet machines. one of the stator cores is shown in Fig. 4.2.

Figure 4.2 Stator core

- **Phase 4: Coil and stator winding**

Open slots means the winding method using flat wire is simplified. The Winding can be done by winding directly around the teeth manually or with a winding machine. Another solution consists in pre-winding coils which will be inserted into the teeth and then connected together. This solution is suitable for mass production. Once arranged in the stator slots, slot wedges at the slot tops hold the windings in the slots. These are electrically non-conductive non-magnetic material. If slotting effects are a problem then magnetic wedges can be used. These can reduce stator harmonics significantly. These techniques help to decrease losses on the surface of the rotor and smooth the airgap flux density distribution. In order to reduce the winding harmonics and to get higher efficiency results, the use of double-layer windings method seem to be the better choice compare to the single-layer winding. The winding should be carefully done in order to obtain the smallest value of the leakage. Double-layer two-thirds short pitch windings were used in this design as shown in Fig. 4.3. There is a

compromise in the choice of the airgap length. The power factor, and hence efficiency, goes down with increasing airgap length - the magnetizing reactance will go down - but the torque can increase.

Figure 4.3 Coil and stator winding realisation

Open stator slots and lap windings makes the windings process straightforward for an AFIM. This allows a reduced space requirement for the end windings, consequently, reduced the copper losses. The windings used copper of 1.0 mm diameter with a total length of 197.56 m per phase.

- **Phase 5: Rotor design and construction**

  The aluminum solid-rotor disc design and construction is one of the most important aspects in the fabrication of the AFIM. An unbalanced rotating rotor will cause vibrations and stresses of the machine. To avoid this balancing of the rotor is necessary. Balancing of rotor will prolong bearing life. The rotor was fabricated using aluminum disc as shown in Fig.4.4.

  The novelty of this design can be emphasised here - it is constructed from the aluminium conductor material with the magnetic steel inserted into the aluminium as shown in Fig. 4.5. These are 10 mm diameter studs. This is an alternative to normal rotor construction, either radial flux or axial flux machines, where the aluminium or copper conductors are cast or fabricated in the rotor core. Table 4.1 summarise the AFIM prototype design parameters


Figure 4.4 Rotor fabrication
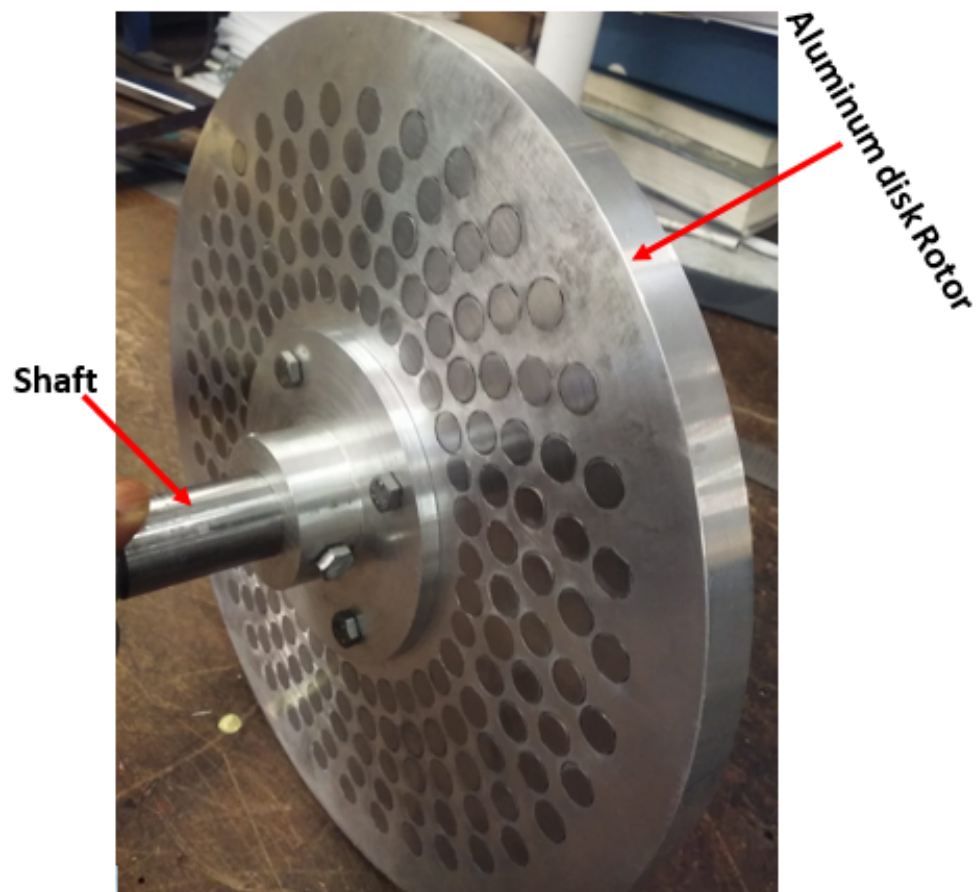
Figure 4.5 Aluminium rotor disc with shaft

Table 4.1 Main parameters of the prototype AFIM

Parameters	Explanation	Value	Unit
D_o	Stator outer diameter	220	mm
D_i	Stator inner diameter	133	mm
$D_{o\text{-rotor}}$	Rotor outer diameter	275	mm
L	height of the Stator	45	mm
L_{rot}	Rotor disc thickness15mm		
M	Number of stator slots	24	
N_b	Number of effective rotor bars35		
$\%_{bar}$	Percentage width of effective bar	35	%
P	Pole number	8	
g	Airgap Length	1	mm
$\emptyset$	Number of phases	3	
N	Synchronous speed	750	rpm
V	Phase voltage	230	V
N_{coil}, N_{ph}	Coil turns and turns per phase	100/800	
P	Nominal power rating	4	kW
f	Frequency	50	Hz

- **Phase 6: General assembly of the designed AFIM**

The general assembly of the designed motor is shown in Fig. 4.6. In order to align the rotor between the two stators a bearing hub was used to attach the disc to the shaft as shown in Fig. 4.5. This caused issues with a buckle of the rotor due to the heavy working of the the disc during manufacture.

Initially the rotor was mounted on the stator back-plates as shown in Fig. 4.6. However,
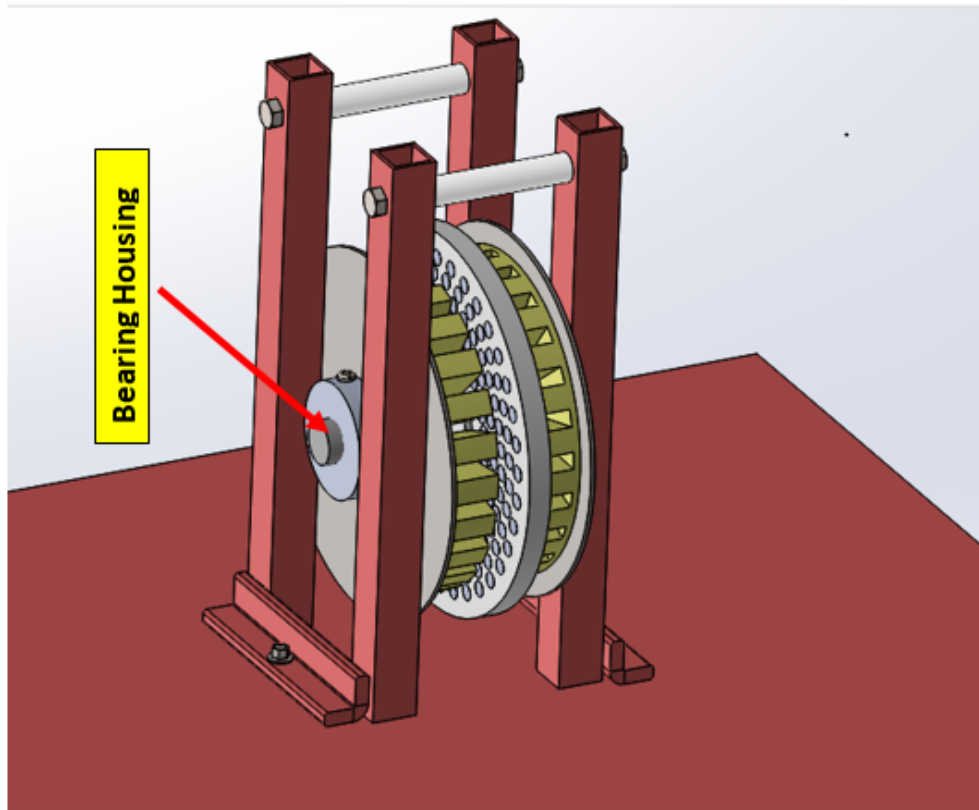
Figure 4.6 Initial prototype motor assembly

initial operation was found to be poor as shown in the results so that the machine was further reworked with the rotor being separately mounted on pedestals to allow future insertion of other rotors of different thicknesses and variation of the airgap length. This is shown in Fig. 4.7.

- **Phase 7: Implementation experimental setup and testing**

  This phase is the implementation of the experimental set up in the laboratory. The 3-phase supply is directly connected to the AFIM via a three-phase auto-transformer as shown in Fig. 4.8.
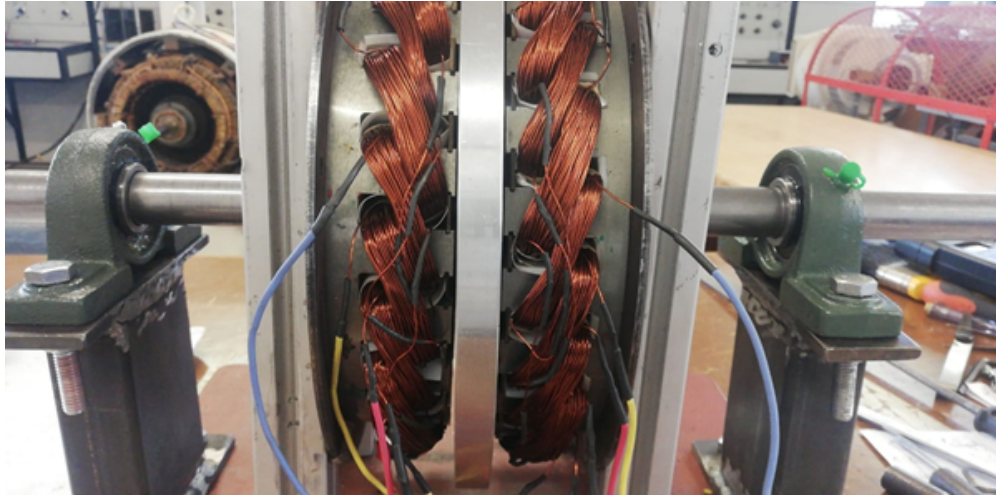
Figure 4.7 Modified prototype motor assembly with separately mounted rotor
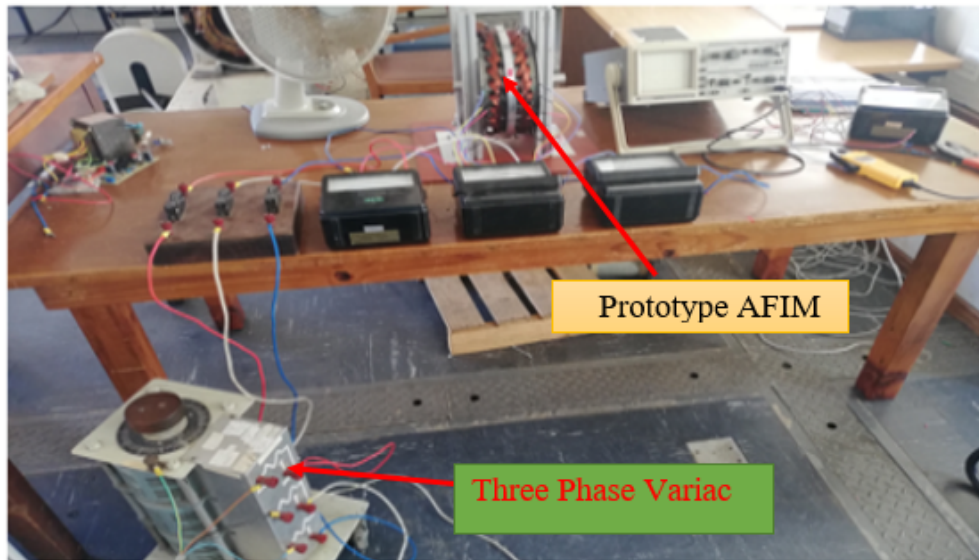

Figure 4.8 AFIM Prototype testing bench

The auto-transformer was used to vary the supply voltage to the motor, while taking different readings. The voltage range was from 0 to 220 V. The power and current traces were obtained using a Fluke MDA-Motor Drive Analyzer.

Two tests were carried out to help validate simulations: the running light test test and the

lock rotor test were carried out. In order to perform the analysis at different airgap, the airgap between the stator and rotor was adjusted. The results analysis is presented in the next section.

4.3   Experimental and Simulation Results Analysis for Equivalent Circuit Parameters

Generally there are two basic type of test carried out to evaluate the performance and efficiency of the prototype machine; they are: running light test and lock rotor test. These can then be used for a comparison of the models and the tests via the variation of the circuit parameters in Fig. 4.9. Note that the voltage is the phase voltage and the rotor has two impedances where $r_2^/$ is the actual referred rotor resistance due to Joule losses in the rotor and $(1-s)/s \times r_2^/$ is the component representing the electro-mechanical energy conversion. The slip s is given by (2.2). Recapping this:

$$s = \frac{n_s - n_r}{n_s}$$

where n_r is the rotor speed and n_s is the synchronous speed. From this it can be seen that the slip is unity at standstill and zero when the rotor is turning at the synchronous speed. The rotor resistive components can merged to give

$$\frac{r_2^/}{s} = r_2^/ + \frac{1-s}{s}r_2^/ \tag{4.1}$$

To give good electro-mechanical conversion then the slip should be small, although not vanishing small so that the rotor circuit is blocked by the term $(1-s)/s$.
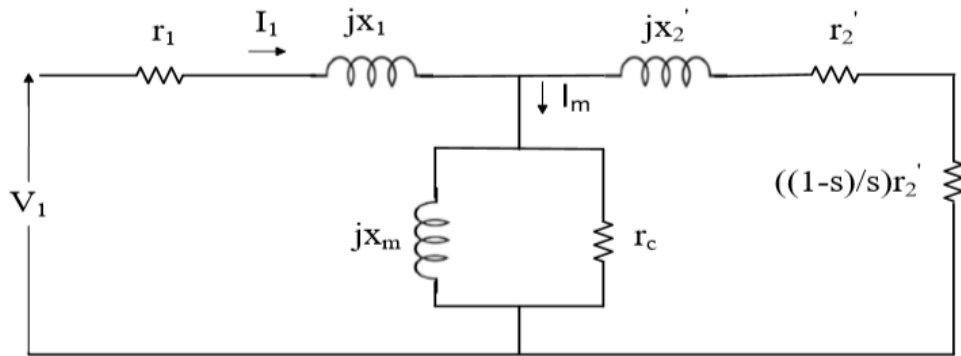
Figure 4.9 Per-phase equivalent circuit of an induction motor

4.3.1 Running Light and Locked Rotor Tests of the AFIM

To obtain the equivalent circuit of the machines then basic running light and locked rotor tests can be conducted. The running light test allows the calulation of the magnetizing components while the locked rotor tests obtain the rotor resistance and the leakage reactances.

4.3.1.1 Running light test

This test is analogous to the transformer no-load test. The test is done when the rotor rotates with synchronous speed; i.e., with no load where the torque is negligible. This test, the rated voltage at the rated frequency should be used to run the motor without any load. The voltage, current and power should be measured and the speed checked. This is a per-phase equivalent circuit so phase values should be used. When the machine is running light then it is possible for the rotor components to be neglected because $(1-s)/s$ is very large, so that the equivalent circuit in Fig. 4.9 can be simplified to Fig. 4.10.
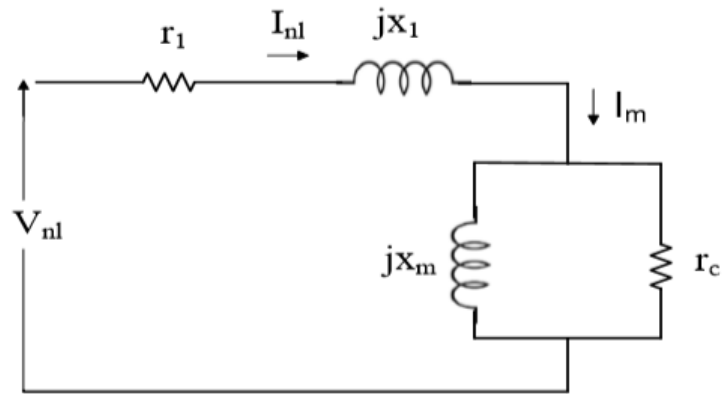
Figure 4.10 Reduced equivalent circuit for the running light test

The input impedance to the running light equivalent circuit in Fig. 4.10 is given by

$$Z_{nl} = \frac{V_{nl}}{I_{nl}} \tag{4.2}$$

where V_{nl} is the phase voltage. Usually $r_1 \ll r_c$ and $X_1 \ll X_m$ so that in this test they can be neglected. r_1 can be directly measured as the phase resistance measured in DC conditions, and X_1 is obtained from the locked rotor test. Hence

$$r_c \approx \frac{P_{nl}}{I_{nl}^2} \tag{4.3}$$

where P_{nl} is the power per phase. The reactive power can be either measured directly or using the voltage, current and power measurements where

$$Q_{nl} = \sqrt{(V_{nl}I_{nl})^2 - P_{nl}^2} \tag{4.4}$$

Therefore the magnetizing reactance can be obtained:

$$X_m \approx \frac{Q_{nl}}{I_{nl}^2} \tag{4.5}$$

Hence X_m and r_c are obtained from measurement of the voltage, current and power. However, this is valid when the neglected terms are much higher for parallel components and much lower for series components.

4.3.1.2   Locked rotor test

The locked rotor test, sometimes called the blocked rotor test is performed to estimate the rotor resistance and leakage impedances.

The circuit in Fig. 4.9 can be simplified to the circuit in Fig. 4.11. This is because the slip is 1 so that the X_m and r_c are usually much great than the other circuit components. This test requires that the rotor be locked so it will not turn and be done at reduced voltage, preferably no more than the rated current. The voltage, current and power are measured.
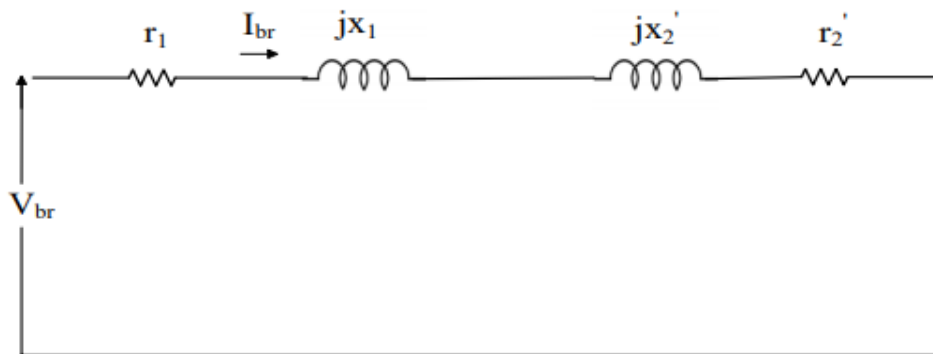

Figure 4.11 Equivalent circuit for locked rotor test

With the rotor locked then

$$Z_{br} = \frac{V_{br}}{I_{br}} = R_{br} + jX_{br} \tag{4.6}$$

where V_{br} the phase voltage

$$R_{br} = \frac{P_{br}}{I_{br}^2} = r_1 + r_2'$$ (4.7)

Since r_1 has been measured then

$$r_2' = R_{br} - r_1$$ (4.8)

The input reactance is

$$X_{br} = \sqrt{Z_{br}^2 - R_{br}^2} = x_1 + x_2'$$ (4.9)

It is difficult to split these. A common approximation is to split them equally so that

$$\frac{X_{br}}{2} = x_1 = x_2'$$ (4.10)

The test procedure was described in phase 7 of the design and testing procedures. The various test were carried out with different airgap as shown below.

4.3.2 Initial Tests - Speed vs Current Characteristic at Different Airgaps

Table 4.2 shows speed current result measurement during no-load test as teh voltage is varied, while Fig. 4.12 shows the graphical analysis. This shows that there were major issues with the design for reasons unknown at the time. The machine appears unable to reach a no load speed close to 750 rpm. By inspection of Fig. 3.20, the *SPEED* model suggests that the rotor resistance is too high with the peak torque at a low slip. If the mechanical loses of the machine are high then a no-load will never be reached. It was decided to rebuild the machine and separately mount the rotor as shown in Fig. 4.7.

Table 4.2 Speed-current characteristics at different airgap

| Speed (rpm)	Current (A) 1 mm airgap	Speed (rpm)	Current (A) 2mm airgap
698	7.5	660	7.5
650	6.7	580	6.7
570	6.1	550	6.1
400	4.9	380	5.1
320	3.7	300	3.8
200	3.2	150	3.1
100	2.2	100	2.8
68	1.8	65	1.9
0	0	0	0
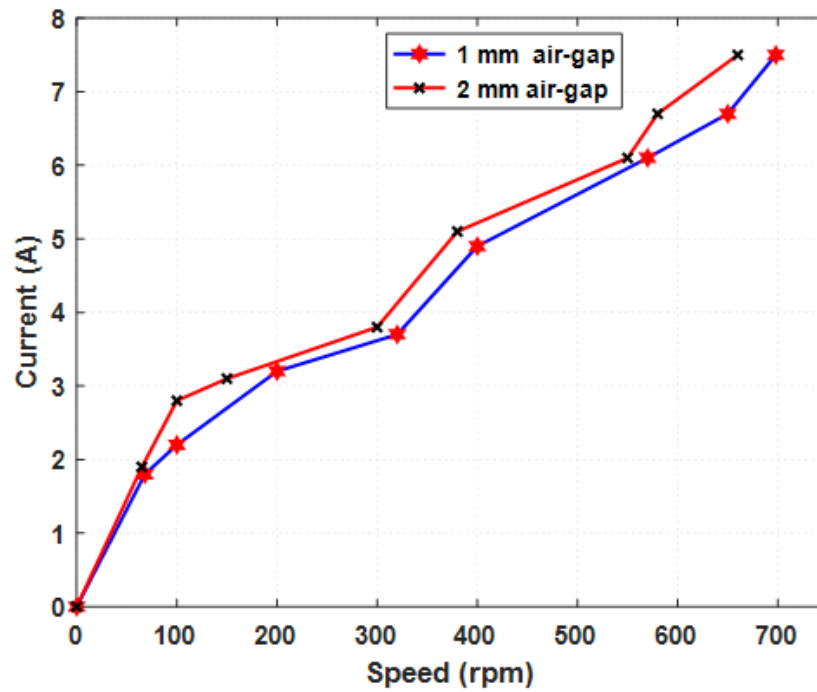
Figure 4.12 Current vs speed characteristics at different airgap

4.3.3 Rebuilt Motor Tests

The machine was rebuilt as discussed earlier. The shaft was replaced as well as the bearings but it still rotated with a buckle which restricted the minimum airgap that could be set. The Fluke meter was used for these measurements which also allowed the inspection of the current waveform as shown in Fig. 4.13. These are sinusoidal.
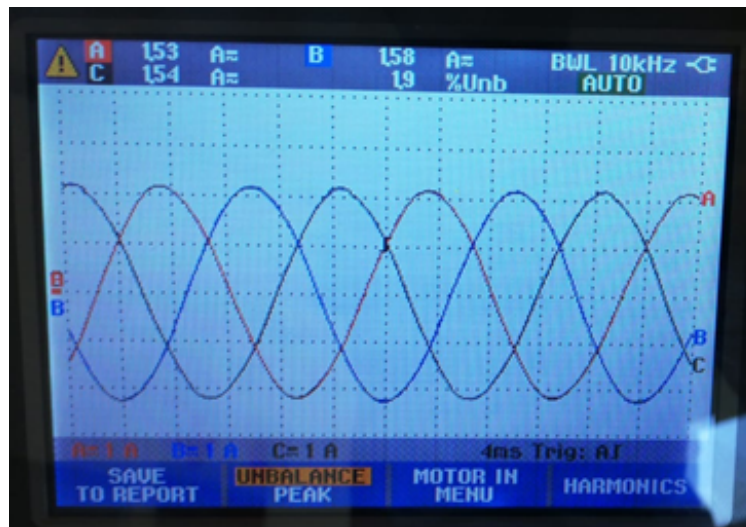
Figure 4.13 Measured current waveforms

4.3.4 Running Light Tests

Several tests were taken with different airgap as shown in Table 4.3. It can be seen that X_m decreases rapidly with increasing airgap and it was considered that only the 1 mm airgap should. This ties in well with the prediction in (3.29) for the basic sizing exercise. The speeds are still not as close to the synchronous as would normally be expected.

Table 4.3 Prototype running light tests

Airgap [mm]	V_{ph} [V]	I_{ph} [A]	P_{ph} [W]	n_r [rpm]	Q_{ph} [VAr]	X_m [Ω]	r_c [Ω]
1	120	1.41	60	707.2	158.2	91.0	240.0
2	120	1.67	71	719.8	187.4	76.8	202.8
4.5	161	3.02	168	718	456.3	56.8	154.3

red

4.3.5   Locked Rotor Tests

Using an airgap length of 1 mm the locked rotor tests. The results are consistent and show that the rotor is does need to be longer with more conductor. The results are shown in Table 4.4

Table 4.4 Prototype locked rotor tests

Airgap [mm]	V_{ph} [V]	I_{ph} [A]	P_{ph} [W]	Q_{ph} [VAr]	$X_1 + X_2'$ [Ω]	$r_1 + r_2'$ [Ω]	r_2' [Ω]
1.2	96.8	2.07	146	137.2	32.0	34.1	26.6
1.2	80.9	1.73	103	94.8	31.7	34.4	26.9
1.2	69.0	1.45	74	67.3	32.0	35.2	27.7

4.3.6   Simulations of the Prototype Machine

4.3.6.1   *SPEED* simulations

The *SPEED* simulation was given in Section 3.4.8. This model was adjusted to have the same winding as the prototype with a 1 mm airgap. The materials were set and the rotor adjusted in

terms of bar and endring dimensions to obtain a reasonable representation. This gave $X_m = 90.7$ Ω, $r_c = 5906$ Ω, $r_1 = 7.45$ Ω, $X_1 = 19.6$ Ω, $r_2' = 26.8$ Ω and $X_2' = 6.93$ Ω. These are close values. The prototype has slightly more leakage reactance but the dimensioning is close.

4.3.6.2 ANSYS Maxwell simulations

These simulations were carried out a locked rotor and running light conditions. The geometry is passed though from RMxpert as shown in Fig. 4.14. This produces the single-pole single-side 3D model shown in Figs. 4.15 and 4.16. Note that the rotor plate appears thin because this is half the rotor length. The boundaries have to be set with master/slave boundaries at each pole side, magnetic insulation boundaries at the back of the stator, and symmetry image at the back of the half rotor.
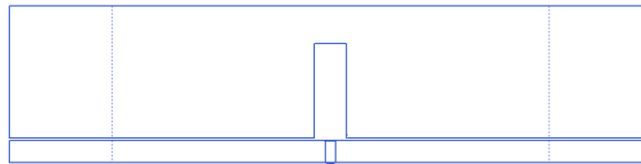

**Figure 4.14** Sizing stator and rotor in ANSYS RMxpert for axial flux machine
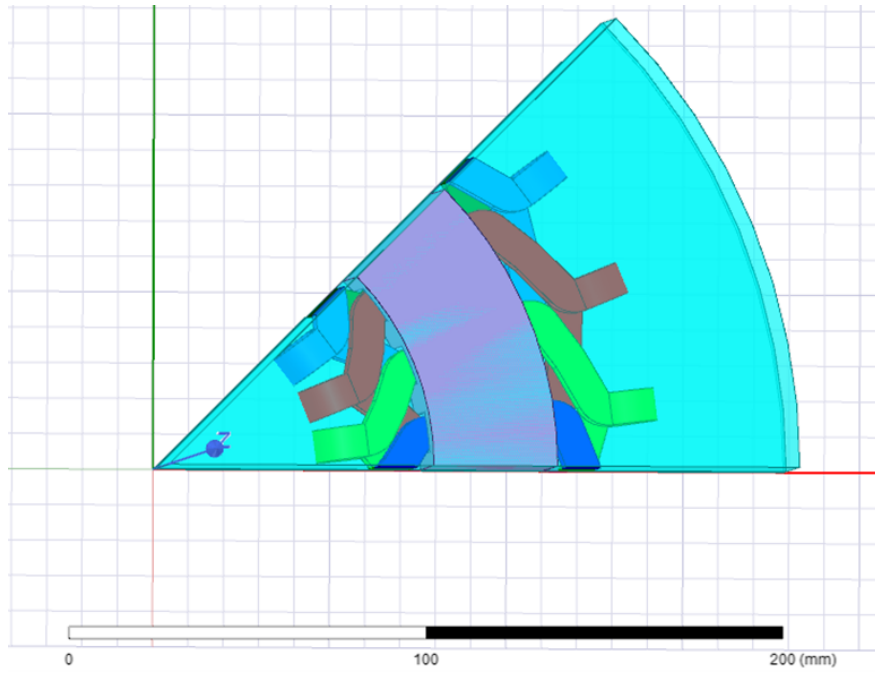
**Figure 4.15** ANSYS Maxwell representation of prototype machine - top
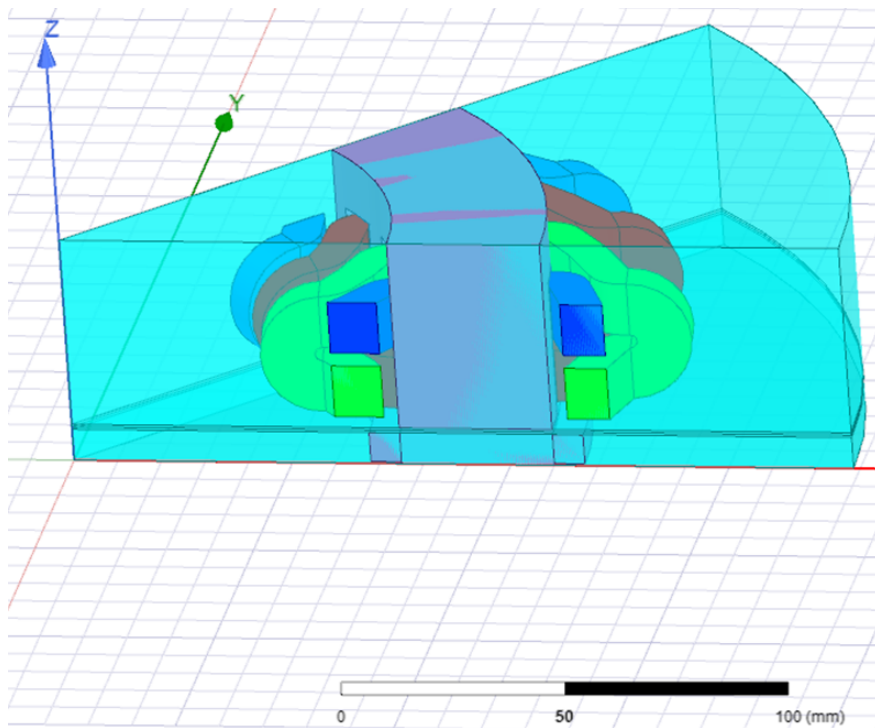
Figure 4.16 ANSYS Maxwell representation of prototype machine - side

112

From the open circuit and locked-rotor simulations the results for the running light tests (Table 4.5) and locked rotor (Table 4.6) were obtained. These were from time-stepped FEA with 0.0005 time steps and 100 mS simulations. The voltages and currents are outputs and it is possible to obtain the transient input power from

$$P_{ph} = \frac{v_{ph1}i_{ph1} + v_{ph2}i_{ph2} + v_{ph3}i_{ph3}}{3} \tag{4.11}$$

Table 4.5 Maxwell model of prototype running light tests

Airgap [mm]	V_{ph} [V]	I_{ph} [A]	P_{ph} [W]	n_r [rpm]	Q_{ph} [VAr]	X_m [Ω]	r_c [Ω]
1	120.2	1.41	50	707	162.5	88.9	289.0

Table 4.6 Maxwell model prototype locked rotor tests

Airgap	V_{ph} [V]	I_{ph} [A]	P_{ph} [W]	Q_{ph} [VAr]	$X_1 + X_2^/$ [Ω]	$r_1 + r_2^/$ [Ω]	$r_2^/$ [Ω]
1	120.9	3.4	260	317.5	27.6	22.6	15.1

4.3.7 Comparison of Results

The results from the sizing, prototype testing, *SPEED* simulations and ANSYS Maxwell simulations can be tabulated as shown in Table 4.7. It can be seen that the equivalent circuit parameters match quite well. The core loss resistance is high and difficult to transition from an axial flux machine to a radial flux equivalent. This is often omitted from the per-phase equivalent circuit, particularly in a variable speed machine where the frequency is varying and inductances are used. The rotor referred resistances map well. The FEA simulation gives a low value which will mean the torque will increase faster when the machine is loaded and the speed drops.

Table 4.7 Comparison of running light and locked rotor tests and simulations

Test/Sim/Calc	X_m [Ω]	r_c [Ω]	$X_1 + X_2^{/}$ [Ω]	r_1 [Ω]	$r_2^{/}$ [Ω]
Calc	91.9	—	—	—	—
Test	91.0	240.0	32	7.5	25.6
SPEED	90.7	5906	19.6 + 6.93	7.45	26.8
ANSYS Maxwell	88.9	289	27.6	7.5	15.1

This comparison give confidence in the modelling techniques which is important when re-designing machines to meet specifications and predict performance.

4.4   Performance Simulation of Improved Design

In Section 3.4.1.7 a redesign of the rotor was suggested since the prototype machine appears to have a rotor that is too short so it performs poorly. In this section the rotor is lengthened and the slot filled with thicker wire.

4.4.1   ANSYS Maxwell Simulation

ANSYS Maxwell was used to simulate the machine and this is shown in Figs. 4.17 and 4.18. This has much thicker bars and deeper bars so that the rotor resistance is much lower. The endrings are quite wide. Fig. 4.18 shows the cage - this is is only for half the axial length of the machine and it is more substantial than the prototype.

114
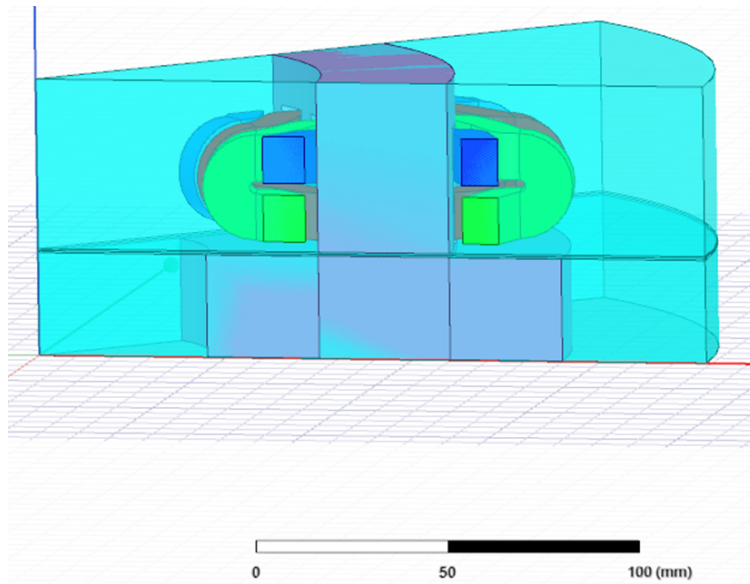
Figure 4.17 ANSYS Maxwell representation of improved machine with long rotor - side
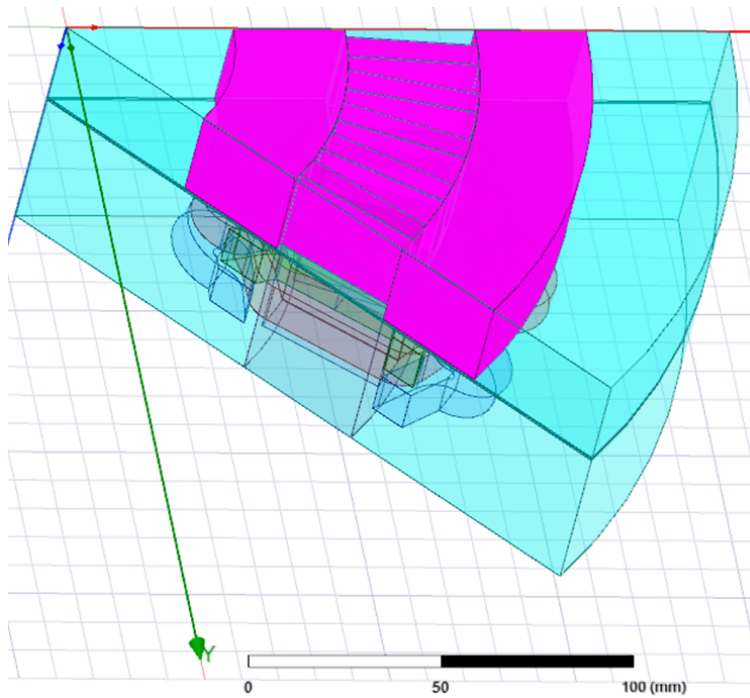

Figure 4.18 ANSYS Maxwell representation of improved machine with long rotor - cage bottom

115

A simulation was carried out at a 730 rpm. The currents are shown in Fig. 4.19 and it can be seen that the convergence is slow. The simulation is 240 ms which 12 current cycles and this was still not quite at steady state. This took over 12 hours to simulate on a modern laptop with 32 GB of RAM. This can be sped up by use of a reduced mesh density and relaxation on some simulation parameters but it is still impractical for the development of an operating area for a variable speed drive. The torque is shown in Fig. 4.20. The unbalanced current produces the torque oscillation. This has a long time period for decay. The input power is shown in Fig. 4.21 and again, there is an oscillation in this. When in steady-state with balanced currents this will be steady. The steady input power can be estimated as about 1500 W while the steady output mechanical power can be estimated as 1146 W. This gives an efficiency of 76.4 % which is an improvement from the prototype machine.
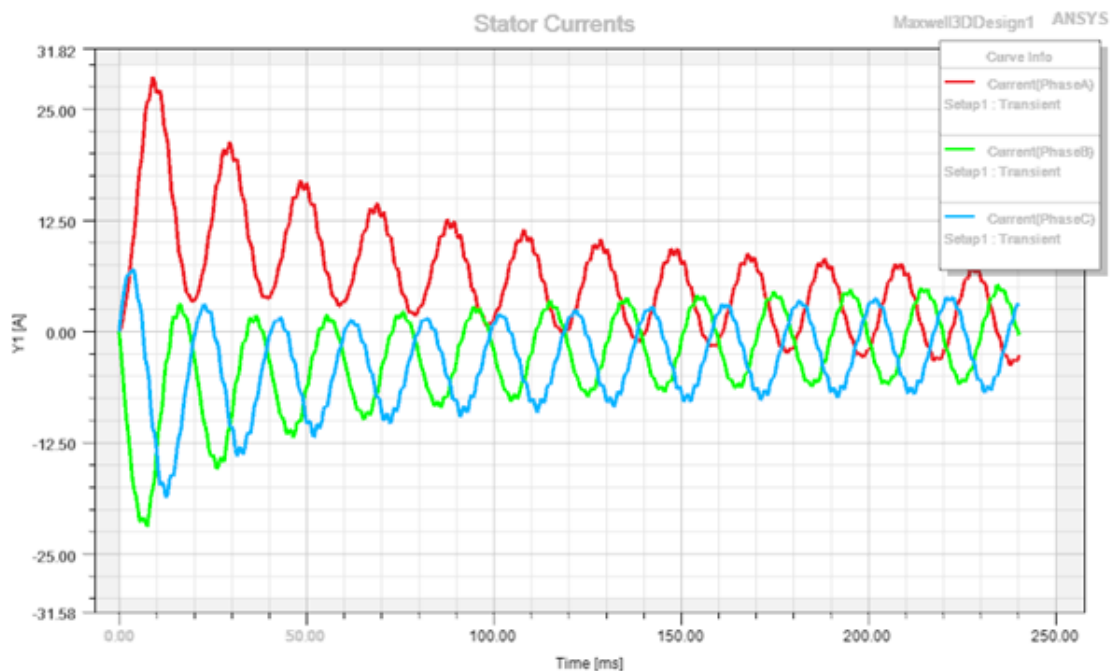

**Figure 4.19** ANSYS Maxwell representation of improved machine current at low loading
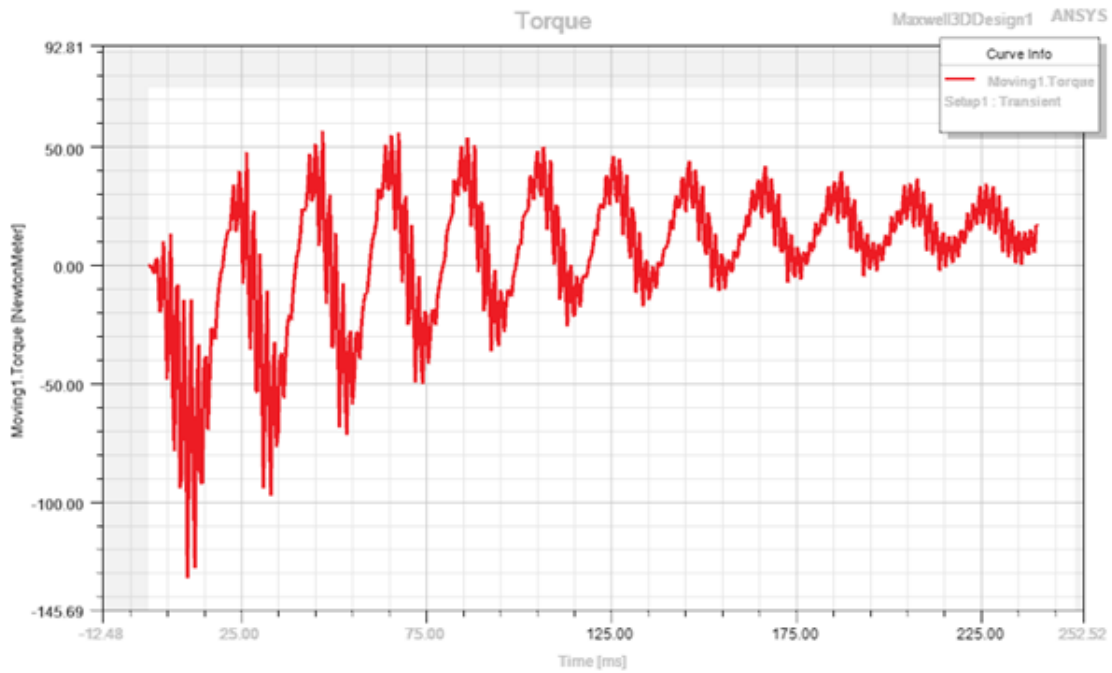
Figure 4.20 ANSYS Maxwell representation of improved machine torque at low loading
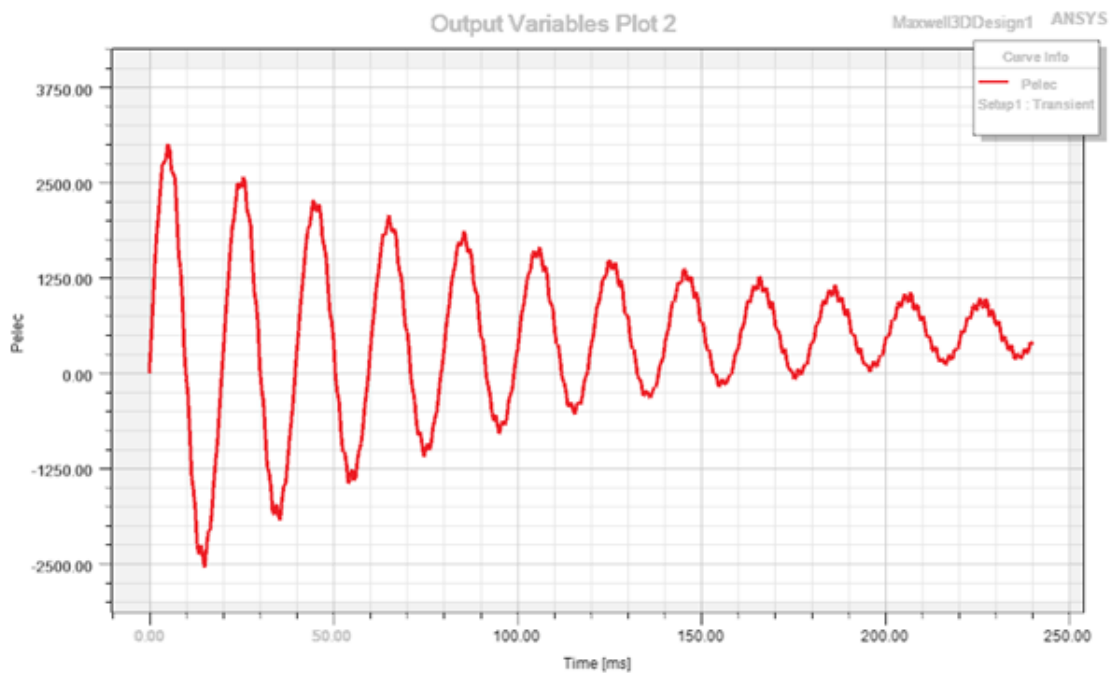

Figure 4.21 ANSYS Maxwell representation of improved machine input electrical power at low load

The ANSYS Maxwell FEA is useful for testing more detailed designs however it is slow to converge and not suitable for rapid design. This is when *SPEED* can be used.

4.4.2 *SPEED* Simulation

A machine with more full stator slots and a longer rotor can be used. This is shown in Fig. 3.21 with a torque-speed curve at a constant frequency shown in Fig. 3.22. These run much faster and can be used for developing operating charts. To do a full design the full range of operation is needed. *SPEED* allows 2D parameter ranging and two dimensions. In Figs. 4.22 and 4.23 have the frequency and speed varied over ranges to assess the maximum torque range up to 1500 rpm and maximum power from 1500 to 4500 rpm. For the maximum power range the efficiency is shown in Fig. 4.24 - the peak efficiency occur at about the rated torque levels.

The control for a variable speed induction motor can control the voltage and frequency. With speed feedback it can therefore control the slip. to do multi-dimensional variations of speed and torque to maximise efficiency is not straightforward. *SPEED* is scriptable and what this allows is for the multi-dimensional design and testing to find the right control solution for a particular machine or geometrical design of a motor for best performance. The scripts can be run in MATLAB and SPEED is called as a calculation routine with opening. This is a powerful tool.
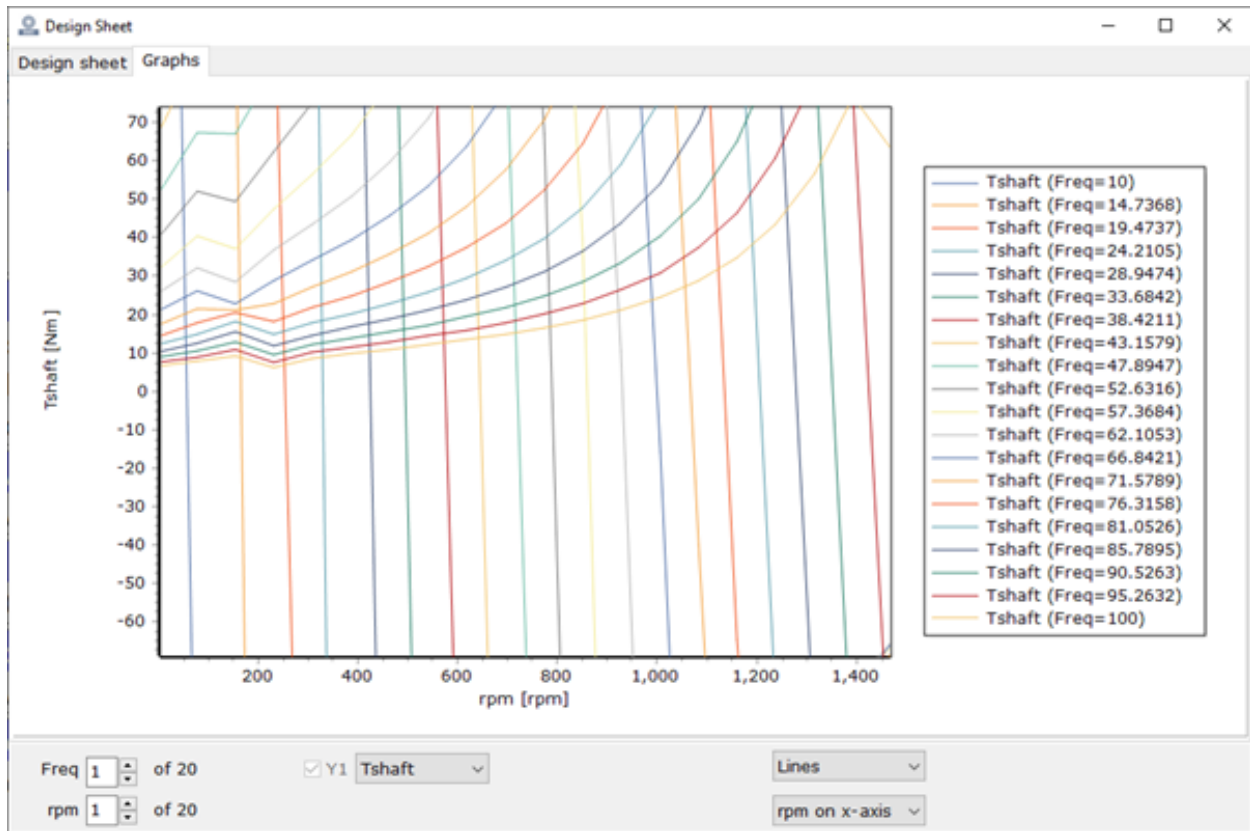
Figure 4.22 *SPEED* representation of improved machine with frequency and speed varied from 0 to 100 Hz and 0 to 1500 rpm
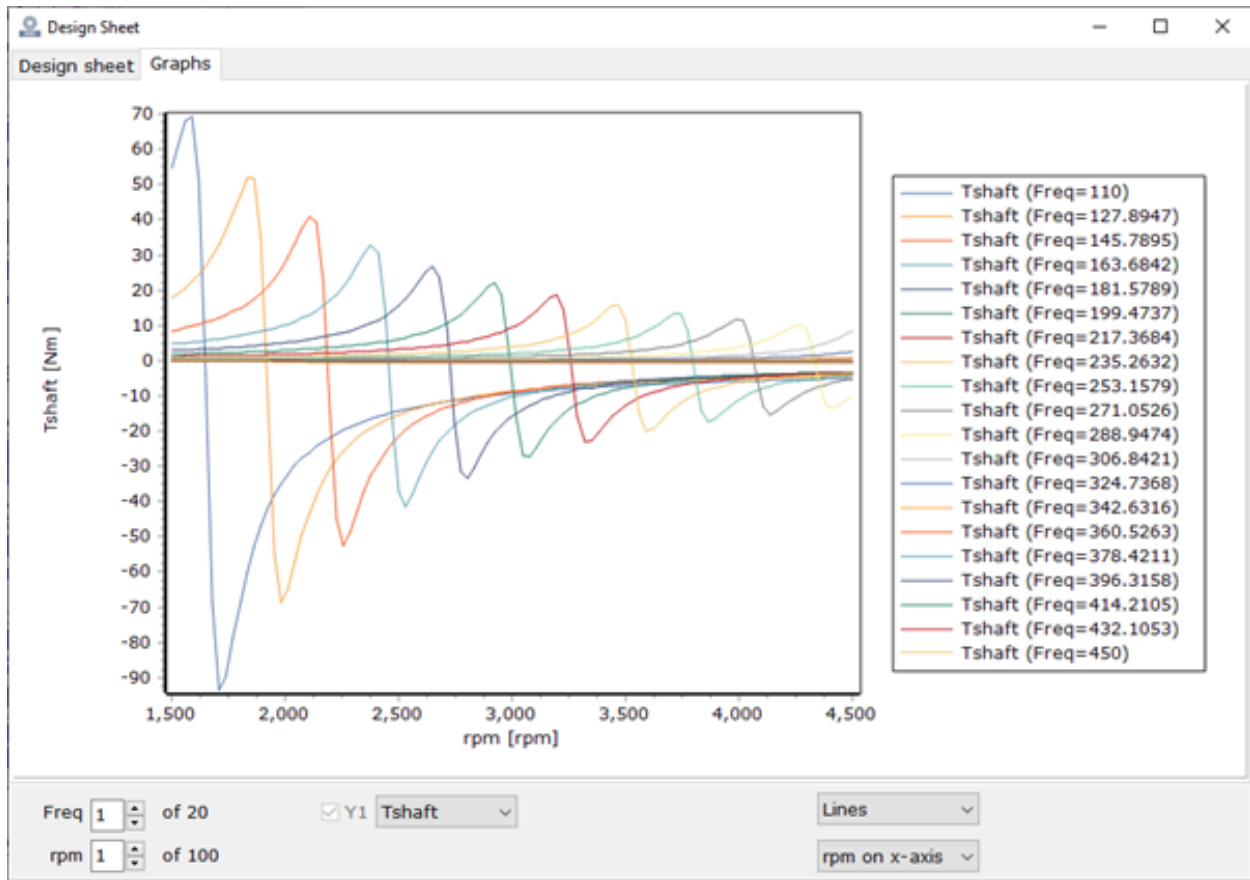
Figure 4.23 *SPEED* representation of improved machine with frequency and speed varied from 100 to 4500 Hz and 1500 to 4500 rpm
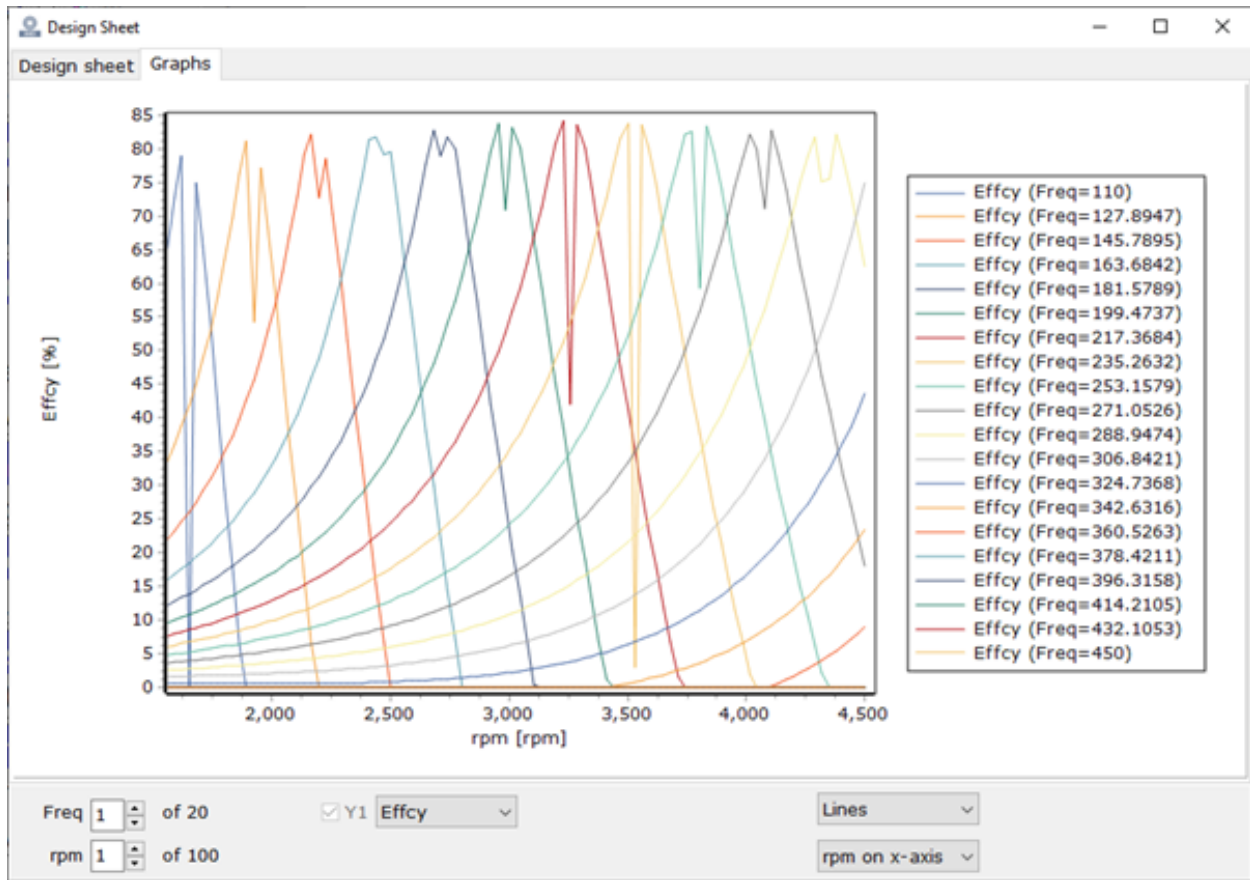
Figure 4.24 *SPEED* representation of improved machine with frequency and speed varied from 100 to 4500 Hz and 1500 to 4500 rpm - efficiency variation

4.5 Conclusions

This chapter shows that the machine does work. It has illustrated that it can be simulated in different ways and these models are reasonable. The basic design was improved and a design which can operate over 75 % efficiency over a range of operating point has been illustrated.

The designed procedure and analysis of the proposed AFIM for use in automotive application is described and discussed. The performance analysis of motor was carried out with various testing

conditions. Throughout the design process and the motor assembly, the aluminum rotor disc of AFIM was subjected to substantial magnetic forces.

From the design point of view the aluminium rotor disc should be able to cope with the loading and the axial forces. During the running of the motor, the aluminum rotor disc appeared to be stable and stiff with the wobble due to manufacturing. The low cost rotor manufacture consists of an aluminum rotor disc with steel studs, which offers a structure with mechanical strength and ruggedness.

Chapter 5

General Conclusion and Future Works

The work presented in this thesis has explored the design of an axial flux electrical machine within the context of an automotive drive. The experimental results of the prototype developed show promising performance enhancements in the axial flux induction machine design for automotive applications.The final design should be able to give about 50 Nm if the rotor is designed properly and the motor controlled correctly. The main objective of this research study was to conduct preliminary designs for surface-mounted low speed axial-flux induction machines with the design arrangement that consists of one rotor and two stators. This design uses a 3D FEA design tool that utilizes the quasi-3D computation method to compute and determine the power and time parameters.

Axial-field electromagnetic differentials using induction machines are a promising solution for electric vehicles rather than a mechanical differential. The machine can have both higher efficiency and power density. Disc-type electrical motors with induction machine excitation appear to be promising in terms of compactness but there still needs to be further design work.

This study required the use of a fast, reliable, multi-physics analytical design tool to explore a wide range of possible solutions in the early stages of the design process when fast design is needed

To keep the gaps between the discs at a distance, some solutions may be:

- The use of tapered roller bearings;

- The compensation of the axial force by means of electromagnetic-based devices; and

The use of fault-tolerant and modular design (weight reduction of machine) direct drive machines will help improve reliability and ease of maintenance. To overcome the problems of cost and availability of permanent rare earth magnets, the use of AFIM could be an interesting alternative solution and will help to facilitate the cost and the control of the flux in the airgap.

5.1 Future Work

Future work may be devoted to further investigate more complex objective functions with additional design variables of the AFIM for automobile applications and to:

- Study of the saturation result on the rotor and the excitation flux paths;

- Study new control techniques as well as the current variations; and

- Cost analysis of the entire process.

Bibliography

[1] Zhi Yang, Fei Shang, Ian P Brown, and Mahesh Krishnamurthy. Comparative study of interior permanent magnet, induction, and switched reluctance motor drives for EV and HEV applications. *IEEE Transactions on Transportation Electrification*, 1(3):245–254, 2015.

[2] Nigel Burton. *History of electric cars*. Crowood, 2013.

[3] Martin Eberhard and Marc Tarpenning. The 21 st century electric car tesla motors. *Tesla Motors*, 17, 2006.

[4] OF Vynakov, EV Savolova, and AI Skrynnyk. Modern electric cars of Tesla Motors company. *Automation technological and business processes*, 8(2):9–18, 2016.

[5] Siang Fui Tie and Chee Wei Tan. A review of energy sources and energy management system in electric vehicles. *Renewable and sustainable energy reviews*, 20:82–102, 2013.

[6] Ion Boldea, Lucian N Tutelea, Leila Parsa, and David Dorrell. Automotive electric propulsion systems with reduced or no permanent magnets: An overview. *IEEE Transactions on Industrial Electronics*, 61(10):5696–5711, 2014.

[7] KT Chau. Overview of Electric Vehicle Machines - From Tesla to Tesla, and Beyond. In *2016 International Conference of Asian Union of Magnetics Societies (ICAUMS)*, pages 1–6. IEEE, 2016.

[8] FC Mushid and DG Dorrell. Review of axial flux induction motor for automotive applications. In *2017 IEEE Workshop on Electrical Machines Design, Control and Diagnosis (WEMDCD)*, pages 146–151. IEEE, 2017.

[9] Iqbal Husain. *Electric and hybrid vehicles: design fundamentals*. CRC press, 2010.

[10] Emine Bostanci, Mehdi Moallem, Amir Parsapour, and Babak Fahimi. Opportunities and challenges of switched reluctance motor drives for electric propulsion: A comparative study. *IEEE Transactions on Transportation Electrification*, 3(1):58–75, 2017.

[11] Pooja Bhatt, Hemant Mehar, and Manish Sahajwani. Electrical Motors for Electric Vehicle– A Comparative Study. *Available at SSRN 3364887*, 2019.

[12] Ramu Krishnan. *Switched reluctance motor drives: modeling, simulation, analysis, design, and applications*. CRC press, 2017.

[13] Philip L Alger and M Harry Hesse. *Induction machines: their behavior and uses*, volume 190. Gordon and Breach New York, 1970.

[14] MG NEMA. Information Guide for General Purpose Industrial AC Small and Medium Squirrel-Cage Induction Motor Standards. 2007.

[15] Riccardo Marino, Patrizio Tomei, and Cristiano M Verrelli. *Induction motor control design*. Springer Science & Business Media, 2010.

[16] Allan B Plunkett, John D D'Atre, and Thomas A Lipo. Synchronous control of a static AC induction motor drive. *IEEE Transactions on Industry Applications*, (4):430–437, 1979.

[17] Tatsuki Suzuki, Masami Nirei, Manbu Horiuchi, Mitsuhide Sato, Yinggang Bu, and Tsutomu Mizuno. Examination of interior winding synchronous motor with improved torque and

reduced ac copper loss. In *2019 International Conference on Electrical Engineering Research & Practice (ICEERP)*, pages 1–6. IEEE, 2019.

[18] Patel B Reddy, TM Jahns, Patrick J McCleer, and Theodore P Bohn. Design, analysis and fabrication of a high-performance fractional-slot concentrated winding surface PM machine. In *2010 IEEE Energy Conversion Congress and Exposition*, pages 1074–1081. IEEE, 2010.

[19] Mohammad Farshadnia, Muhammad Ali Masood Cheema, Alireza Pouramin, Rukmi Dutta, and John Edward Fletcher. Design of optimal winding configurations for symmetrical multi-phase concentrated-wound surface-mount pmsms to achieve maximum torque density under current harmonic injection. *IEEE Transactions on Industrial Electronics*, 65(2):1751–1761, 2017.

[20] Metin Aydin, Surong Huang, and Thomas A Lipo. Torque quality and comparison of internal and external rotor axial flux surface-magnet disc machines. *IEEE transactions on Industrial Electronics*, 53(3):822–830, 2006.

[21] Delvis Anibal González, Juan Antonio Tapia, and Alvaro Letelier Bettancourt. Design consideration to reduce cogging torque in axial flux permanent-magnet machines. *IEEE Transactions on Magnetics*, 43(8):3435–3440, 2007.

[22] Rathna Chitroju. *Improved performance characteristics of induction machines with non-skewed symmetrical rotor slots*. PhD thesis, KTH, 2009.

[23] Zahra Nasiri-Gheidari and Hamid Lesani. A survey on axial flux induction motors. *Przeglad Elektrotechniczny*, 2:300–305, 2012.

[24] Anurag M Lulhe and Tanuja N Date. A technology review paper for drives used in electrical vehicle (ev) & hybrid electrical vehicles (hev). In *2015 International Conference on Control,*

Instrumentation, Communication and Computational Technologies (ICCICCT), pages 632–636. IEEE, 2015.

[25] F Caricchi, F Crescimbini, E Santini, and C Santucci. Influence of the radial variation of the magnet pitch in slotless permanent magnet axial flux motors. In *IAS'97. Conference Record of the 1997 IEEE Industry Applications Conference Thirty-Second IAS Annual Meeting*, volume 1, pages 18–23. IEEE, 1997.

[26] Z Nasiri-Gheidari and H Lesani. Optimal design of adjustable air-gap, two-speed, capacitor-run, single-phase axial flux induction motors. *IEEE Transactions on energy conversion*, 28(3):543–552, 2013.

[27] Sinisa Jurkovic, Khwaja M Rahman, and Peter J Savagian. Electric traction motors for Cadillac CT6 plugin hybrid-electric vehicle. In *2016 IEEE Energy Conversion Congress and Exposition (ECCE)*, pages 1–9. IEEE, 2016.

[28] MA Tapia, AE Hoffer, and JA Tapia. Analysis of the magnetizing current requirement of an axial flux induction machine. In *2016 IEEE International Conference on Automatica (ICA-ACCA)*, pages 1–6. IEEE, 2016.

[29] Amin Nobahari, Ahmad Darabi, and Amir Hassannia. Various skewing arrangements and relative position of dual rotor of an axial flux induction motor, modelling and performance evaluation. *IET Electric Power Applications*, 12(4):575–580, 2018.

[30] Sonja Tidblad Lundmark, Johan Linder, and Mikael Rittander. Outer rotor high torque density pm motors with a peripheral position sensor. In *2016 XXII International Conference on Electrical Machines (ICEM)*, pages 858–864. IEEE, 2016.

[31] Shahbaz Amin, Sahib Khan, and Syed Sabir Hussain Bukhari. A comprehensive review on

axial flux machines and its applications. In *2019 2nd International Conference on Computing, Mathematics and Engineering Technologies (iCoMET)*, pages 1–7. IEEE, 2019.

[32] Ion Boldea and Syed A Nasar. *The induction machine design handbook*. CRC press, 2018.

[33] Mario Alejandro Tapia Montero, Alvaro Ernesto Hoffer Garces, Juan Antonio Tapia Ladino, and Rogel Rodolfo Wallace Collao. Simulation and Analysis of an Axial Flux Induction Machine. *IEEE Latin America Transactions*, 15(7):1263–1269, 2017.

[34] Zahra Nasiri-Gheidari and Farid Tootoonchian. Axial flux resolver design techniques for minimizing position error due to static eccentricities. *IEEE Sensors Journal*, 15(7):4027–4034, 2015.

[35] STEG Stephen, Matthew James Carton, and Bryce Allen Peters. Axial flux motor, November 2 2017. US Patent App. 15/358,238.

[36] Mark Andrew Johnson. Brushless motor, December 20 2018. US Patent App. 16/011,954.

[37] Preston L Schiller, Jeffrey R Kenworthy, N Aarsæther, T Nyseth, A Røiseland, P McLaverty, RN Abers, M Douglass, J Friedmann, RN Abers, et al. When Tesla's autopilot goes wrong. In *An introduction to sustainable transportation: policy, planning and implementation*, volume 1, pages 1–10. Lutterworth Press, Cambridge, MA, and Chelsea Green Publishing Company . . . , 2018.

[38] Metin Aydin, Ronghai Qu, and Thomas A Lipo. Cogging torque minimization technique for multiple-rotor, axial-flux, surface-mounted-pm motors: alternating magnet pole-arcs in facing rotors. In *38th IAS Annual Meeting on Conference Record of the Industry Applications Conference, 2003.*, volume 1, pages 555–561. IEEE, 2003.

[39] Sakuntala Mahapatra, Raju Daniel, Deep Narayan Dey, and Santanu Kumar Nayak. Induction motor control using PSO-ANFIS. *Procedia Computer Science*, 48:753–768, 2015.

[40] James Goss, Mircea Popescu, Dave Staton, Dougie Hawkins, and Aldo Boglietti. Electrical vehicles-practical solutions for power traction drive systems. In *2017 IEEE Workshop on Electrical Machines Design, Control and Diagnosis (WEMDCD)*, pages 80–88. IEEE, 2017.

[41] Greg Heins, Dan M Ionel, Dean Patterson, Steve Stretz, and Mark Thiele. Combined experimental and numerical method for loss separation in permanent-magnet brushless machines. *IEEE Transactions on Industry Applications*, 52(2):1405–1412, 2015.

[42] S Vivier and G Friedrich. Comparison between single-model and multi-model optimization methods for multiphysical design. In *2016 XXII International Conference on Electrical Machines (ICEM)*, pages 1399–1404. IEEE, 2016.

[43] Weizhong Fei, Patrick Chi Kwong Luk, Jian Xin Shen, Bin Xia, and Yu Wang. Permanent-magnet flux-switching integrated starter generator with different rotor configurations for cogging torque and torque ripple mitigations. *IEEE Transactions on Industry Applications*, 47(3):1247–1256, 2011.

[44] Jacek F Gieras, Rong-Jie Wang, and Maarten J Kamper. *Axial flux permanent magnet brushless machines*. Springer Science & Business Media, 2008.

[45] Ion Boldea. *Linear electric machines, drives, and MAGLEVs handbook*. CRC press, 2017.

[46] ZQ Zhu, Y Oner, LJ Wu, and X Ge. Analytical sub-domain model for predicting open-circuit field of permanent magnet Vernier machine accounting for tooth tips. *COMPEL: The International Journal for Computation and Mathematics in Electrical and Electronic Engineering*, 2016.

[47] Ankita Dwivedi, Santosh Kumar Singh, Rakesh K Srivastava, and Som N Mahendra. Comparative study and performance evaluation of analytical methods for surface mounted permanent magnet brushless motors. *IET Power Electronics*, 9(11):2289–2297, 2016.

[48] Giulio De Donato, Fabio Giulii Capponi, and Federico Caricchi. No-load performance of axial flux permanent magnet machines mounting magnetic wedges. *IEEE Transactions on industrial electronics*, 59(10):3768–3779, 2011.

[49] G De Donato, F Giulii Capponi, and F Caricchi. Influence of magnetic wedges on the load performance of axial flux permanent magnet machines. In *IECon 2010-36th Annual Conference on IEEE Industrial Electronics Society*, pages 876–882. IEEE, 2010.

[50] ZQ Zhu, Zh P Xia, LJ Wu, and Geraint W Jewell. Analytical modeling and finite-element computation of radial vibration force in fractional-slot permanent-magnet brushless machines. *IEEE Transactions on Industry Applications*, 46(5):1908–1918, 2010.

[51] Tianjie Zou, Dawei Li, Ronghai Qu, Jian Li, and Dong Jiang. Analysis of a dual-rotor, toroidal-winding, axial-flux vernier permanent magnet machine. *IEEE Transactions on Industry Applications*, 53(3):1920–1930, 2017.

[52] Emin Yildiriz and Güven Önbilgin. Design studies of axial flux hybrid excitation synchronous machine with magnetic bridge. In *2013 8th International Conference on Electrical and Electronics Engineering (ELECO)*, pages 234–237. IEEE, 2013.

[53] A Benoudjit and N Nait Said. New dual-airgap axial and radial-flux induction motor for on wheel drive electric propulsion systems. In *POWERCON'98. 1998 International Conference on Power System Technology. Proceedings (Cat. No. 98EX151)*, volume 1, pages 615–619. IEEE, 1998.

[54] Liliang Gao, John E Fletcher, and Libo Zheng. Low-speed control improvements for a two-level five-phase inverter-fed induction machine using classic direct torque control. *IEEE Transactions on Industrial Electronics*, 58(7):2744–2754, 2010.

[55] Alfio Consoli, Giacomo Scelba, Giuseppe Scarcella, and Mario Cacciato. An effective energy-saving scalar control for industrial ipmsm drives. *IEEE Transactions on Industrial Electronics*, 60(9):3658–3669, 2012.

[56] William Sierzchula, Sjoerd Bakker, Kees Maat, and Bert Van Wee. The competitive environment of electric vehicles: An analysis of prototype and production models. *Environmental Innovation and Societal Transitions*, 2:49–65, 2012.

[57] Ali Emadi, Kaushik Rajashekara, Sheldon S Williamson, and Srdjan M Lukic. Topological overview of hybrid electric and fuel cell vehicular power system architectures and configurations. *IEEE Transactions on vehicular technology*, 54(3):763–770, 2005.

[58] Richard A Schmidt, Timothy D Lee, Carolee Winstein, Gabriele Wulf, and Howard N Zelaznik. *Motor control and learning: A behavioral emphasis*. Human kinetics, 2018.

[59] Yirga Belay Muna and Cheng-Chien Kuo. Magnetic field distribution of magnetic encoder with tmr sensor using finite element analysis. *Microsystem Technologies*, pages 1–19, 2020.

[60] S Peaiyoung, T Kulworawanichpong, S Sujitjorn, et al. Magnetic Field Simulation of an Induction Motor Using Nonlinear Time-Stepping Finite Element Method. In *International Conference on Electrical Engineering/Electronics, Computer, Telecommunications and Information Technology (ECTI-CON 2005)*, pages 734–737, 2005.

[61] Jie Mei, C. H. T Lee, and J. L. Kirtley. Design of axial flux induction motor with reduced back iron for electric vehicles. *IEEE Transactions on Vehicular Technology*, 69(1):293–301, 2020.

[62] James Larminie and John Lowry. *Electric vehicle technology explained*. John Wiley & Sons, 2012.

[63] XD Xue, KWE Cheng, and NC Cheung. Selection of electric motor drives for electric vehicles. In *2008 Australasian Universities Power Engineering Conference*, pages 1–6. IEEE, 2008.

[64] J. R. Hendershot and T. J. E. Miller. *Design of brushless permanent-magnet motors*. Clarendon Press, Oxford, 1994.

[65] Johannes JH Paulides, Laurentiu Encica, Elena A Lomonova, and Andre JA Vandenput. Active roll compensation for automotive applications using a brushless direct-drive linear permanent magnet actuator. In *2006 37th IEEE Power Electronics Specialists Conference*, pages 1–6. IEEE, 2006.

[66] D. G. Dorrell. Combined thermal and electromagnetic analysis of permanent-magnet and induction machines to aid calculation. *IEEE Transactions on Industrial Electronics*, 55(10):3566–3574, 2008.

[67] N Simpson and PH Mellor. Exploiting cloud computing in the multi-physics design and optimisation of electromagnetic devices. In *2015 IEEE 16th Workshop on Control and Modeling for Power Electronics (COMPEL)*, pages 1–8. IEEE, 2015.

[68] Juha Pyrhönen, Pia Lindh, Maria Polikarpova, Emil Kurvinen, and Ville Naumanen. Heat-transfer improvements in an axial-flux permanent-magnet synchronous machine. *Applied Thermal Engineering*, 76:245–251, 2015.